UNIVERSIDADE
BEIRA INTERIOR

Computational Evaluation of Heat Exchangers in Hydrogen-Fueled Gas Turbines

Luís Martinho de Figueiredo Moura Diogo

Dissertação para obtenção do Grau de Mestre em
Engenharia Aeronáutica
(Ciclo de estudos integrado)

Orientador: Prof. Doutor Francisco Miguel Ribeiro Proença Brojo

Covilhã, outubro de 2024

Declaração de Integridade

Eu, Luís Martinho de Figueiredo Moura Diogo, que abaixo assino, estudante com número de inscrição 42437 de/o Mestrado Integrado em Engenharia Aeronáutica da Faculdade de Engenharia, declaro ter desenvolvido o presente trabalho e elaborado o presente texto em total consonância com o **Código de Integridade da Universidade da Beira Interior**.

Mais concretamente afirmo não ter incorrido em qualquer das variedades de Fraude Académica, e que aqui declaro conhecer, que em particular atendi à exigida referenciação de frases, extratos, imagens e outras formas de trabalho intelectual, e assumindo assim na íntegra as responsabilidades da autoria.

Universidade da Beira Interior, Covilhã 09/10/2024

Resumo

Esta Dissertação apresenta a avaliação computacional de permutadores de calor utilizados em turbinas a gás alimentadas a hidrogénio, abordando a crescente necessidade de sistemas de propulsão eficientes e sustentáveis. Foi desenvolvida uma ferramenta computacional para modelar e prever métricas chave de desempenho dos permutadores de calor, incluindo taxas de transferência de calor, quedas de pressão, NTU e eficácia, numa ampla gama de condições operacionais. O estudo aplica abordagens de nó único e de múltiplos nós. No entanto, a validação e os estudos paramétricos são realizados exclusivamente utilizando o método de nó único. Estes estudos analisam de forma exaustiva o impacto de parâmetros críticos, como a temperatura de estagnação do combustor, o caudal mássico, a área da garganta e as configurações dos canais de arrefecimento, no desempenho geral dos permutadores de calor.

A validação mostrou previsões bastante precisas para números de Mach de voo de 1,5 e 2, com desvios mínimos. No entanto, à medida que os números de Mach aumentam para 3 e além, a precisão diminui devido às limitações inerentes do método de nó único, que simplifica em excesso os gradientes de fluxo e temperatura dentro do combustor e dos canais de arrefecimento. Os estudos paramétricos revelaram que o aumento dos caudais mássicos e a otimização das áreas do gargalo resultaram em melhorias significativas tanto nas taxas de transferência de calor quanto na eficiência de arrefecimento. Notavelmente, as configurações de contrafluxo superaram consistentemente os designs de fluxo paralelo, alcançando até 12% mais eficácia, especialmente em temperaturas de estagnação elevadas. Estes resultados sublinham a importância de otimizar cuidadosamente o design dos permutadores de calor para melhorar a eficiência das turbinas a gás alimentadas a hidrogénio, particularmente em aplicações aeroespaciais de alto desempenho. Trabalhos futuros concentrar-se-ão na validação da abordagem de múltiplos nós para melhorar a precisão do modelo na previsão das variações espaciais de temperatura, pressão e características de fluxo. Além disso, a incorporação dos efeitos de interação com a parede e da resistência térmica refinará ainda mais as previsões de transferência de calor, otimizando o design dos permutadores de calor para sistemas de propulsão a hidrogénio.

Palavras-chave

Permutadores de calor, Taxas de transferência de calor, Turbina a gás alimentada a hidrogénio criogénico, Coeficiente de transferência de calor convectivo, Análise NTU-eficácia

Abstract

This Dissertation presents the computational evaluation of heat exchangers used in hydrogen-fueled gas turbines, addressing the growing need for efficient and sustainable propulsion systems. A computational tool was developed to model and predict key performance metrics of heat exchangers, including heat transfer rates, pressure drops, NTU, and effectiveness, across a wide range of operating conditions. The study applies both single-node and multi-node approaches. The validation and parametric studies, however, are performed exclusively using the single-node method. These studies thoroughly analyze the impact of critical parameters, including combustor stagnation temperature, mass flow rate, throat area, and cooling channel configurations, on the overall performance of heat exchangers.

The validation showed highly accurate predictions at aircraft Mach numbers 1.5 and 2, with minimal deviations. However, as aircraft Mach numbers increased to 3 and beyond, the accuracy decreased due to the inherent limitations of the single-node method, which oversimplifies the flow and temperature gradients within the combustor and cooling channels. Parametric studies revealed that increasing mass flow rates and optimizing throat areas resulted in significant improvements in both heat transfer rates and cooling efficiency. Notably, counterflow configurations consistently outperformed parallel flow designs, yielding up to 12% greater effectiveness, particularly at elevated stagnation temperatures. These findings underscore the importance of carefully optimizing heat exchanger design to enhance the efficiency of hydrogen-fueled gas turbines, especially in high-performance aerospace applications. Future work will focus on validating the multi-node approach to enhance the model's accuracy in predicting spatial variations in temperature, pressure, and flow characteristics. Additionally, incorporating wall interaction effects and thermal resistance will further refine heat transfer predictions, optimizing the design of heat exchangers for hydrogen-fueled propulsion systems.

Keywords

Heat exchangers, Heat transfer rates, Cryogenic Hydrogen-fueled gas turbine, Convective heat transfer coefficient, NTU-effectiveness analysis

Contents

List of Figures

List of Tables

Nomenclature

A	Area	(m^2)
c_p	Specific heat at constant pressure	J/kg·K
C	Heat capacity rate	W/K
D	Diameter	m
G	Gibbs Free Energy	-
h	Convective heat transfer coefficient	W/m^2·K
H	Cooling Channel Height	m
k	Thermal conductivity	W/m·K
L	Length	m
m	Mass	kg
$\dot{m}$	Mass flow rate	kg/s
Ma	Mach number	-
n	Number of moles	mol
Nu	Nusselt number	-
p	Static Pressure	Pa
p^0	Stagnation Pressure	Pa
Δp	Pressure difference	Pa
P	Power	W
Pe	Perimeter	m
Pr	Prandtl number	-
q	Heat flux	W/m^2
Q	Heat transfer rate	W
r	Pressure ratio	-
R	Universal gas constant	J/mol·K
Re	Reynolds number	-
s	Entropy	J/K
T	Static Temperature	K
T^0	Stagnation Temperature	K
ΔT	Temperature difference	K
U	Overall heat transfer coefficient	W/m^2·K
v	Velocity	m/s
V	Volume	m^3
W	Cooling Channel Width	m

Greek Symbols

α	Thermal diffusivity	m^2/s

ε	Effectiveness	-
γ	Specific heat ratio	-
μ	Dynamic viscosity	Pa·s
ν	Kinematic viscosity	m^2/s
ξ	Friction factor	-
ρ	Density	kg/m^3
σ	Stefan-Boltzmann constant	$W/m^2 \cdot K^4$
τ	Shear stress	Pa
ϕ	Relative humidity	-
ψ	Stream function	-

Subscripts

a	Air
c	Cold fluid
h	Hot fluid
i	Inlet
o	Outlet
s	Surface
w	Wall

Acronyms

CFD	Computational Fluid Dynamics
FEA	Finite Element Analysis
LMTD	Log Mean Temperature Difference
NTU	Number of Transfer Units

Chapter 1

Introduction

1.1 Motivation

Hydrogen is increasingly recognized as a key player in the transition to cleaner and more efficient energy systems, particularly in the aerospace sector. As a zero-carbon fuel, hydrogen offers significant environmental benefits, making it an attractive alternative for propulsion systems aiming to reduce their carbon footprint. In addition to its environmental advantages, hydrogen-fueled propulsion systems promise higher efficiency and performance, particularly when integrated with well-optimized thermal management systems such as heat exchangers. These systems play a critical role in maintaining optimal operating conditions by efficiently transferring heat in engines, ensuring better fuel utilization and overall system reliability.

However, designing effective heat exchangers in hydrogen-fueled systems presents numerous challenges. Due to the complexities involved in thermal management, particularly in handling hydrogen's unique properties under varying operating conditions, there is a need for tools that can assist in the early stages of engine pre-design. This is especially true when seeking efficiency gains without incurring the high computational costs typically associated with detailed simulations.

This thesis is motivated by the need to develop a simple and computationally inexpensive tool that can be used to evaluate the performance of heat exchangers in hydrogen-fueled propulsion systems. The tool is designed to provide quick and reliable estimates of key performance parameters, making it a valuable resource for the initial stages of propulsion system design. By simplifying the evaluation process, this tool will aid engineers and researchers in making informed design decisions early on, without the need for costly and time-consuming simulations. Ultimately, this research contributes to enhancing the efficiency of hydrogen propulsion systems, supporting the broader goal of cleaner, more efficient aerospace technologies.

1.2 Objectives

The primary objective of this thesis is to develop a computational tool capable of evaluating and optimizing the thermal performance of hydrogen-fueled propulsion systems equipped with heat exchangers. This tool is designed to provide a fast and computationally efficient way to assess key performance metrics, such as heat transfer rates, pressure drops, NTU, and effectiveness, across a range of operating conditions and Mach numbers. Its simplified approach aims to assist in the preliminary design and optimization of propulsion systems,

particularly in the early stages where rapid feedback is essential.

The tool features two primary methods of analysis: a single-node approach, which has been validated in the present work, and a multi-node method, which is available for future work. The single-node method is suited for cases where detailed temperature profiles inside the combustor are not available, offering quick estimates of heat transfer and fluid flow. On the other hand, the multi-node method is intended to provide more granular insights into temperature distribution and flow behavior within the combustor. While the multi-node method was not validated in this study, it is designed to improve the accuracy of the results in cases where more detailed input data is available, allowing for a better representation of the thermal gradients and local phenomena within the combustor and cooling channels.

In this context, the specific objectives of the thesis are:

- To implement a computational method that models the heat transfer and fluid flow within the combustor and cooling channels of hydrogen-fueled engines.
- To validate the computational tool using the single-node approach against existing reference data, ensuring reliable estimates of heat exchanger performance under different Mach number conditions.
- To outline the functionality of the multi-node method, which can provide more detailed predictions in future work when more information about temperature distribution is available.
- To assess the limitations of the single-node approach and propose recommendations for future improvements in the thermal management of propulsion systems.
- To demonstrate the applicability of the tool in optimizing heat exchanger designs for hydrogen-fueled engines, with a focus on efficiency gains and system reliability.

The ultimate goal is to deliver a versatile and user-friendly tool that can streamline the design process for propulsion systems, facilitating the development of more efficient and sustainable aerospace technologies. This research contributes to broader efforts in improving hydrogen propulsion systems by enabling faster evaluations of thermal performance and lays the groundwork for more accurate, detailed modeling through the multi-node method in future work.

1.3 Dissertation Outline

The present dissertation is organized into five chapters. These are as follows: Introduction, Literature Review, Methodology, Results, and Conclusion.

The first chapter provides the motivation behind the study, outlining the goals of developing a computational model to assess the thermal performance of hydrogen-fueled propulsion

systems with heat exchangers. It also presents the objectives of the dissertation and provides an overview of how the content is structured.

The Literature Review offers a foundation by summarizing existing research on heat exchangers and propulsion systems, with a focus on hydrogen-fueled designs. This chapter highlights the importance of efficient heat management in propulsion systems, exploring previous studies and frameworks that guided the development of the current model. Additionally, the review discusses the various empirical correlations, such as the Bartz formula, which are used in thermal calculations.

The Methodology chapter describes the computational approaches applied in the model. It explains both the single-node and multi-node methods for evaluating heat transfer and fluid properties in the combustor and cooling channels. The chapter also details the mathematical formulations of the governing equations and the assumptions made, such as the ideal gas law and inviscid flow. Furthermore, this chapter outlines the development of the computational tool and its design to provide quick, preliminary evaluations during the early stages of propulsion system design.

The Results chapter presents a comprehensive analysis of the model's predictions in comparison with reference data from existing literature, focusing on key performance parameters such as heat transfer rates, pressure drop, NTU, and effectiveness. The validation section assesses the model's accuracy across different Mach numbers, identifying both its strengths and limitations, particularly at higher Mach numbers where the assumptions and simplifications in the model begin to diverge from the complex physical phenomena observed in practice. In addition to the validation, the chapter includes a series of parametric studies that evaluate how variations in critical parameters—such as combustor stagnation temperature, mass flow rates, throat area, and flow configuration—affect the heat exchanger's performance. These studies provide deeper insights into the sensitivity of the model's predictions to changes in operational and geometric parameters, offering guidance for optimizing heat transfer and cooling system efficiency in high-performance propulsion systems.

The Conclusion summarizes the main findings of the project, reflecting on the accuracy and applicability of the single-node method in predicting heat exchanger performance. It also suggests directions for future research, particularly the validation of the multi-node method and the incorporation of more detailed thermal and flow profiles to improve the accuracy of the model at higher speeds.

Chapter 2

Literature Review

2.1 Heat Exchangers

Heat exchangers are fundamental devices engineered to transfer thermal energy between two or more fluids, between a solid surface and a fluid, or even between solid particulates and a fluid, across different temperatures and in thermal contact. These systems typically exhibit minimal external heat and work interactions, focusing instead on heating or cooling fluid streams and facilitating phase changes such as evaporation and condensation. Heat exchangers also play a crucial role in processes aimed at heat recovery or rejection and in various chemical processing applications, including sterilization, pasteurization, distillation, and crystallization. The design of most heat exchangers ensures that the fluids exchanging heat do not come into direct contact. Instead, they transfer heat through a separating wall or transiently into and out of such a wall. These devices are broadly classified into two types:

- **Recuperators:** Fluids are permanently separated by a heat transfer surface.
- **Regenerators:** The heat transfer surface intermittently stores and releases heat, allowing minimal fluid leakage due to matrix rotation or valve switching.

2.1.1 Flow Configurations in Heat Exchangers

The configuration of hot and cold fluid flows relative to each other in a heat exchanger is crucial for efficient utilization of the heat transfer area. This efficiency is essential not only for meeting the heat load requirements but also for managing factors such as pressure drop, header design, thermal stresses on materials, and integration into specific usage locations.

The fundamental flow arrangements in heat exchangers include counter-flow, parallel-flow, cross-flow, and advanced multipass configurations, each with distinct temperature profiles and heat transfer efficiencies.

- **Counter-Flow**: In this arrangement, the fluids flow in opposite directions, allowing for a more uniform temperature gradient and more efficient heat transfer, as shown on the left side of Figure 2.1. This configuration achieves higher heat transfer rates with a smaller area, mitigating issues like decreasing temperature differences towards the outlet that are common in parallel arrangements.

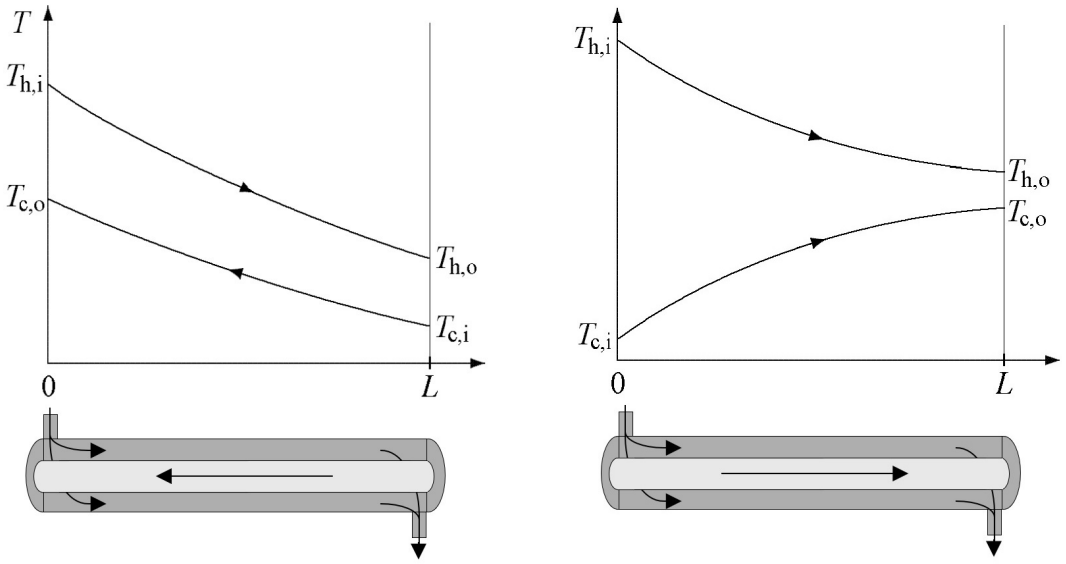

Figure 2.1: Temperature profiles and flow direction in a heat exchanger configured in counter-flow (left) and parallel-flow (right) configurations.

- **Parallel-Flow**: While sometimes less efficient in terms of heat transfer area, parallel-flow offers benefits such as more uniform heat transfer surface temperatures, as illustrated on the right side of Figure 2.1. This is crucial when dealing with high-temperature fluids, as it allows for the use of less expensive materials due to lower maximum surface temperatures. Additionally, the higher minimum temperature in a parallel-flow setup can prevent undesirable conditions such as fluid freezing or acid condensation, depending on the fluid characteristics.

- **Cross-Flow**: In cross-flow arrangements, where fluids move perpendicularly to each other, efficiency varies based on whether the flows are mixed or unmixed. Mixed flows allow free movement in the transverse direction, while unmixed flows are channeled by the heat exchanger design to prevent such movement. While cross-flow does not generally match the efficiency of counter-flow, it is often simpler to design, especially when considering header and distribution challenges.

- **Advanced Multipass Configurations**: To optimize heat exchangers, engineers often use multipass arrangements where fluids circulate through the exchanger more than once. True multipass heat exchangers enhance thermal performance through complex flow dynamics that cannot be simplified into a single pass without a complete redesign. These configurations significantly impact the overall heat transfer efficiency by exposing the fluid to different temperatures at each pass. This approach is particularly beneficial when high heat transfer rates are required without a proportional increase in the heat transfer area. Multipass designs can convert a basic flow arrangement into a more effective configuration, combining efficient heat transfer with simpler header configurations. This balance between efficiency and practical design considerations makes multipass configurations a valuable option for complex heat exchanger requirements.

2.1.2 Heat Exchanger Constructions

Heat exchangers are essential in various engineering applications, each designed to meet specific operational and efficiency requirements. The construction type of a heat exchanger significantly impacts its thermal performance, maintenance needs, and operational lifespan. Here, we explore the common constructions used in the industry:

The physical construction of a heat exchanger not only determines its suitability for particular applications but also influences its thermal efficiency, ease of maintenance, and operational durability. Each type has unique characteristics that make it ideal for certain applications over others, influenced by factors such as fluid properties, temperature ranges, pressure levels, and spatial constraints.

- **Double-Pipe Heat Exchangers**: These consist of two concentric pipes that allow two fluids to exchange heat efficiently. The simplicity of this design enables effective heat transfer in scenarios where space is limited, making it suitable for smaller-scale applications.
- **Shell-and-Tube Heat Exchangers**: These are among the most prevalent types, particularly favored in process and petrochemical industries due to their robustness and versatility. The basic structure includes a shell and a tube bundle, with various configurations to enhance efficiency.
- **Plate Heat Exchangers (PHEs)**: These are constructed from a series of thin, rectangular metal plates arranged in a stack, facilitating efficient heat transfer. They are compact, lightweight, and cost-effective, making them a preferred choice for specific heat duty requirements.
- **Spiral Heat Exchangers**: These utilize a distinctive configuration involving two metal sheets rolled into a spiral form, allowing for efficient heat transfer and inherent self-cleaning capabilities.
- **Compact Heat Exchangers**: Characterized by their high surface area-to-volume ratio, these exchangers are crucial for handling fluids like gases, where the heat transfer coefficient is lower compared to liquids. They come in various designs, often utilizing tube-fin systems or plate-type configurations.

The design of a heat exchanger is critically linked to its effectiveness in transferring heat between fluids while minimizing energy loss. Factors such as ease of cleaning, the ability to handle high pressures and temperatures, and the efficiency of heat transfer are critical considerations that influence the choice of construction type. From the robustness of shell and tube designs to the high efficiency of compact heat exchangers, the diversity in construction types showcases the adaptability of heat exchangers to various technological and environmental demands.

In the context of gas turbine combustors, the choice of heat exchanger construction becomes particularly critical due to the extreme operating conditions encountered. Shell-and-tube and compact heat exchangers are frequently employed in gas turbines because of their ability to withstand high temperatures and pressures while maintaining efficient heat transfer rates. The robust design of shell-and-tube exchangers ensures durability under the cyclic thermal loads typical of turbine operation, while their flexibility in configuration allows for optimized heat recovery processes, such as in regenerators or intercoolers.

Compact heat exchangers, with their high surface area-to-volume ratios, are also highly valued in gas turbines, especially in applications where space is at a premium. Their ability to handle gaseous fluids efficiently makes them ideal for preheating air or fuel, thereby enhancing the overall thermal efficiency of the turbine. The integration of such heat exchangers into gas turbines not only helps in improving fuel combustion but also plays a vital role in reducing emissions and increasing the operational lifespan of critical turbine components by managing thermal stresses more effectively.

Understanding the fundamental design principles behind each type provides valuable insights into their selection and implementation in systems ranging from simple residential heating to complex chemical processing.

2.1.3 Heat Exchangers in Gas Turbine Combustors

Heat exchangers in gas turbine combustors operate under extreme conditions, handling higher temperatures and pressures. These specialized devices are compact and integrated directly into the turbine's structure, using advanced materials and design features to withstand thermal stress and corrosion. Unlike conventional bulkier heat exchangers, they employ mechanisms like finned surfaces and microchannels to maximize efficiency.

One primary function of these heat exchangers is to preheat the combustion air, enhancing fuel combustion efficiency and reducing harmful emissions. This preheating allows for higher combustor temperatures, improving the turbine's thermal efficiency. By raising the temperature of the incoming air, these heat exchangers ensure more efficient fuel combustion, leading to better fuel economy and more complete combustion.

Additionally, heat exchangers manage thermal loads on critical components within the combustor. The high temperatures in a gas turbine can cause significant thermal stress and potential damage to components such as turbine blades and nozzles. By removing excess heat, heat exchangers prolong the operational life and maintain the structural integrity of the combustor, crucial for the durability and reliability of the turbine.

Heat exchangers also recover waste heat from the exhaust gases, which can be redirected to preheat the incoming air or fuel, further boosting the turbine's efficiency. Integrating these advanced heat transfer mechanisms and materials ensures that gas turbine combustor heat exchangers play a vital role in optimizing performance and longevity, enabling efficient and reliable operation in harsh conditions.

Effective thermal management in gas turbines is essential for enhancing efficiency, reducing fuel consumption, and minimizing emissions. Heat exchangers improve heat transfer efficiency by preheating the air-fuel mixture using recovered exhaust heat, significantly boosting overall thermal efficiency. Ghazvini and Narayanan (2011) highlighted that preheating the reactant gases improves combustion efficiency and reduces emissions, making recuperators essential for efficient thermal management in gas turbines [1].

Operationally, heat exchangers enhance fuel efficiency, stabilize combustion processes, extend the lifespan of turbine components, and reduce emissions. By preheating the air entering the combustion chamber, they extract more energy from the fuel, leading to lower operational costs and enhanced performance. McDonald (1989) emphasized that the use of recuperators in gas turbines can lead to substantial improvements in thermal efficiency, translating into better fuel economy and reduced operational expenses [2].

Heat exchangers also contribute to the stabilization of combustion processes by maintaining stable temperature profiles, reducing oscillations, and preventing pulsations. Zhao et al. (2019) found that heat exchangers play a vital role in stabilizing combustion processes and mitigating pulsation effects [3].

Moreover, heat exchangers help extend the operational lifespan of turbine components by managing the temperature distribution within the combustor, reducing thermal stresses that can lead to mechanical wear and fatigue. Moskowitz et al. (1983) discussed how controlling temperature gradients within the combustor helps mitigate thermal stresses, thereby extending the life of critical turbine components [4].

Advanced heat exchanger designs, such as ceramic heat exchangers, enable gas turbines to operate at higher efficiencies and with greater reliability due to their superior thermal and mechanical properties. Smyth (1997) highlighted that ceramic heat exchangers, due to their superior thermal and mechanical properties, enable gas turbines to operate at higher efficiencies and with greater reliability [5].

Heat exchangers also play a crucial role in reducing emissions by facilitating stable combustion with leaner mixtures, thus lowering the emissions of NOx and other pollutants. Ganji et al. (1976) showed that heat recirculation through heat exchangers allows for complete combustion with leaner fuel mixtures, thus reducing harmful emissions [6]. In micro-gas turbines, recuperative heat exchangers recover exhaust heat, preheating the air before it enters the combustor, leading to higher efficiency and reduced environmental impact. Cao and Xu (2007) discussed the benefits of using recuperative heat exchangers in micro-gas turbines, highlighting their role in improving efficiency and reducing emissions [7].

The versatility of heat exchangers allows them to be used in various applications, including power generation, industrial processes, and cogeneration systems. Marksberry and Lindahl (1980) emphasized that heat exchangers facilitate the efficient use of fuel and heat energy across different sectors, making them a versatile and essential component in modern energy systems [8].

In conclusion, the operational benefits of heat exchangers in gas turbine combustors are extensive. They enhance fuel efficiency, stabilize combustion processes, extend the lifespan of turbine components, reduce emissions, and offer versatility in various applications. The continued development and integration of advanced heat exchanger designs will further enhance the performance, efficiency, and sustainability of gas turbine systems, making them indispensable in modern energy technology.

2.2 Theoretical Foundations of Heat Exchanger Operation

2.2.1 Heat Transfer Mechanisms

Heat transfer is a fundamental process in the operation of heat exchangers and is essential for the efficient exchange of thermal energy between different fluids. The mechanisms of heat transfer can be broadly classified into three categories: conduction, convection, and radiation. Each of these mechanisms plays a crucial role in determining the thermal performance of a heat exchanger and is influenced by various factors, including fluid properties, flow arrangements, and temperature gradients. Understanding these mechanisms is pivotal for the design, analysis, and optimization of heat exchangers, particularly in ensuring that they meet the thermal demands of industrial applications while maintaining efficiency and reliability.

2.2.1.1 Conduction

Conduction is the process by which heat energy is transferred through a solid or between two solids in direct contact. This mode of heat transfer is driven by a temperature gradient, where heat flows from the region of higher temperature to the region of lower temperature. The rate of heat transfer by conduction is governed by Fourier's law, which in its general form is given by:

$$q = -k\nabla T \tag{2.1}$$

where q is the heat flux (W/m^2), k is the thermal conductivity of the material (W/m·K), and ∇T is the temperature gradient (K/m). The thermal conductivity k is a material-specific property that measures the material's ability to conduct heat. For instance, metals like copper and aluminum have high thermal conductivities, making them suitable for use in heat exchanger construction where efficient heat transfer is required.

In the context of heat exchangers, conduction primarily occurs through the walls of the heat exchanger, where heat is transferred from the hot fluid on one side to the cold fluid on the other. The effectiveness of this process depends on the thermal conductivity of the material

used in the heat exchanger construction and the thickness of the walls. For a plane wall, the heat transfer rate can be expressed as:

$$Q = \frac{kA(T_1 - T_2)}{L} \tag{2.2}$$

where A is the area normal to the heat flow (m^2), T_1 and T_2 are the temperatures on either side of the wall (K), and L is the thickness of the wall (m). In practical applications, multiple layers of materials may be involved, leading to a thermal resistance network where the total thermal resistance is the sum of individual resistances.

2.2.1.2 Convection

Convection is the process of heat transfer between a solid surface and a fluid (liquid or gas) in motion, or within the fluid itself due to the fluid's bulk movement. Convection can be further categorized into natural convection, where fluid motion is induced by buoyancy forces due to density differences, and forced convection, where fluid motion is driven by external means such as pumps or fans. The heat transfer rate in convection is described by Newton's law of cooling:

$$Q = hA(T_s - T_\infty) \tag{2.3}$$

where Q is the heat transfer rate (W), h is the convective heat transfer coefficient ($W/m^2 \cdot K$), A is the surface area (m^2), T_s is the surface temperature (K), and T_∞ is the temperature of the fluid far from the surface (K).

The convective heat transfer coefficient h is a critical parameter that depends on several factors, including the nature of the fluid, the flow velocity, the surface geometry, and the type of flow (laminar or turbulent). In forced convection, h tends to be higher due to the increased fluid velocity, which enhances the mixing and reduces the thermal boundary layer thickness.

In heat exchangers, convection occurs on both the shell side and the tube side, with the rate of heat transfer being influenced by factors such as fluid velocity, fluid properties, and surface roughness. The design of the heat exchanger aims to optimize these conditions to maximize the convective heat transfer coefficient and thus the overall heat transfer rate.

2.2.1.3 Radiation

Radiation is the transfer of heat energy through electromagnetic waves, primarily in the infrared spectrum. Unlike conduction and convection, radiation does not require a medium and can occur across a vacuum. The heat transfer rate by radiation is governed by the Stefan-

Boltzmann law:

$$Q = \varepsilon \sigma A (T_s^4 - T_\infty^4) \tag{2.4}$$

where Q is the radiative heat transfer rate (W), ε is the emissivity of the surface (dimensionless), σ is the Stefan-Boltzmann constant (5.67×10^{-8} W/m^2·K^4), A is the surface area (m^2), T_s is the surface temperature (K), and T_∞ is the temperature of the surroundings (K).

Radiation is particularly significant in high-temperature heat exchangers where surface temperatures are elevated, and it can be a substantial mode of heat transfer in addition to conduction and convection. The emissivity ε is a measure of a material's ability to emit thermal radiation compared to an ideal blackbody, which has an emissivity of 1. Materials with high emissivity, such as non-metallic surfaces, are more effective at radiating heat. In practical applications, radiation often occurs in tandem with convection, particularly in environments where temperature gradients are steep and where reflective or absorptive coatings on heat exchanger surfaces are used to manage radiative heat transfer.

In summary, the heat transfer mechanisms of conduction, convection, and radiation each play vital roles in the operation of heat exchangers. The interplay between these mechanisms, along with material properties, flow conditions, and temperature gradients, defines the overall thermal performance of the exchanger. Understanding and optimizing these mechanisms are essential for achieving efficient and reliable heat exchanger designs, particularly in demanding industrial applications where thermal management is critical.

2.2.2 Governing Equations

The operation of heat exchangers is fundamentally governed by a set of mathematical principles rooted in thermodynamics and fluid dynamics. These principles include energy balance equations, continuity equations, and the application of dimensionless numbers. Understanding these mathematical foundations is essential for the design, analysis, and optimization of heat exchangers, as they provide the framework for predicting the performance and efficiency of these devices under various operating conditions.

2.2.2.1 Energy Balance Equations

The energy balance equation, derived from the first law of thermodynamics, is fundamental to the analysis of heat exchangers. This principle asserts that the energy within a closed system must be conserved. In the context of heat exchangers, this law manifests as the requirement that the rate of heat transfer from the hot fluid must equal the rate of heat gain by the cold fluid, assuming no heat losses to the surroundings.

General Energy Balance in Heat Exchangers In a typical heat exchanger, where two fluids are separated by a solid boundary and do not mix, the energy balance can be represented as:

$$Q = \dot{m}_h c_{p,h}(T_{h,i} - T_{h,o}) = \dot{m}_c c_{p,c}(T_{c,o} - T_{c,i}) \tag{2.5}$$

where:

- Q is the heat transfer rate (W),
- $\dot{m}_h$ and $\dot{m}_c$ are the mass flow rates of the hot and cold fluids, respectively (kg/s),
- $c_{p,h}$ and $c_{p,c}$ are the specific heat capacities at constant pressure for the hot and cold fluids, respectively (J/kg·K),
- $T_{h,i}$ and $T_{h,o}$ are the inlet and outlet temperatures of the hot fluid (K),
- $T_{c,i}$ and $T_{c,o}$ are the inlet and outlet temperatures of the cold fluid (K).

This equation highlights the conservation of energy across the heat exchanger and is applicable to both steady-state and transient conditions, though it is most commonly applied in steady-state analyses. In cases where heat losses to the environment are negligible, the heat lost by the hot fluid equals the heat gained by the cold fluid.

Energy Balance in Counterflow Heat Exchanger In a counterflow heat exchanger, the fluids move in opposite directions, which maximizes the temperature difference between the fluids at any point along the length of the heat exchanger. The energy balance in a counterflow heat exchanger can be expressed by integrating the local energy balance along the flow direction:

$$\frac{dT_h}{dx} = -\frac{UPe}{\dot{m}_h c_{p,h}}(T_h - T_c) \tag{2.6}$$

$$\frac{dT_c}{dx} = \frac{UPe}{\dot{m}_c c_{p,c}}(T_h - T_c) \tag{2.7}$$

where:

- U is the overall heat transfer coefficient (W/m^2·K),
- Pe is the perimeter of the heat exchanger surface through which heat is transferred (m),

- x is the coordinate along the length of the heat exchanger (m),
- T_h and T_c are the local temperatures of the hot and cold fluids, respectively (K).

These differential equations are solved simultaneously to determine the temperature profiles of the fluids along the heat exchanger. The outlet temperatures $T_{h,out}$ and $T_{c,out}$ are then used to calculate the overall rate of heat transfer using the energy balance equation.

Energy Balance in Parallel Flow Heat Exchanger In a parallel flow heat exchanger, both fluids move in the same direction. The energy balance in a parallel flow configuration can similarly be described by differential equations, but the temperature difference between the fluids decreases along the flow direction:

$$\frac{dT_h}{dx} = -\frac{UPe}{\dot{m}_h c_{p,h}}(T_h - T_c) \tag{2.8}$$

$$\frac{dT_c}{dx} = \frac{UPe}{\dot{m}_c c_{p,c}}(T_h - T_c) \tag{2.9}$$

However, in parallel-flow heat exchangers, the maximum possible outlet temperature for the cold fluid is lower than that achievable in counterflow exchangers, making them less efficient in terms of heat transfer.

Differential Energy Balance In cases where the temperature varies significantly along the length of the heat exchanger, a differential form of the energy balance is often employed. For a small differential element of the heat exchanger, the heat transferred can be expressed as:

$$dQ = UP(T_h - T_c)dx \tag{2.10}$$

Integrating this equation along the length of the heat exchanger provides the total heat transfer rate:

$$Q = \int_0^L UP(T_h(x) - T_c(x))dx \tag{2.11}$$

where L is the length of the heat exchanger. This approach is particularly useful in analyzing heat exchangers with varying cross-sectional areas or non-uniform temperature profiles.

Energy Balance with Phase Change When one of the fluids undergoes a phase change (e.g., condensation or evaporation), the energy balance equation must account for the latent heat of the phase change. The rate of heat transfer associated with the phase change is given by:

$$Q = \dot{m} h_{fg} \tag{2.12}$$

where h_{fg} is the latent heat of vaporization or condensation (J/kg). In such cases, the energy balance equation is modified to include both sensible and latent heat components:

$$Q = \dot{m}_h (c_{p,h}(T_{h,i} - T_{h,o}) + h_{fg}) \tag{2.13}$$

This equation is essential for designing heat exchangers used in processes such as refrigeration, air conditioning, and power generation, where phase changes are common.

2.2.2.2 Continuity Equations

The continuity equation is another fundamental principle that applies to heat exchangers, ensuring the conservation of mass within the system. For incompressible fluids, the mass flow rate must remain constant across any cross-section of the heat exchanger. The general form of the continuity equation is given by:

$$\dot{m} = \rho A v = \text{constant} \tag{2.14}$$

where:

- $\dot{m}$ is the mass flow rate (kg/s),
- ρ is the fluid density (kg/m^3),
- A is the cross-sectional area of the flow (m^2),
- v is the fluid velocity (m/s).

In the context of heat exchangers, the continuity equation implies that any change in the cross-sectional area along the flow path must be accompanied by a corresponding change in fluid velocity to maintain a constant mass flow rate. This relationship is crucial for analyzing the pressure drop across the heat exchanger and for determining the velocity profiles, which in turn affect the heat transfer coefficients.

The continuity equation is also instrumental in the design of heat exchanger components such as tubes, plates, and fins, where the flow area may vary to optimize heat transfer performance. In multipass heat exchangers, the continuity equation must be satisfied across each pass, ensuring that the mass flow rate is appropriately divided among the parallel flow paths.

2.2.2.3 Dimensionless Numbers

Dimensionless numbers are pivotal in the analysis and design of heat exchangers as they encapsulate the complex interrelationships between various physical quantities into simpler forms. The most commonly used dimensionless numbers in heat exchanger analysis are the Reynolds number, Prandtl number, and Nusselt number.

Reynolds Number (Re) The Reynolds number is a dimensionless quantity that characterizes the flow regime within the heat exchanger, indicating whether the flow is laminar or turbulent. It is defined as:

$$Re = \frac{\rho v D_h}{\mu} = \frac{v D_h}{\nu} \tag{2.15}$$

where:

- ρ is the fluid density (kg/m^3),
- v is the fluid velocity (m/s),
- D_h is the hydraulic diameter of the flow channel (m),
- μ is the dynamic viscosity of the fluid (Pa·s),
- ν is the kinematic viscosity of the fluid (m^2/s).

The Reynolds number is crucial for determining the flow regime, which directly influences the heat transfer coefficient. For $Re < 2300$, the flow is typically laminar, while $Re > 4000$ indicates turbulent flow. In the turbulent regime, the heat transfer coefficient increases due to enhanced mixing, which promotes better thermal contact between the fluid and the heat exchanger surfaces.

Prandtl Number (Pr) The Prandtl number is a dimensionless number that relates the momentum diffusivity (viscosity) to the thermal diffusivity of the fluid. It is defined as:

$$Pr = \frac{\mu c_p}{k} = \frac{\nu}{\alpha} \tag{2.16}$$

where:

- μ is the dynamic viscosity of the fluid (Pa·s),
- c_p is the specific heat capacity at constant pressure (J/kg·K),
- k is the thermal conductivity of the fluid (W/m·K),
- α is the thermal diffusivity of the fluid (m^2/s).

The Prandtl number indicates the relative thickness of the momentum and thermal boundary layers. For fluids with a high Prandtl number, the thermal boundary layer is thinner than the velocity boundary layer, leading to higher heat transfer rates. In heat exchanger design, the Prandtl number is used in conjunction with the Reynolds number to determine the convective heat transfer coefficient through empirical correlations.

Nusselt Number (Nu) The Nusselt number is a dimensionless number that represents the ratio of convective to conductive heat transfer across the boundary layer. It is defined as:

$$Nu = \frac{hD_h}{k} \tag{2.17}$$

where:

- h is the convective heat transfer coefficient ($W/m^2 \cdot K$),
- D_h is the hydraulic diameter (m),
- k is the thermal conductivity of the fluid (W/m·K).

The Nusselt number provides a measure of the enhancement of heat transfer through convection relative to pure conduction. A higher Nusselt number indicates more efficient convective heat transfer. In heat exchanger design, the Nusselt number is typically determined from empirical correlations based on the Reynolds and Prandtl numbers, which are specific to the flow geometry and conditions.

These dimensionless numbers are integral to the design and analysis of heat exchangers, as they simplify the complex interactions between fluid dynamics and heat transfer into more manageable forms. By utilizing these numbers, engineers can predict heat transfer coefficients, pressure drops, and overall heat exchanger performance under various operating conditions.

In conclusion, the mathematical foundations of heat exchanger behavior are built upon the principles of energy conservation, mass conservation, and the use of dimensionless numbers to characterize fluid flow and heat transfer. Understanding these principles is essential for the effective design, optimization, and operation of heat exchangers in a wide range of industrial applications.

2.2.3 Heat Exchanger Performance Key Metrics

In the design and analysis of heat exchangers, several key metrics are used to assess the thermal performance, efficiency, and operational viability of these devices. These metrics are not only crucial for ensuring that the heat exchanger meets the desired thermal and mechanical requirements but also for optimizing the design to achieve better energy efficiency and cost-effectiveness.

2.2.3.1 Overall Heat Transfer Coefficient (U)

The overall heat transfer coefficient U is a crucial metric in evaluating the performance of a heat exchanger. It represents the ability of the heat exchanger to transfer heat across the entire surface area, accounting for all modes of heat transfer (conduction, convection, and potentially radiation) and any thermal resistances present in the system.

For a heat exchanger with fins or multiple surface types, the overall heat transfer coefficient U can be defined using the total heat transfer surface area A_{tot} and the total thermal resistance R_{tot}. The relationship is expressed as:

$$U = \frac{1}{A \cdot R_{\text{tot}}} \tag{2.18}$$

where:

- A is the heat transfer area of the exchanger.
- R_{tot} is the total thermal resistance, which may include resistances due to conduction, convection, and fouling on both the hot and cold sides.

This generalized form provides a flexible approach to calculating U, making it applicable to various heat exchanger designs, including those with complex geometries or enhanced surfaces such as fins.

In cases where the thermal contact resistance between different surface types (e.g., finned and plain) can be neglected, the overall thermal resistance R_{tot} simplifies to the sum of individual resistances. However, in more complex designs, these interactions must be carefully accounted for to ensure accurate determination of U.

2.2.3.2 Heat Capacity Rates and Their Ratios

The heat capacity rate (C) of a fluid in a heat exchanger is defined as:

$$C = \dot{m} c_p \tag{2.19}$$

where $\dot{m}$ is the mass flow rate of the fluid and c_p is its specific heat capacity at constant pressure. The minimum ($C_{\min}$) and maximum ($C_{\max}$) heat capacity rates are vital in determining the heat exchanger's performance. $C_{\min}$ limits the maximum possible heat transfer, while the heat capacity rate ratio (C_r) indicates the balance between the two fluids:

$$C_r = \frac{C_{\min}}{C_{\max}} \tag{2.20}$$

In cases where one fluid undergoes a phase change, C_r approaches zero, and the heat exchanger's effectiveness primarily depends on the characteristics of the fluid undergoing the phase change.

2.2.3.3 Log Mean Temperature Difference (LMTD)

The Log Mean Temperature Difference (LMTD) is a crucial concept in heat exchanger design, representing the average temperature difference between the hot and cold fluids across the heat exchanger. The LMTD accounts for the varying temperature differences along the length of the heat exchanger, making it a more accurate representation than a simple arithmetic mean.

The LMTD is calculated using the temperature differences at the two ends of the heat exchanger, denoted as ΔT_1 and ΔT_2. The general formula for LMTD is:

$$\Delta T_{\text{lm}} = \frac{\Delta T_2 - \Delta T_1}{\ln\left(\frac{\Delta T_2}{\Delta T_1}\right)} \tag{2.21}$$

As illustrated in Figure 2.2, the values of ΔT_1 and ΔT_2 differ depending on the flow arrangement:

Counterflow Arrangement: For a counterflow heat exchanger, where the hot and cold fluids flow in opposite directions, the temperature differences are defined as:

$$\Delta T_1 = (T_{h,i} - T_{c,o}) \quad \text{and} \quad \Delta T_2 = (T_{h,o} - T_{c,i}), \tag{2.22}$$

where $T_{\text{h,i}}$ and $T_{\text{h,o}}$ are the inlet and outlet temperatures of the hot fluid, respectively, and $T_{\text{c,i}}$

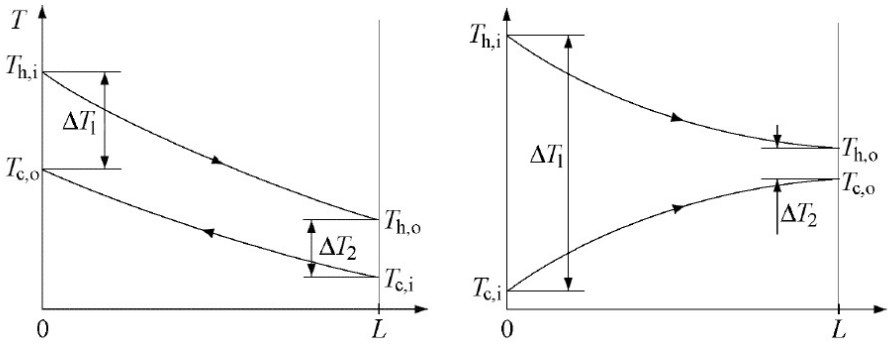

Figure 2.2: Temperature differences ΔT_1 and ΔT_2 in counterflow (left) and parallel-flow (right) configurations.

and $T_{\mathrm{c,o}}$ are the inlet and outlet temperatures of the cold fluid, respectively.

Parallelflow Arrangement: For a parallel-flow heat exchanger, where the hot and cold fluids flow in the same direction, the temperature differences are given by:

$$\Delta T_1 = (T_{h,i} - T_{c,i}) \quad \text{and} \quad \Delta T_2 = (T_{h,o} - T_{c,o}), \tag{2.23}$$

where $T_{\mathrm{h,i}}$ and $T_{\mathrm{h,o}}$ are the inlet and outlet temperatures of the hot fluid, respectively, and $T_{\mathrm{c,i}}$ and $T_{\mathrm{c,o}}$ are the inlet and outlet temperatures of the cold fluid, respectively.

Application of LMTD: The LMTD is then used to determine the heat transfer rate Q in a heat exchanger, given by:

$$Q = UA\Delta T_{\mathrm{lm}}, \tag{2.24}$$

where:

- U is the overall heat transfer coefficient,
- A is the heat transfer surface area,
- ΔT_{lm} is the log mean temperature difference.

This method is particularly useful for designing heat exchangers where the temperatures of the fluids vary significantly from one end of the exchanger to the other. The LMTD method provides a more accurate and practical approach for calculating the temperature differences in such cases.

2.2.3.4 Number of Transfer Units (NTU)

The Number of Transfer Units (NTU) is a dimensionless parameter that quantifies the thermal size of a heat exchanger relative to the minimum heat capacity rate. It is defined as:

$$\text{NTU} = \frac{UA}{C_{\min}} \tag{2.25}$$

where U represents the overall heat transfer coefficient, A is the total heat transfer area, and $C_{\min}$ is the minimum heat capacity rate of the two fluids in the exchanger. The NTU is directly proportional to the heat transfer area and the overall heat transfer coefficient, making it a crucial parameter in determining the heat exchanger's effectiveness.

2.2.3.5 Effectiveness (ε)

Effectiveness (ε) is another dimensionless metric that measures how efficiently a heat exchanger transfers heat compared to the maximum possible heat transfer. It is defined as:

$$\varepsilon = \frac{q_{\text{actual}}}{q_{\max}} \tag{2.26}$$

where q_{actual} is the actual heat transfer rate, and $q_{\max}$ is the maximum possible heat transfer rate if the fluid with the minimum heat capacity rate underwent the maximum possible temperature change.

2.2.3.6 ε-NTU Method

The ε-NTU method is a powerful and widely used approach in heat exchanger analysis, especially when the outlet temperatures of the fluids are not known in advance. This method relates the effectiveness (ε) of a heat exchanger to the number of transfer units (NTU), which is a dimensionless parameter reflecting the heat exchanger's size relative to its thermal capacity.

One of the strengths of the ε-NTU method is its ability to handle different heat exchanger configurations, including counterflow, parallel flow, crossflow, and complex multipass arrangements. The relationships between ε and NTU are established for various flow configurations, providing engineers with the necessary tools to analyze and design heat exchangers based on their specific operational requirements.

For each flow configuration, the relationship between ε and NTU is determined through theoretical analysis or empirical correlations. These relationships are often presented in the form of equations or graphs, making it easier to apply the method across different heat exchanger

types and operating conditions.

For instance, in a counterflow heat exchanger, the ε-NTU relationship is typically more favorable than in a parallel flow configuration, meaning that for the same NTU, a counterflow arrangement will achieve a higher effectiveness.

For complex flow arrangements, such as crossflow heat exchangers with mixed and unmixed flows, the ε-NTU relationships become more intricate. These cases often require the use of charts or detailed equations provided in specialized literature.

In many practical applications, the ε-NTU method is preferred because it allows for direct determination of the heat exchanger's performance without needing to iterate on the outlet temperatures. Once the NTU and the heat capacity rate ratio C_r are known, the effectiveness can be easily determined, and from there, the heat transfer rate can be calculated.

The ε-NTU method is particularly advantageous in the preliminary design stages of heat exchangers, where quick assessments of different configurations are necessary. Its flexibility in accommodating various flow arrangements and operational conditions makes it a cornerstone of heat exchanger analysis and design.

In summary, the ε-NTU method provides a robust framework for analyzing and designing heat exchangers, offering clear relationships between the effectiveness and the heat exchanger's thermal characteristics across a wide range of configurations and operating conditions.

2.2.3.7 Pressure Drop (Δp)

In heat exchanger systems, fluid must be pumped through the exchanger, and the required pumping power is significantly affected by the pressure drop across the exchanger. The pressure drop Δp [Pa] and the pumping power P_{pump} [W] are related by the following equation:

$$P_{\text{pump}} = \Delta p \frac{q_m}{\rho \eta_p} \tag{2.27}$$

where ρ represents the fluid density, q_m is the mass flow rate, and η_p is the efficiency of the pump or fan. The relationship between pressure drop and pumping power highlights the trade-off inherent in heat exchanger design: higher fluid velocities through the exchanger increase the pressure drop but simultaneously improve convective heat transfer coefficients, thus enhancing the overall heat transfer performance. Consequently, designing an efficient heat exchanger necessitates a careful balance between maximizing heat transfer and maintaining an acceptable pressure drop.

When a maximum allowable pressure drop is specified, either by application requirements or by customer needs, achieving the smallest possible heat transfer area typically means maximizing the pressure drop within those constraints. In scenarios where no maximum pressure

drop is predefined, the optimal design strategy often aims to minimize the total life cycle cost, which includes both the initial investment in the heat exchanger and the ongoing operational costs associated with fluid pumping.

Pressure drop in heat exchangers can be attributed to several factors, and it is generally classified into two main categories based on its location within the system:

- **Core Pressure Drop**: This occurs within the heat exchanger core, where the fluid directly interacts with the heat transfer surfaces. The core pressure drop is closely related to the heat exchanger's design, including the type of surfaces used, the flow arrangement, and the characteristics of the fluid.
- **Entry and Exit Pressure Drops**: These are encountered at the inlet and outlet sections of the heat exchanger, including manifolds, ducts, headers, and other devices used to distribute and collect the fluid. These drops are influenced by the geometry and design of these components, as well as the flow conditions at the points of entry and exit.

A well-designed heat exchanger aims to minimize pressure drops in parts other than the core, thereby allowing maximum utilization of the allowable pressure drop for enhancing heat transfer. This is particularly challenging in plate-type heat exchangers due to their construction, where both surface friction and the geometry of the flow channels play critical roles.

The primary causes of pressure drop in heat exchangers can be categorized into the following:

1. **Flow Entry Effects**: Pressure drops caused by the acceleration of fluid and the sudden contraction of flow channels as the fluid enters the heat exchanger core. These effects are particularly pronounced in designs where the fluid must navigate narrow or abrupt channel transitions.
2. **Surface Friction**: Frictional losses occur due to the interaction between the fluid and the heat transfer surfaces. This includes both form drag, resulting from the shape and roughness of the surfaces, and frictional drag along the channel walls.
3. **Momentum Changes**: Pressure drops arise from changes in fluid density, often due to temperature variations, which in turn affect the velocity of the fluid. As the fluid undergoes heating or cooling, its density changes, leading to corresponding changes in momentum and pressure.
4. **Flow Exit Effects**: Pressure drops resulting from the deceleration of fluid and the sudden expansion of flow channels as the fluid exits the heat exchanger. These effects are exacerbated when the fluid must transition from a high-velocity core to a broader collection area.

In addition to these, the height difference between fluid entry and exit ports can contribute significantly to the total pressure drop, especially when dealing with liquid fluids. While this is influenced by how the heat exchanger is installed within the system, the fundamental approach to minimizing pressure drop remains focused on managing the core and flow-related pressure losses.

The equation for pressure drop through a heat exchanger can be further detailed by considering factors such as flow regime (laminar or turbulent), channel geometry, and fluid properties. These details are crucial for accurately predicting pressure drops and designing heat exchangers that optimize both thermal performance and fluid dynamics.

In conclusion, understanding and optimizing key performance metrics such as NTU, effectiveness, overall heat transfer coefficient, and pressure drop are essential in the design and operation of efficient heat exchangers. These metrics provide a comprehensive understanding of the heat exchanger's thermal and operational performance, ensuring that the system meets its intended objectives while maintaining energy efficiency and reliability. By carefully balancing these parameters, engineers can design heat exchangers that not only perform effectively but also operate within acceptable pressure drop limits, thereby minimizing energy consumption and operational costs.

2.3 Computational and Experimental Evaluation Techniques

Evaluating heat exchanger performance is crucial, especially in high-stakes applications like gas turbines where efficiency, reliability, and safety are paramount. Accurate evaluation is necessary to ensure that heat exchangers meet stringent operational requirements, directly impacting overall turbine efficiency, fuel consumption, and emissions.

In gas turbines, the evaluation of heat exchanger performance is vital for optimizing energy transfer and ensuring component durability. Any inefficiency can lead to significant operational and economic consequences. Computational techniques, allow for detailed modeling of thermal and fluid dynamics, predicting performance metrics with high accuracy. These predictions help identify potential issues early in the design phase.

However, computational models are based on approximations and assumptions that may not fully capture real-world conditions. Therefore, experimental validation is essential to ensure that computational predictions align with actual performance. The combination of computational and experimental methods leads to more reliable and optimized heat exchanger designs.

Historically, heat exchanger performance was assessed through experimental testing alone, which was time-consuming and costly. With the advent of computational tools, detailed modeling became possible, significantly reducing the need for physical prototypes. These tools enable engineers to explore a wider range of design variables and operating conditions.

Today, the most effective approach integrates both computational and experimental meth-

ods. Computational models predict and optimize performance, while experimental techniques validate these predictions, providing a feedback loop that enhances the accuracy and reliability of heat exchanger designs.

2.3.1 Overview of Computational Modeling Tools and Software

In the design and optimization of heat exchangers, particularly within gas turbines, computational modeling tools and software play an indispensable role. These tools facilitate the accurate simulation and analysis of complex physical phenomena, such as fluid dynamics, heat transfer, and chemical reactions, which are critical for enhancing the performance and efficiency of gas turbine systems. This section provides an overview of the key categories of computational modeling tools and software, exploring their functionalities, applications, and relevance to heat exchanger design.

2.3.1.1 Types and Most Relevant Software in Modeling Gas Turbine Heat Exchangers

In the modeling and simulation of gas turbine heat exchangers, various computational tools and software types play critical roles in optimizing design, predicting performance, and ensuring reliability under extreme operating conditions. These tools are categorized based on their primary functions and the specific aspects of heat exchanger performance they address. The most relevant types of software in this domain include:

- **Computational Fluid Dynamics (CFD) Software**: These tools are essential for simulating fluid flow, heat transfer, and related phenomena within heat exchangers, providing detailed insights into the behavior of fluids under various operating conditions.
- **Heat Transfer Analysis Software**: Focused on the accurate modeling of thermal energy exchanges, these tools ensure that heat exchangers are optimized for thermal performance and structural integrity.
- **Finite Element Analysis (FEA) Software**: FEA tools are crucial for evaluating thermal stresses within heat exchanger materials, ensuring that designs can withstand the thermal gradients encountered during operation.
- **Combustion Simulation Software**: These specialized tools model chemical kinetics and combustion processes, integral to understanding the interactions between combustion and heat exchange in gas turbines.
- **Thermodynamic Simulation Tools**: These tools simulate the thermodynamic behavior of fluids, providing accurate fluid property data essential for precise thermodynamic calculations.

- **Integrated Multiphysics Platforms**: Offering a holistic approach, these platforms integrate multiple physical phenomena, enabling comprehensive simulations that encompass fluid dynamics, heat transfer, and structural mechanics.

- **Specialized Gas Turbine Design Tools**: Tailored specifically for gas turbine components, these tools provide integrated CFD, FEA, and system modeling capabilities, ensuring comprehensive design and performance optimization.

Each of these software types contributes uniquely to the modeling and simulation of gas turbine heat exchangers, with specific examples of tools and their respective applications, advantages, and disadvantages detailed below in Tables 2.1, 2.2, and 2.3.

The integration of these diverse computational tools and software into the design and analysis of gas turbine heat exchangers has significantly advanced the field. By leveraging the strengths of each type—whether it's the detailed fluid dynamics modeling provided by CFD software, the precise thermal stress analysis of FEA tools, or the comprehensive system-level simulations enabled by multiphysics platforms—engineers can create robust, efficient, and reliable heat exchanger designs. The continued development and refinement of these tools, along with their synergistic use, will play a crucial role in meeting the evolving demands of modern gas turbine systems. This holistic approach ensures that every aspect of heat exchanger performance is optimized, from thermal efficiency to structural integrity, ultimately contributing to more efficient and sustainable energy solutions.

2.3.1.2 Advancements in Computational Tools for Gas Turbine Heat Exchangers

The computational modeling landscape for gas turbine heat exchangers has undergone significant evolution in recent years, driven by the demand for higher efficiency, reduced emissions, and enhanced system reliability. These advancements have been propelled by improvements in Computational Fluid Dynamics (CFD), the integration of multiphysics simulations, the application of High-Performance Computing (HPC), and the emerging role of data-driven modeling techniques, including artificial intelligence (AI) and machine learning (ML). This section explores these key advancements and their implications for the design and optimization of gas turbine heat exchangers.

One of the most notable advancements in computational tools for gas turbine heat exchangers is the enhancement of CFD capabilities. Traditional CFD models have been instrumental in simulating fluid dynamics and heat transfer within these systems. However, recent developments have introduced more sophisticated turbulence models, such as Large Eddy Simulation (LES) and Direct Numerical Simulation (DNS), which offer unprecedented detail in capturing the complex fluid dynamics within gas turbines. LES, for instance, resolves the large-scale turbulent structures directly, while modeling the smaller scales, providing a more accurate depiction of turbulence effects in heat exchanger applications [9]. DNS, on

Table 2.1: Types and Most Relevant Software in Modeling Gas Turbine Heat Exchangers (Part 1)

Tool/Software Type	Example	Applications	Advantages	Disadvantages
Computational Fluid Dynamics (CFD)	ANSYS Fluent/CFX	Turbulent Flow Simulation Heat Transfer Optimization Design Improvement	Advanced turbulence models Extensive material libraries Multiphysics capabilities	High computational requirements Steep learning curve
	Siemens STAR-CCM+	Multiphysics Simulation Thermal Stress Analysis Optimization of Heat Exchanger Design	Handles complex Multiphysics Advanced mesh generation	Requires significant computational resources Expensive to license
	OpenFOAM	Custom Solver Development Turbulent Flow and Heat Transfer Combustion Modeling	Extensive customization Open-source and flexible	Requires programming expertise Limited commercial support
Finite Element Analysis (FEA)	ANSYS Mechanical	Thermal-Structural Coupling Stress Analysis Material Failure Prediction	Comprehensive FEA capabilities Seamless integration with ANSYS CFD	High licensing cost Complex setup for multiphysics simulations
	Abaqus	Thermal-Structural Coupling Stress Analysis Material Failure Prediction	Advanced thermal-structural analysis capabilities	Expensive Steep learning curve

Table 2.2: Types and Most Relevant Software in Modeling Gas Turbine Heat Exchangers (Part 2)

Tool/Software Type	Example	Applications	Advantages	Disadvantages
Heat Transfer Analysis Software	COMSOL Multiphysics	Coupled Heat Transfer and Structural Analysis Thermal Stress Evaluation Design Optimization	Intuitive interface Powerful post-processing tools	Expensive Limited CFD capabilities
	ESATAN-TMS	Aerospace Thermal Analysis High-Temperature Operations Thermal Load Evaluation	Validated against real-world data Excels in high-demand environments	Niche software Expensive with specialized training requirements
	HEATRAN	Complex Geometry Analysis Thermal Efficiency Optimization Heat Load Management	Highly accurate in modeling thermal phenomena within complex geometries	Limited to heat transfer analysis Lacks multiphysics integration
Integrated Multiphysics Platforms	MATLAB /Simulink	Custom Modeling Stress Analysis System-Level Simulation Control Strategy Optimization	Powerful mathematical tools Flexible modeling environment	Not specialized for CFD or FEA Requires integration with other tools
	Modelica (e.g., Dymola)	System-Level Modeling Multiphysics Integration Control System Design	Flexible, powerful environment for system-level simulations	Steep learning curve May require coupling with other software

Table 2.3: Types and Most Relevant Software in Modeling Gas Turbine Heat Exchangers (Part 3)

Tool/Software Type	Example	Applications	Advantages	Disadvantages
Combustion Simulation Software	CHEMKIN	Chemical Kinetics Simulation Emission Reduction Fuel Efficiency Optimization	Highly accurate in modeling detailed combustion reactions	Specialized software Limited applicability outside combustion modeling
	Cantera	Combustion Process Optimization Species Distribution Thermal Efficiency Assessment	Open-source with Python integration Flexible for simulating complex chemical reactions	Requires significant expertise Customization is complex
Thermodynamic Simulation Tools	CoolProp	Thermodynamic Property Calculation Fluid Behavior Simulation Mixture Property Analysis	High accuracy in fluid property data Open-source flexibility	Limited to thermodynamic properties Learning curve for complex simulations
Specialized Gas Turbine Design Tools	AxSTREAM	Gas Turbine Component Design Performance Optimization System Integration	All-in-one solution for gas turbine design Robust support for complex turbomachinery	High cost Steep learning curve
	GasTurb	Turbine Performance Analysis Design Scenario Testing Efficiency Improvements	User-friendly Specialized for gas turbine performance analysis	Limited in scope to gas turbine performance Requires integration with other tools

the other hand, resolves all scales of turbulence, offering the highest level of detail but at a significantly higher computational cost [10].

These advanced turbulence models allow engineers to predict more accurately the behavior of fluids within heat exchangers, particularly in high-stakes environments like gas turbines, where precise temperature control and fluid flow are critical. The adoption of these models has led to improved design processes, enabling the optimization of heat exchanger geometries to enhance thermal efficiency and reduce pressure drops [11]. Despite their computational intensity, the ability of LES and DNS to simulate real-world fluid behaviors with high fidelity makes them invaluable tools in modern heat exchanger design [12].

The integration of multiphysics simulations represents another significant advancement in the field. Tools such as COMSOL Multiphysics have enabled the simultaneous simulation of multiple physical processes—fluid dynamics, heat transfer, structural mechanics, and even electromagnetic phenomena—within a single platform [13]. This holistic approach is particularly advantageous in the design of gas turbine heat exchangers, where interactions between different physical processes can significantly impact performance.

For example, in a gas turbine, the thermal expansion of materials under high temperatures can lead to mechanical stresses that may compromise the structural integrity of the heat exchanger. By using multiphysics simulations, engineers can model these interactions comprehensively, ensuring that the heat exchanger design is robust and capable of withstanding the demanding conditions of turbine operation. This integrated approach not only improves the reliability of the design but also shortens the development cycle by reducing the need for iterative physical testing [14].

High-Performance Computing (HPC) has also played a crucial role in advancing computational tools for gas turbine heat exchangers. The introduction of parallel processing and HPC clusters has drastically reduced the time required to perform complex simulations. This capability allows for more comprehensive analyses, where multiple design scenarios can be tested in a fraction of the time previously required [9].

HPC has made it feasible to employ more detailed models, such as LES and DNS, that were once considered too computationally expensive for routine use. By leveraging HPC, engineers can perform optimization studies that explore a wider range of design parameters, leading to heat exchanger designs that are not only more efficient but also more cost-effective to manufacture and operate. Moreover, HPC enables the execution of uncertainty quantification studies, where variations in operating conditions and material properties can be systematically explored to ensure that the final design is resilient to real-world variability [14].

The rise of data-driven modeling and machine learning represents a frontier in computational heat exchanger design. These techniques are increasingly being integrated into traditional modeling workflows to enhance the accuracy of simulations and predict system behavior under a variety of conditions. Machine learning algorithms can be trained on large datasets generated from simulations and experimental data to identify patterns and make predictions that might not be apparent through conventional analysis [15].

For instance, AI can be used to optimize heat exchanger designs by predicting the performance of different configurations based on historical data. This capability allows for the rapid screening of design alternatives, accelerating the design process and reducing reliance on trial-and-error methods. Additionally, machine learning models can be employed to predict the occurrence of phenomena such as fouling or material degradation, enabling the development of heat exchangers that are more durable and require less maintenance [16].

2.3.1.3 Challenges and Opportunities

While the advancements in computational tools for gas turbine heat exchangers have been significant, several challenges remain, presenting both hurdles and opportunities for future research and development.

One of the primary challenges in computational heat exchanger design is balancing the complexity of models with the need for accurate results. Advanced models, such as LES and DNS, offer detailed insights but at the cost of increased computational resources and time. Simplified models, while faster, may lack the fidelity required for high-stakes applications like gas turbines. The challenge lies in developing models that are both accurate and computationally efficient. This area represents an opportunity for innovation in algorithm development, where hybrid models that combine the strengths of both detailed and simplified approaches could emerge as a solution [17, 18].

The scalability of simulations is another challenge, particularly as designs become more complex and demand higher computational power. High computational costs can limit the ability to conduct extensive design optimization studies, especially for small and medium-sized enterprises. Addressing this challenge will require the development of more efficient algorithms and the continued advancement of HPC technologies [19]. There is also an opportunity to explore cloud-based computing solutions, which could democratize access to high-powered simulations by offering scalable resources on demand [20].

The full potential of AI and machine learning in heat exchanger modeling has yet to be realized. While these technologies offer exciting possibilities for enhancing model accuracy and predictive capabilities, their integration into established workflows is still in its infancy. Future research could focus on improving the interpretability of machine learning models and developing frameworks that seamlessly integrate AI with traditional simulation tools [21]. This represents a promising area for innovation, with the potential to revolutionize how heat exchangers are designed and optimized.

Finally, addressing uncertainties in input data and operating conditions is crucial for designing resilient heat exchangers. Uncertainty quantification methods, coupled with robust design techniques, can help ensure that heat exchangers perform reliably under a wide range of conditions. This challenge offers an opportunity to develop new methodologies that incorporate uncertainty analysis into the early stages of design, leading to more resilient and reliable heat exchangers for gas turbines [22].

In conclusion, the advancements in computational tools for gas turbine heat exchangers have significantly enhanced our ability to design more efficient, reliable, and environmentally friendly systems. However, challenges remain, and addressing them will require continued innovation and collaboration across disciplines.

2.3.2 Experimental Validation and Synergistic Techniques

2.3.2.1 Importance of Experimental Validation

In high-risk engineering applications like gas turbines, the accuracy of computational models is critical. While computational simulations provide valuable insights into the thermal and fluid dynamics of heat exchangers, their reliability must be verified with empirical data. This is where experimental validation becomes essential. It serves as a crucial checkpoint, ensuring that the assumptions, boundary conditions, and numerical methods used in simulations accurately reflect real-world behavior. Without this validation, even the most sophisticated models could lead to errors that jeopardize the safety, efficiency, and performance of gas turbine systems.

In gas turbines, where operating conditions involve extreme temperatures and pressures, any discrepancy between simulated and actual performance can result in catastrophic failures. Therefore, validating computational models against experimental data is not just beneficial but necessary. It allows engineers to confirm that their models can predict the behavior of heat exchangers under the most demanding conditions, providing a solid foundation for further design optimization and operational decision-making.

Several experimental techniques are particularly valuable in validating the performance of heat exchangers:

- **Thermocouple Arrays:** These are used to measure temperature distributions within heat exchangers. Thermocouples provide precise temperature data at various points within the system, helping validate the thermal models developed through computational simulations.

- **Flow Visualization Techniques:** Methods such as Particle Image Velocimetry (PIV) and Laser Doppler Anemometry (LDA) are used to analyze flow patterns within the heat exchanger. These techniques help in validating fluid dynamics simulations by providing detailed insights into the actual flow behavior, which can be compared against the computational predictions.

- **Heat Flux Sensors:** These sensors measure the local heat transfer rates within the heat exchanger. The data gathered from heat flux sensors is crucial for refining the thermal models and improving the accuracy of computational simulations regarding heat transfer processes.

2.3.2.2 Integration of Computational and Experimental Techniques

Feedback Loop The integration of computational and experimental techniques creates a robust feedback loop that enhances the accuracy and reliability of heat exchanger designs. Experimental data obtained from thermocouples, flow visualization tools, and heat flux sensors are fed back into the computational models. This iterative process allows engineers to adjust the models, fine-tuning parameters such as boundary conditions, turbulence models, and material properties until the simulation results align closely with the experimental observations. This continuous refinement process not only improves the predictive capability of the models but also builds confidence in their use for design and operational purposes.

Future Directions Looking ahead, the integration of computational and experimental techniques is expected to evolve significantly with advancements in technology. Real-time data integration, where experimental measurements are continuously fed into the computational models during operation, is one promising direction. This approach would enable adaptive simulations that adjust to changing operating conditions, providing real-time insights and predictions. Additionally, the development of digital twins—virtual replicas of physical systems that are updated in real-time with data from their physical counterparts—holds great potential for enhancing the predictive accuracy of heat exchanger models. These digital twins could be used for predictive maintenance, optimizing operational parameters, and extending the life of gas turbine components. As these technologies mature, they will likely lead to even closer integration of computational and experimental techniques, further improving the design, performance, and reliability of heat exchangers in gas turbines.

Chapter 3

Methodology

The computational process for this analysis is structured in several key stages. First, the input data required for both the hot and cold fluid streams is loaded from a configuration file. This data includes details on the mass flow rates, pressures, temperatures, and geometric properties of the heat exchanger components. Following this, the model sequentially calculates the thermodynamic and transport properties of the hot and cold fluids, which are essential for determining the heat transfer characteristics. The computed properties serve as the foundation for further steps, where the heat exchanger's performance is evaluated, focusing on the heat transfer rate, effectiveness, and pressure drops. Once all calculations are complete, the results are compiled and saved in a structured output format, typically a JSON file, facilitating easy analysis and further validation.

The overall flow of the computational method is illustrated in Figure 3.1. This flowchart provides a high-level overview of the process, highlighting the sequence of tasks involved, from reading input data to calculating fluid properties, and finally evaluating the performance metrics of the heat exchanger. Each step is designed to ensure accuracy in the prediction of critical parameters like the convective heat transfer coefficient, effectiveness, and the Number of Transfer Units (NTU). The inclusion of multiple nodes in the model allows for detailed assessments at different points along the heat exchanger, capturing the variability in fluid properties and heat transfer rates.

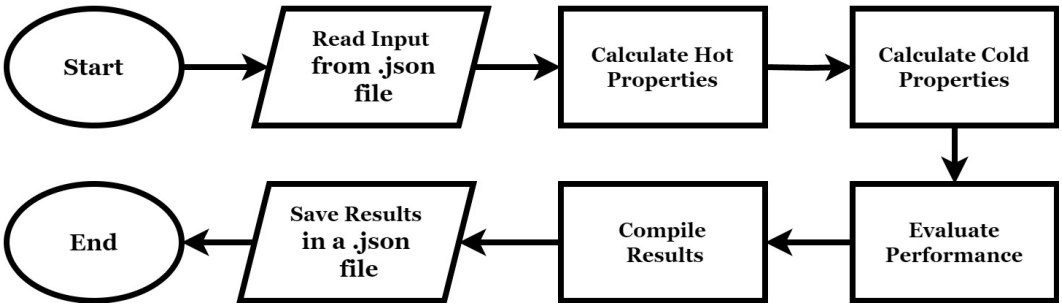

Figure 3.1: High-Level Flowchart of the Computational Process for Heat Exchanger Analysis

In this analysis, the wall separating the hot fluid in the combustion chamber from the cold fluid in the cooling channels is assumed to be adiabatic. This assumption implies that the wall does not participate in heat transfer, and therefore, the thermal resistance of the wall R_w is considered negligible. The focus is instead placed on the thermal resistances of the hot fluid R_h and the cold fluid R_c, which govern the heat transfer process between the two fluids.

Figure 3.2 provides a schematic representation of the heat exchanger system. The combustion chamber, representing the hot fluid side, transfers heat directly to the cooling channels

on the cold fluid side, with no significant heat loss through the wall. The temperatures of the hot fluid (T_h) and the cold fluid (T_c), along with their respective thermal resistances (R_h and R_c), determine the effectiveness of the heat exchange process.

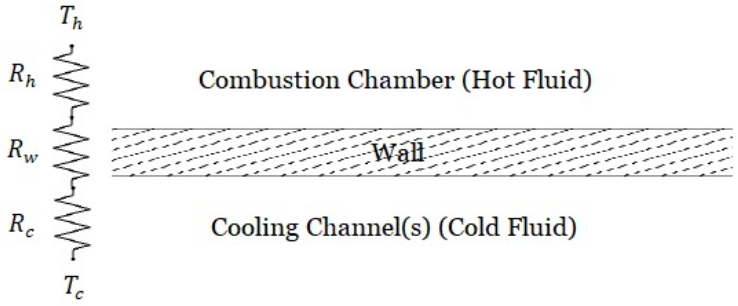

Figure 3.2: Schematic of Heat Exchanger System

3.1 Hot Fluid (Combustion Chamber)

The combustion chamber is a critical component in a gas turbine system, serving as the primary source of thermal energy. In the context of the heat exchanger system, it functions as the hot fluid side, where high-temperature gases generated by the combustion of fuel are directed toward the turbine. These gases transfer heat to the walls of the combustion chamber, which is subsequently absorbed by the cooling channels. This process is vital for maintaining the operational efficiency and structural integrity of the turbine by managing the extreme temperatures encountered during combustion.

This section of the thesis focuses on the computational analysis of the combustion chamber as the hot fluid side of the heat exchanger system. The analysis accounts for both scenarios where a single stagnation temperature is provided as input and where a temperature distribution across multiple nodes is considered. This dual approach enhances the versatility of the computational tool, allowing it to adapt to different levels of data availability and varying complexity of the input conditions. To accurately simulate the properties of the combustion gases, the model integrates Cantera, a powerful tool for calculating thermodynamic and transport properties based on the chemical composition and state of the gas mixture. Additionally, several assumptions are made throughout the analysis to simplify the model while focusing on the key aspects of heat transfer and fluid dynamics. These assumptions and the use of Cantera are crucial for ensuring that the model provides reliable predictions of the combustion chamber's performance under various operating conditions.

3.1.1 Assumptions

In the computational analysis of the hot fluid side within the combustion chamber, several key assumptions are made to simplify the model while maintaining the focus on the critical aspects of heat transfer and fluid dynamics. These assumptions are grounded in the

theoretical foundations discussed in Chapter (2), particularly in the sections dealing with thermodynamic properties and fluid dynamics.

- **Ideal Gas Behavior:** As established in Section (2.2.2.2) on governing equations, the combustion gases are modeled as ideal gases. This assumption is justified by the high-temperature conditions typical in combustion chambers, allowing the use of the ideal gas law, to relate the pressure, temperature, and density of the gases efficiently.

$$p_h = \rho_h R_h T_h \tag{3.1}$$

- **Adiabatic Walls:** The walls of the combustion chamber are assumed to be adiabatic, meaning there is no heat transfer between the hot gases inside the chamber and the surroundings. As discussed in the literature review, this assumption simplifies the energy balance by ensuring that all the heat generated by the combustion process remains within the system, affecting only the internal energy and temperature of the gases.
- **Frozen Flow Assumption:** The flow within the combustion chamber is assumed to be chemically frozen, implying that after the combustion process, the chemical composition of the gases remains constant with no further chemical reactions occurring. This assumption aligns with the theoretical considerations of chemical kinetics and equilibrium, allowing the use of fixed gas compositions when calculating thermodynamic properties.
- **Uniform Inlet Conditions:** The inlet conditions for the combustion chamber, including temperature, pressure, and mass flow rate, are assumed to be uniform across the entire entrance of the chamber. This simplification, reduces the complexity of the boundary conditions at the inlet, focusing the analysis on the internal dynamics of the flow.
- **Constant Stagnation Properties:** In cases where a single stagnation temperature is provided as input, the stagnation pressure and temperature are assumed to be constant throughout the entire combustion chamber. As discussed in the review of thermodynamic systems, this assumption simplifies the calculations by reducing the number of variables that need to be updated during the iteration process.
- **Simplified Geometric Representation:** The combustion chamber is modeled using a simplified geometric representation, assuming that the cross-sectional area and other geometric properties are either constant or vary in a straightforward manner (e.g., linear tapering). This assumption is based on typical simplifications in computational fluid dynamics as discussed in Section (2.3.1).
- **Inviscid Flow Assumption:** The flow within the combustion chamber is assumed to be inviscid, meaning that the effects of viscosity are neglected. This assumption, consistent with the high-speed flow analysis mentioned in the literature review, allows the focus to remain on the primary thermodynamic processes without the added complexity of viscous effects.

- **Perfect Gas Mixture:** The combustion gases are treated as a perfect mixture of ideal gases, including species such as nitrogen, oxygen, and combustion products like water vapor and carbon dioxide. This assumption, along with the frozen flow assumption, facilitates the accurate calculation of the gas mixture properties using standard methods for ideal gases.

3.1.2 Chemical Composition and Thermodynamic Equilibrium of Combustion Chamber Gases

The combustion gases within the combustion chamber are treated as a complex mixture resulting from the combustion of hydrogen (H_2) with air, which is treated as a perfect mixture of nitrogen (N_2), oxygen (O_2), and argon (Ar). The exact molar fractions of these gases are:

- **Nitrogen (N_2)**: Approximately 78% by volume,
- **Oxygen (O_2)**: Approximately 21% by volume,
- **Argon (Ar)**: Approximately 0.93% by volume.

When hydrogen combusts in this air mixture, a series of chemical reactions occur, producing a variety of species. The main product is water vapor (H_2O), but the high temperatures and pressures in the combustion chamber also lead to the formation of several other species, such as:

- **Hydroxyl radicals (OH)**,
- **Hydrogen peroxide (H_2O_2)**,
- **Atomic hydrogen (H)**,
- **Nitrogen oxides (NO, NO_2)**,
- **Ammonia (NH_3)**.

In total, up to 19 reacting species may be formed, depending on the exact conditions within the chamber. These species are derived from the atoms of hydrogen, oxygen, and nitrogen, and their concentrations are determined by the chemical equilibrium of the system.

In this model, the gases are treated as an ideal gas mixture, which simplifies the calculation of properties such as pressure, temperature, and density. The ideal gas law is applied to each component of the gas mixture, allowing for the prediction of the overall behavior of the combustion gases:

$$pV = nRT \tag{3.2}$$

However, the extreme conditions within the combustion chamber, including high temperatures and pressures, can lead to deviations from ideal gas behavior. These non-ideal effects are particularly relevant when considering the interactions between different species and the formation of additional products not captured by a simple ideal gas model.

To accurately model the equilibrium state of the gas mixture, the principle of Gibbs free energy minimization is employed. Gibbs free energy (G) is a thermodynamic potential that represents the amount of reversible work that a system can perform at constant temperature and pressure. It is defined as:

$$G = \sum_i n_i \mu_i = \sum_i n_i \left(h_i - T s_i\right) \tag{3.3}$$

where:

- n_i is the number of moles of species i,
- μ_i is the chemical potential of species i,
- h_i is the enthalpy of species i,
- T is the temperature,
- s_i is the entropy of species i.

At chemical equilibrium, the Gibbs free energy of the system is at its minimum value, meaning that the system has reached its most stable state. The minimization of Gibbs free energy is a key step in determining the equilibrium concentrations of the various species in the combustion gases. This process ensures that the predicted composition reflects the actual physical state of the gases under the specific temperature and pressure conditions in the combustion chamber.

By carefully modeling the fluid composition and applying the principle of Gibbs free energy minimization, the model provides accurate predictions of the combustion chamber's performance under various operating conditions. This approach ensures that the properties of the gas mixture reflect its true physical state, even under the extreme conditions encountered in the combustion chamber.

3.1.2.1 Use of Cantera

To accurately compute the thermodynamic and transport properties of the combustion gases, the computational model integrates Cantera, a sophisticated software tool specifically designed for simulating chemically reacting flows and determining the properties of gas mixtures. Cantera combines advanced chemical kinetics, thermodynamics, and transport theory to model the behavior of the combustion gases under various operating conditions.

Cantera's calculations begin with the determination of the equilibrium composition of the gas mixture. This is achieved through the minimization of Gibbs free energy, a principle that governs chemical equilibrium. At a given temperature and pressure, Cantera employs an iterative algorithm that adjusts the concentrations of different species in the mixture until the total Gibbs free energy is minimized. This state indicates that the system has reached chemical equilibrium, where no further net change in species concentrations occurs. The equilibrium composition obtained is then used as a basis for calculating various thermodynamic properties essential for modeling the combustion process.

Thermodynamic Properties Cantera calculates several key thermodynamic properties based on the equilibrium composition using methods grounded in statistical mechanics and thermodynamic principles:

- **Specific Heat Capacity (c_p)**: Cantera calculates the specific heat capacity at constant pressure (c_p) by evaluating the change in enthalpy with respect to temperature at constant pressure. This is done using the equilibrium species concentrations and the partition functions of each species, which account for the different energy states (translational, rotational, vibrational, and electronic) of the molecules.

- **Ratio of Specific Heats ($\gamma = c_p/c_v$)**: The ratio of specific heats is determined by computing both c_p and c_v (specific heat at constant volume). c_v is similarly derived from the internal energy change with respect to temperature. The ratio γ is crucial for modeling adiabatic processes and influences the sound speed in the gas mixture, calculated using relations from thermodynamics and fluid dynamics.

- **Enthalpy (H) and Entropy (S)**: Enthalpy is calculated from the sum of the enthalpies of each species at their respective equilibrium concentrations, taking into account the standard state enthalpy and the temperature-dependent changes. Entropy is computed using the species partition functions and equilibrium concentrations, reflecting the disorder within the system. These calculations are integral to assessing the energy and entropy balances in the combustion chamber.

Transport Properties In addition to thermodynamic properties, Cantera calculates transport properties using kinetic theory and statistical mechanics, which are critical for modeling the flow and heat transfer characteristics of the combustion gases:

- **Viscosity**: Cantera computes the dynamic viscosity of the gas mixture using the Chapman-Enskog theory, which models the transport properties based on molecular collisions. The viscosity is calculated by considering the interaction potentials between different species and their relative concentrations. This property influences the flow behavior, including the development of boundary layers and internal friction in the combustion chamber.

- **Thermal Conductivity**: Thermal conductivity is calculated by Cantera using a similar approach, where the transport of energy through molecular collisions is modeled. The

Chapman-Enskog method is used again to determine how efficiently the gas mixture conducts heat, based on species concentrations and molecular weights. This property is crucial for understanding heat transfer within the combustion chamber, which affects the temperature distribution and cooling efficiency.

- **Mass Diffusion Coefficients**: Cantera calculates the diffusion coefficients for different species using both binary diffusion models and more complex multi-component diffusion models, depending on the system. The calculations are based on the relative movement of species due to concentration gradients and are influenced by molecular size and interaction potentials. Accurate modeling of mass diffusion is essential for predicting how species mix within the combustion chamber, affecting combustion uniformity and pollutant formation.

Cantera's robust computational framework allows for the precise simulation of both chemical and physical processes within the combustion chamber. By integrating Cantera into the computational model, the behavior of the combustion gases is simulated with high accuracy, ensuring that the chemical equilibrium and transport phenomena are appropriately captured. This integration enables the model to predict the performance of the combustion chamber under various operating conditions with confidence, thereby aiding in the optimization of the overall gas turbine system.

3.1.3 Computational Modeling of Combustion Chamber Dynamics

The accurate simulation of combustion chamber dynamics is essential for understanding and optimizing the performance of gas turbine engines. This section presents a comprehensive computational approach to modeling the thermodynamic and heat transfer processes within the combustion chamber. The modeling process is divided into two primary stages: the calculation of static fluid properties and the subsequent heat transfer analysis. By carefully considering both the static and dynamic behavior of the fluid, this model provides a detailed representation of the thermal environment within the combustion chamber, which is crucial for designing efficient and reliable turbine systems.

The first stage, the Static Fluid Properties Calculation, involves determining the key thermodynamic properties along the chamber, setting the foundation for the entire computational process. Following this, the Heat Transfer Calculation assesses how energy is transferred from the hot gases to the chamber walls, utilizing either a single-node or multi-node approach depending on the level of detail required. Each stage is meticulously executed to ensure that the complex interactions between the fluid and the chamber surfaces are accurately captured.

3.1.3.1 Static Fluid Properties Calculation

This stage is applied to both the single-node and multi-node approaches, ensuring that the fluid properties are consistently evaluated across different spatial resolutions within the com-

bustor. The first stage of the computational process involves calculating the static properties of the fluid within the combustion chamber. This step is crucial as it sets the foundation for determining key thermodynamic properties such as the static temperature $T_{h,i}$, Mach number $\mathrm{Ma}_{h,i}$, static pressure $p_{h,i}$, density $\rho_{h,i}$, and specific heats. The process is initiated by defining the stagnation conditions, chamber and throat geometry, mass flow rates, and node structure, and it proceeds through the following steps:

1. **Initialization of Stagnation Conditions and Geometrical Parameters:**

   - The computation begins by setting the known stagnation properties, including stagnation temperature T_h^0 and stagnation pressure p_h^0. These properties represent the total conditions at the inlet, considering the effects of both air and fuel (hydrogen) mass flow rates.
   - The chamber geometry, including its length, cross-sectional area, and throat dimensions, is also defined at this stage. These geometrical parameters are critical for subsequent calculations of flow velocity and area-related properties.
   - The total mass flow rate $\dot{m}_h$, which includes contributions from both the air and the injected fuel, is established. This rate is used in conjunction with the chamber geometry to ensure accurate calculations of flow properties.
   - The computational domain is divided into nodes, where the number of nodes N_{nodes} is determined by the length of the temperature input array. The index i is used to represent each node, ranging from 1 to N_{nodes}. If only one temperature is provided, it is interpreted as the overall stagnation temperature for the entire chamber, rather than just the inlet condition.
   - Initial guesses for static temperature $T_{h,i}$ and Mach number $\mathrm{Ma}_{h,i}$ at each node i are made. These initial values are refined during the iterative process, ensuring convergence to the correct static properties throughout the chamber.

2. **Energy and Mass Flow Continuity:**

   - The static temperature $T_{h,i}$ and Mach number $\mathrm{Ma}_{h,i}$ at each node are solved simultaneously in an iterative process, ensuring the conservation of energy and mass throughout the combustion chamber. Initially, a guess for $T_{h,i}$ and $\mathrm{Ma}_{h,i}$ is made at each node, and the solver iteratively refines these values until convergence is achieved.
   - The energy conservation equation, which relates the stagnation temperature $T_{h,i}^0$, static temperature $T_{h,i}$, and Mach number $\mathrm{Ma}_{h,i}$, is given by:

$$T_{h,i} = T_{h,i}^0 \left(1 + \frac{\gamma_{h,i} - 1}{2} \cdot \mathrm{Ma}_{h,i}^2\right)^{-1} \tag{3.4}$$

     This equation ensures that the static temperature at each node is consistent with the energy content of the flow. The stagnation temperature $T_{h,i}^0$ remains constant

along the flow unless there is heat exchange or friction, while the static temperature decreases with increasing Mach number due to the conversion of thermal energy into kinetic energy.

- The mass flow rate $\dot{m}_h$ is conserved across each node, as described by the continuity equation. In this case, the mass flow rate at each node is a function of the static density $\rho_{h,i}$, the cross-sectional area A_i, and the velocity $v_{h,i}$. To calculate these properties, the following equation for mass flow is used:

$$\dot{m}_h = \rho_{h,i} \cdot A_i \cdot v_{h,i} \tag{3.5}$$

where A_i is the cross-sectional area and $v_{h,i}$ is the flow velocity at node i. Additionally, the velocity $v_{h,i}$ can be related to the Mach number $\text{Ma}_{h,i}$, the specific heat ratio $\gamma_{h,i}$, the specific gas constant R_h, and the static temperature $T_{h,i}$ through the equation:

$$v_{h,i} = \text{Ma}_{h,i} \cdot \sqrt{\gamma_{h,i} \cdot R_h \cdot T_{h,i}} \tag{3.6}$$

This relationship shows that velocity is directly proportional to the Mach number, and is dependent on the local thermodynamic properties of the gas at node i.

- To solve for the Mach number $\text{Ma}_{h,i}$, the following mass flow continuity equation is employed:

$$\text{Ma}_{h,i} = \frac{\dot{m}_h}{\rho_{h,i} \cdot A_i \cdot \sqrt{\gamma_{h,i} \cdot R_h \cdot T_{h,i}}} \tag{3.7}$$

This equation ensures that the Mach number is consistent with the mass flow rate, density, and flow velocity at each node. The iterative solver adjusts the static temperature $T_{h,i}$ and Mach number $\text{Ma}_{h,i}$ at each node until the values satisfy both the energy and mass flow conservation equations.

- The iterative process begins with initial guesses for $T_{h,i}$ and $\text{Ma}_{h,i}$, which are refined during each iteration. The solver uses the ‘fsolve‘ method to minimize the error between the guessed and calculated values for the static temperature and Mach number until the difference is within a predefined tolerance. This process is repeated for each node until the temperature and Mach number converge.

3. **Momentum Conservation and Pressure Distribution:**

- The static pressure $p_{h,i}$ is computed by maintaining momentum conservation, which accounts for the pressure drop along the length of the chamber:

$$p_{h,i} = \frac{p_{h,i}^0}{\left(\frac{T_{h,i}^0}{T_{h,i}}\right)^{\frac{\gamma_{h,i}}{\gamma_{h,i}-1}}} \tag{3.8}$$

where $\gamma_{h,i}$ is the specific heat ratio at node i.

- The iterative solver adjusts the pressure distribution $p_{h,i}$ and the Mach number $\text{Ma}_{h,i}$ across each node i until the momentum equation is satisfied throughout the chamber.

4. **Finalization of Static Properties:**

   - Once the temperature, pressure, and Mach number have converged, additional static properties are calculated. These include specific heat capacities $c_{p,h,i}$, the specific gas constant R_h, and the speed of sound $a_{h,i}$ for each node i.
   - These properties are crucial for the subsequent heat transfer calculations and are obtained using the Cantera software, which provides accurate thermodynamic and transport properties based on the chemical composition of the gas mixture at each node.

3.1.3.2 Heat Transfer Calculation

After determining the static fluid properties, the model proceeds to calculate the heat transfer between the hot gases and the combustion chamber walls. This part of the process is divided into two methods, depending on whether the chamber is modeled with a single node or multiple nodes.

Method 1: Single Node Heat Transfer Calculation

1. **Calculation of Prandtl and Reynolds Numbers:**

   - The first step in the heat transfer calculation involves determining the Prandtl number Pr_h and Reynolds number Re_h for the hot gases. These dimensionless numbers are crucial as they characterize the flow and thermal properties of the gas mixture. The general definitions of these numbers are provided in Section (2.2.2.3) of the Literature Review, where equations (2.16) and (2.15) detail the Prandtl and Reynolds numbers respectively.
   - The Prandtl number is calculated as:

   $$\text{Pr}_h = \frac{c_{p,h} \cdot \mu_h}{k_h} \tag{3.9}$$

   where $c_{p,h}$ is the specific heat at constant pressure, μ_h is the dynamic viscosity, and k_h is the thermal conductivity of the hot gases.
   - The Reynolds number is determined using:

   $$\text{Re}_h = \frac{\dot{m}_h \cdot D_h}{\mu_h \cdot A_h} \tag{3.10}$$

   where $\dot{m}_h$ is the mass flow rate, D_h is the hydraulic diameter of the chamber, μ_h is the dynamic viscosity, and A_h is the cross-sectional area.

2. **Calculation of Adiabatic Hot Wall Temperature and Averaged Properties:**

- The adiabatic wall temperature $T_{hw,\text{adiabatic}}$ represents the theoretical maximum temperature that the chamber wall could reach if it were perfectly insulated, meaning no heat is lost to the surroundings. This temperature is a crucial factor in understanding and predicting the heat transfer from the hot gases to the chamber wall.
- The adiabatic wall temperature is calculated using the following equation:

$$T_{hw,\text{adiabatic}} = T_h \cdot \left(1 + \frac{0.5 \cdot \text{Pr}_h^{1/3} \cdot (\gamma_h - 1) \cdot \text{Ma}_h^2}{2}\right) \tag{3.11}$$

  where:
  - T_h is the static temperature of the hot gases at the node,
  - Pr_h is the Prandtl number, which reflects the ratio of momentum diffusivity (viscosity) to thermal diffusivity,
  - γ_h is the ratio of specific heats (also known as the adiabatic index),
  - Ma_h is the Mach number, representing the ratio of the gas velocity to the speed of sound.
- The constant 0.5 in the equation is an empirical factor that adjusts the formula to better fit experimental data, particularly under conditions of compressible and turbulent flow, as often encountered in high-speed combustion chambers. This specific form of the equation has been referenced in previous studies of air-breathing engines and heat exchangers, such as those described by Tanatsugu et al. [23].
- After determining $T_{hw,\text{adiabatic}}$, the properties of the gas mixture, such as viscosity μ_h, thermal conductivity k_h, and specific heat $c_{p,h}$, are recalculated at the average temperature between T_h and $T_{hw,\text{adiabatic}}$. This recalculation is essential because these properties are highly temperature-dependent, and using an average temperature provides more accurate values for subsequent heat transfer calculations.

3. **Calculation of the Heat Transfer Coefficient h_h:**
   - The heat transfer coefficient h_h is then calculated using an empirical correlation developed by D.R. Bartz, which is widely used for predicting heat transfer in rocket combustion chambers under highly turbulent and accelerating flow conditions [24]. The correlation used is:

$$h_h = 0.026 \cdot \mu_h^{0.2} \cdot \left(\frac{k_h}{\mu_h}\right)^{0.6} \cdot c_{p,h}^{0.4} \cdot \frac{\dot{m}_h^{0.8}}{A_{\text{combustor}}^{0.9}} \cdot \left(\frac{0.25 \cdot \pi \cdot D_{\text{throat}}}{(D_{\text{combustor}} - D_{\text{throat}})/L_{\text{throat}}}\right) \tag{3.12}$$

   - This formula accounts for the flow characteristics and the specific geometry of the combustion chamber and throat, making it suitable for conditions where the gas flow is highly turbulent and subjected to rapid acceleration, typical of rocket engines.

4. **Calculation of Heat Transfer:**

   - The heat transfer Q from the hot gases to the chamber wall is calculated using the heat transfer coefficient:

$$Q = h_h \cdot \left(T_{hw,\text{adiabatic}} - T_h\right) \cdot A_h \tag{3.13}$$

     where $T_{hw,\text{adiabatic}}$ is the adiabatic wall temperature, T_h is the static temperature, and A_h is the chamber surface area.

   - This calculation provides the total rate of heat transfer from the hot gases to the chamber wall for a single-node model.

Method 2: Multi-Node Heat Transfer Calculation

1. **Discretization of the Combustion Chamber:**

   - The combustion chamber is discretized into multiple nodes to capture the temperature and pressure variations along its length. This approach allows for a more detailed analysis of the heat transfer process by breaking down the chamber into smaller segments, where each segment represents a different location along the length of the chamber.

   - Each node is treated as a distinct segment with its own local fluid properties and heat transfer characteristics. The properties at each node are calculated using the average temperature between adjacent nodes, providing a more accurate representation of the thermodynamic and transport properties within the chamber.

2. **Calculation of Node Properties Using Cantera:**

   - For each node i, the properties of the hot gases, such as the ratio of specific heats γ_h, viscosity μ_h, thermal conductivity k_h, specific heat capacity $c_{p,h}$, density ρ_h, and specific gas constant R_h, are calculated using Cantera. These properties are computed at the average temperature between the static temperatures of the current node i and the next node $i+1$, as follows:

$$T_{\text{avg},i} = \frac{T_h[i] + T_h[i+1]}{2} \tag{3.14}$$

   - This average temperature is crucial because it reflects the conditions under which heat transfer occurs between the nodes, making it more representative of the actual thermal processes taking place within the chamber.

3. **Calculation of Heat Transfer:**

   - The heat transfer $Q[i]$ at each node is calculated using the enthalpy difference between adjacent nodes. This approach is based on the first law of thermodynamics, which states that the change in internal energy of a system is equal to the heat

added minus the work done by the system. As the hot gases flow through the combustion chamber, their enthalpy (which includes both internal energy and flow work) decreases due to heat transfer to the chamber walls. By applying the enthalpy difference between nodes, we can accurately capture the heat lost from the gas to the chamber walls.

- The heat transfer is given by:

$$Q[i] = \dot{m}_h \cdot c_{p,h}[i] \cdot (T_h[i] - T_h[i+1]) \tag{3.15}$$

  where:

  - $\dot{m}_h$ is the mass flow rate of the hot gases,
  - $c_{p,h}[i]$ is the specific heat capacity at constant pressure, evaluated at the average temperature between node i and node $i+1$,
  - $T_{h,\text{stag}}[i]$ is the stagnation temperature at node i,
  - $T_{h,\text{stag}}[i+1]$ is the stagnation temperature at the subsequent node $i+1$.

- The heat transfer at the last node $Q[N_{\text{nodes}} - 1]$ is considered to be zero because there is no subsequent node with which to calculate a temperature difference. Essentially, heat transfer occurs between adjacent nodes, and with no node beyond the last one, there is no temperature gradient to drive heat transfer at that location. This implies that the heat transfer in a multi-node model is distributed across $N-1$ sections, and the final node serves as the boundary condition where the heat transfer process concludes.

- The total heat transfer Q^{total} for the entire chamber is then the sum of the heat transfer across all nodes:

$$Q^{\text{total}} = \sum_{i=1}^{N_{\text{nodes}}} Q[i] \tag{3.16}$$

This method provides a detailed analysis of how heat is transferred along the length of the combustion chamber. By considering the temperature distribution and thermal performance under varying operating conditions, this approach enables the accurate modeling of heat transfer, particularly in cases where non-uniformities along the chamber length are significant.

The computational modeling of the combustion chamber dynamics, as outlined in this section, provides a robust framework for analyzing and optimizing the thermal behavior of gas turbine engines. By first establishing the static fluid properties and then conducting a detailed heat transfer analysis, the model offers insights into the temperature distribution, pressure variations, and energy transfer processes within the combustion chamber. This comprehensive approach ensures that the model can accommodate a range of operating conditions and chamber designs, making it a valuable tool for both research and practical applications.

3.1.4 Flowchart

Following the detailed explanation of the computational methodologies for the hot fluid (combustion chamber), a high-level flowchart is presented in Figure 3.3. This flowchart provides a visual representation of the main computational steps involved in determining the properties and behavior of the hot fluid, starting from the initial input data to the final calculation of the heat transfer rate.

Each step in the flowchart corresponds to a key function within the code, illustrating the iterative process of solving for static and stagnation properties across multiple nodes in the combustion chamber. It also highlights how intermediate quantities, such as adiabatic wall temperature and convective heat transfer coefficients, are calculated. By visually organizing the calculation steps, the flowchart demonstrates the process of modeling the heat transfer and fluid flow through the combustion chamber, as described in Section 3.1.

For more in-depth details of the code's structure and implementation, please refer to the full Python code provided in Annex A.2.

3.2 Cold Fluid (Cooling Channels)

In gas turbine systems, the cooling channels are integral to the thermal management strategy, ensuring that the extreme temperatures generated within the combustion chamber do not compromise the structural integrity of the engine. These channels are designed to circulate a coolant, hydrogen, alongside the combustion chamber walls. The role of hydrogen in this context is particularly advantageous: it not only absorbs heat effectively due to its high specific heat capacity but also serves a dual purpose. After being heated in the cooling process, the hydrogen is subsequently directed into the combustion chamber, where it acts as a fuel. This innovative approach enhances the overall efficiency of the system by recycling the coolant as an energy source.

The primary focus of this section is to provide a detailed computational analysis of the cooling channels. This analysis aims to simulate the thermodynamic behavior of the hydrogen as it travels through the channels, absorbing heat from the combustion chamber walls. The model calculates key properties such as temperature distribution, pressure drops, and heat transfer rates, providing insights into the cooling efficiency and the overall thermal management of the system.

To achieve a comprehensive understanding of the cooling process, the analysis considers both single-node and multi-node approaches. These approaches enable the capture of spatial variations in temperature and pressure along the length of the cooling channels. The integration of advanced computational tools like Cantera or CoolProp further enhances the accuracy of the simulations, ensuring that the model can predict cooling performance under a variety of operating conditions. This modeling is crucial not only for optimizing the cooling process but also for improving the overall efficiency and reliability of the gas turbine system.

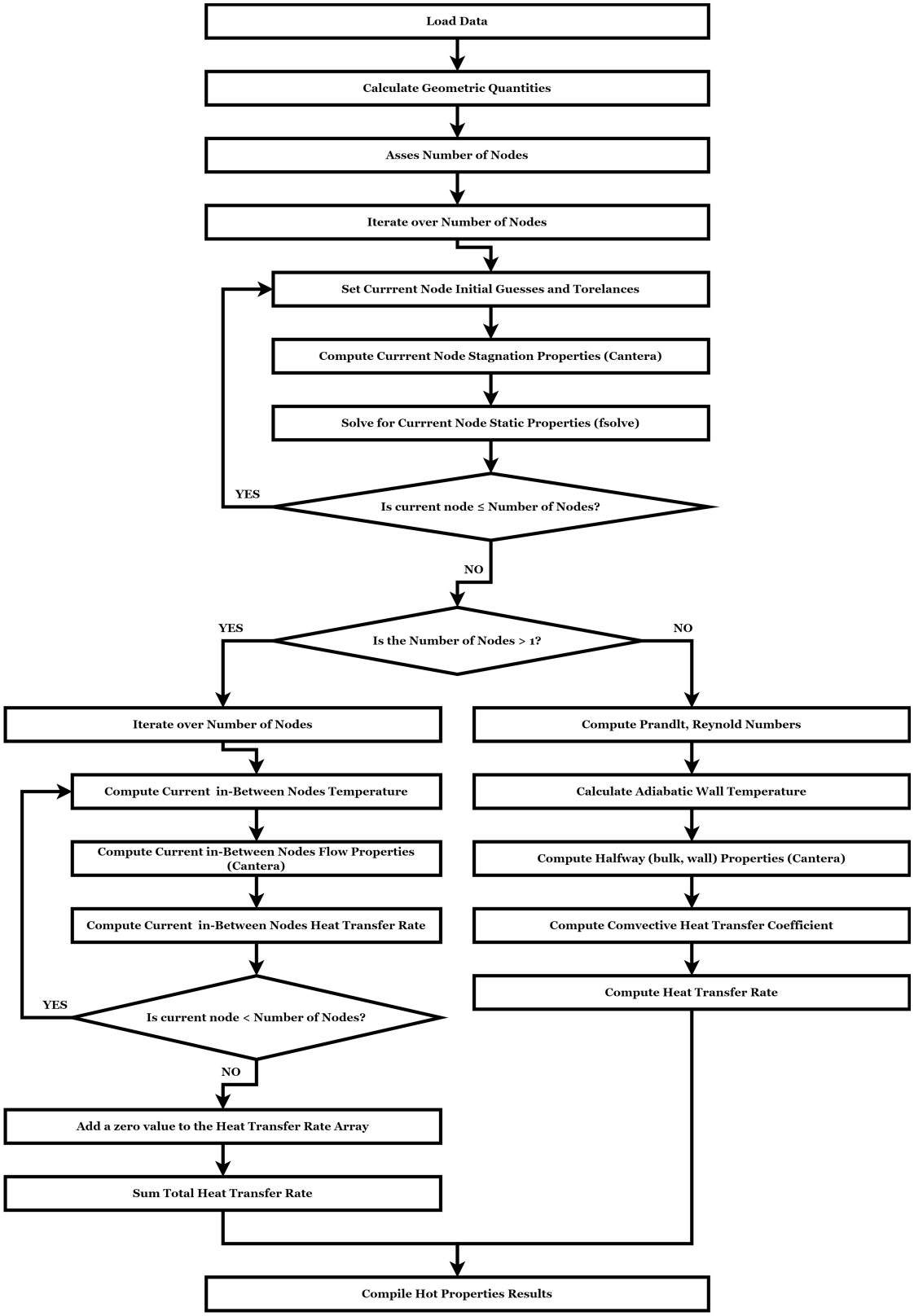

Figure 3.3: Flowchart of Hot Fluid (Combustion Chamber) Calculations

3.2.1 Assumptions

In the computational modeling of the cooling channels, several key assumptions are made to streamline the calculations and ensure that the model remains computationally efficient while accurately predicting the thermal and fluid behavior of the hydrogen coolant. These assumptions are essential for simplifying the complex interactions within the cooling system and are based on the physical characteristics of the hydrogen coolant and the geometry of the channels.

- **Real Gas Behavior for Hydrogen:** The model assumes that hydrogen exhibits real gas behavior, especially crucial due to its phase change from supercritical liquid to supercritical gas within the cooling channels. This assumption is necessary for accurately capturing the thermophysical properties of hydrogen as it absorbs heat and undergoes phase transformations.
- **Uniform Channel Geometry:** The geometry of the cooling channels is assumed to vary linearly from inlet to outlet in both width and height. This linear variation simplifies the calculation of the hydraulic diameter (D_h) and sectional area at each node along the channel, which are critical parameters for determining the flow characteristics and heat transfer rates.
- **Adiabatic Channel Walls:** The walls of the cooling channels are assumed to be adiabatic, meaning there is no heat transfer between the coolant and the surrounding environment. This simplifies the energy balance by ensuring that all heat removed from the combustion chamber is absorbed by the coolant.
- **Neglected Gravitational Effects:** The pressure drop due to height differences between the fluid entry and exit points within the cooling channels is neglected. This assumption is based on the fact that gravitational effects are minimal compared to frictional losses and are therefore considered insignificant in the overall pressure drop calculation.
- **Zero Entrance and Exit Pressure Drop:** The model assumes that there are no additional pressure drops at the entrance and exit of the cooling channels. This means that the total pressure drop within the system is attributed solely to the frictional losses within the core of the channels.
- **Inlet Conditions Based on Pumped or Tank Conditions:** The model accounts for two scenarios regarding the inlet conditions of the cooling channels. In one scenario, hydrogen is pumped from a tank, requiring an entropy-based calculation to determine the inlet temperature. In the other scenario, the inlet conditions, such as temperature and pressure, are directly provided. This assumption allows the model to accommodate different initial conditions based on the cooling system's design.
- **Constant Mass Flow Rate Through Channels:** It is assumed that the mass flow rate of hydrogen through each cooling channel remains constant. This simplification

means that there is no consideration for any mass exchange with the surroundings, allowing for consistent flow property calculations along the channel's length.

- **Parallel Flow or Counterflow Heat Transfer:** The heat exchange between the hot combustion gases and the cooling hydrogen is modeled under either parallel flow or counterflow configurations. This assumption simplifies the analysis by treating the entire system uniformly under one of these two heat exchange methods, which significantly impacts the temperature gradients and heat transfer rates along the channels.

These assumptions play a crucial role in the computational modeling of the cooling channels, enabling the model to simulate the thermodynamic and fluid dynamic behavior of hydrogen as a coolant effectively. By making these assumptions, the model strikes a balance between computational efficiency and the accuracy needed to predict the cooling performance under various operating conditions.

3.2.2 Hydrogen Behavior and Properties

Hydrogen serves as the primary coolant in the system, undergoing significant thermodynamic transformations as it progresses through the cooling channels. Initially stored in a cryogenic tank, hydrogen enters the cooling system in a supercritical state, where it must effectively absorb the intense heat generated in the combustion chamber. Understanding the behavior of hydrogen under these conditions is critical for accurate modeling of the cooling process.

3.2.2.1 Cryogenic to Supercritical Transition

Hydrogen is stored at cryogenic temperatures in the tank, often close to its boiling point under high pressure. As it passes through the pump, hydrogen undergoes a phase transition from a liquid to a supercritical fluid. Upon entering the cooling channels, it remains in this supercritical state as it absorbs heat from the walls of the combustion chamber. This transition to a supercritical fluid is a crucial aspect of the cooling process, as it significantly influences the thermophysical properties of hydrogen, such as its density, specific heat capacity, viscosity, and thermal conductivity.

The model assumes real gas behavior for hydrogen, which is essential for capturing the complex changes in its properties as it transitions through different states. Hydrogen undergoes a phase change from liquid to supercritical fluid as it passes through the pump, and its subsequent heat absorption in the supercritical state significantly affects the efficiency of heat transfer and the overall cooling performance.

3.2.2.2 Influence of Assumptions on Hydrogen Behavior

Several assumptions play a crucial role in shaping the behavior and calculations of hydrogen in the cooling channels. The real gas behavior assumption is critical near the critical point, where hydrogen deviates from ideal gas behavior. The model also assumes a linear variation in channel geometry, which directly impacts the distribution of velocity, pressure, and temperature of hydrogen, thereby influencing heat transfer rates and cooling efficiency. Additionally, assuming a constant mass flow rate simplifies the calculations related to pressure drops and temperature changes, ensuring consistency in flow analysis. Finally, the configuration of the flow, whether parallel or counterflow, significantly affects the temperature gradients across the hydrogen coolant, which in turn impacts the efficiency of heat absorption and the overall performance of the cooling system.

These assumptions are carefully selected to balance the need for a manageable model complexity with the goal of producing accurate and reliable predictions of hydrogen's behavior in the cooling channels.

3.2.2.3 Use of CoolProp

The model utilizes CoolProp, an advanced open-source thermodynamic library, to determine the thermophysical properties of hydrogen throughout the cooling channels. CoolProp is particularly effective for fluids exhibiting non-ideal behavior, like hydrogen under supercritical conditions. It calculates essential properties such as specific heat capacity (c_p), viscosity (μ), density (ρ), thermal conductivity (k), the specific gas constant (R), and Reynolds number (Re) based on rigorous equations of state that account for the real gas behavior of hydrogen. By leveraging a comprehensive fluid property database, CoolProp provides accurate predictions across a wide range of temperatures and pressures.

CoolProp calculates these properties based on fundamental principles of thermodynamics and fluid dynamics, using detailed equations of state (EOS) that account for the real gas behavior of fluids like hydrogen. By leveraging a comprehensive database of fluid properties, CoolProp can provide accurate predictions for a wide range of temperatures and pressures. This capability is crucial for modeling the dynamic and complex behavior of hydrogen as it flows through the cooling channels, ensuring that the model accurately reflects the physical processes at play.

The integration of CoolProp into the computational model allows for precise simulations of hydrogen's behavior under various operating conditions, enabling the optimization of the cooling system's design and performance.

3.2.3 Computational Modeling of Cooling Channel Dynamics

The cooling channels in a gas turbine engine are vital for maintaining the structural integrity and operational efficiency of the combustion chamber. Hydrogen serves as both a coolant

and a fuel, absorbing excess heat from the chamber walls before being used in combustion. This section presents the computational model developed to predict the fluid dynamics and heat transfer processes within the cooling channels. The model is divided into two main parts: the initialization of inlet conditions and the determination of outlet conditions along the channel.

3.2.3.1 Initialization of Inlet Conditions

The computational process begins with the initialization of the inlet conditions for the hydrogen coolant. This step involves defining the inlet temperature, pressure, mass flow rate, and geometrical properties of the cooling channels.

1. **Distribution of Mass Flow Rate:** The overall mass flow rate of the coolant $\dot{m}_c$ is first distributed across the number of cooling channels, resulting in a mass flow rate per channel $\dot{m}_{c,\text{per\_channel}}$. This distribution is essential for understanding how the coolant flows through each individual channel.

2. **Calculation of Geometrical Properties and Surface Areas:** The geometrical dimensions of the cooling channels, including the width W_{inlet}, height H_{inlet}, and hydraulic diameter D_h, are first calculated. These properties are crucial as they directly influence the flow characteristics and heat transfer capabilities of the coolant.

   - For a single-node model, the dimensions are averaged across the entire channel length.
   - For multiple nodes, the width and height at each node i are determined by linear interpolation between the inlet and outlet dimensions. The linear interpolation for width $W[i]$ and height $H[i]$ at each node i is given by:

$$W[i] = W_{\text{inlet}} + i \times \frac{W_{\text{outlet}} - W_{\text{inlet}}}{N_{\text{nodes}} - 1} \tag{3.17}$$

$$H[i] = H_{\text{inlet}} + i \times \frac{H_{\text{outlet}} - H_{\text{inlet}}}{N_{\text{nodes}} - 1} \tag{3.18}$$

   - The hydraulic diameter $D_h[i]$ is calculated using the following formula:

$$D_h[i] = \frac{2 \times W[i] \times H[i]}{W[i] + H[i]} \tag{3.19}$$

   - The sectional area $A_{\text{node}}[i]$ and surface area $A_{\text{surface}}[i]$ for each node are computed as follows:

$$A_{\text{node}}[i] = W[i] \times H[i] \tag{3.20}$$

$$A_{\text{surface}}[i] = W[i] \times L_{\text{combustor}} \tag{3.21}$$

where $L_{\text{combustor}}$ is the length of the combustor.

3. **Setting Inlet Conditions:** The initialization also involves setting the inlet conditions for temperature and pressure, depending on whether the hydrogen originates from a cryogenic tank or is directly introduced at the inlet.

   - **Tank Conditions:** If hydrogen is sourced from a cryogenic tank, the initial temperature T_{tank} and pressure p_{tank} are specified. The pressure is adjusted by a pump pressure ratio r_{pump} to determine the inlet pressure $p_{\text{inlet}}[0]$:

   $$p_{\text{inlet}}[0] = p_{\text{tank}} \times r_{\text{pump}} \tag{3.22}$$

   To maintain thermodynamic consistency, the entropy s at the tank conditions is computed first using the CoolProp library:

   $$s = s(T_{\text{tank}}, p_{\text{tank}}) \tag{3.23}$$

   Then, the inlet temperature $T_{\text{inlet}}[0]$ is determined using an entropy balance, ensuring that the entropy remains constant from the tank to the channel inlet. This is solved iteratively, often using a root-finding algorithm like ‘fsolve‘ in Python, where:

   $$s(T_{\text{inlet}}[0], p_{\text{inlet}}[0]) = s_{\text{tank}} \tag{3.24}$$

   The computational implementation for this process might involve defining a function that returns the difference between the entropy at the guessed inlet temperature and the tank entropy. The inlet temperature is then adjusted until the difference is minimized to zero, indicating consistency with the tank conditions.

   - **Inlet Conditions:** If hydrogen is introduced directly at the inlet, its temperature $T_{\text{inlet}}[0]$ and pressure $p_{\text{inlet}}[0]$ are specified directly, bypassing the need for entropy calculations.

This initial setup provides a robust foundation for accurately modeling the coolant's behavior as it progresses through the channel.

3.2.3.2 Determination of Outlet Conditions Along the Channel

After establishing the inlet conditions, the model proceeds to calculate the outlet conditions at each node along the cooling channel. This process involves iteratively determining the temperature, pressure, and other relevant properties at each outlet node.

1. **Heat Transfer Rate Calculation:** The heat transfer rate $Q_{\text{channel}}[i]$ is computed for each node, with considerations made for the flow configuration—whether it is parallel

flow or counterflow relative to the combustion chamber. The code considers both configurations and distributes the heat transfer rate accordingly across multiple cooling channels:

- **Parallel Flow:** In a parallel flow configuration, the coolant and the hot gases flow in the same direction. The heat transfer rate $Q_{\text{channel}}[i]$ at each node i is calculated by dividing the heat transfer rate $Q[i]$ by the number of cooling channels. This reflects how the total heat transfer is shared across all channels:

$$Q_{\text{channel}}[i] = \frac{Q[i]}{\text{number\_of\_channels}} \tag{3.25}$$

- **Counterflow:** In a counterflow configuration, the coolant flows in the opposite direction to the hot gases. Here, the code reverses the node indexing to ensure that the heat transfer rate $Q_{\text{channel}}[i]$ is calculated based on the interaction between the last node of the cooling channel and the first node of the combustion chamber. Specifically:
  - For nodes other than the last one:

$$Q_{\text{channel}}[i] = \frac{Q[N_{\text{nodes}} - 2 - i]}{\text{number\_of\_channels}} \tag{3.26}$$

  - For the last node, the heat transfer rate is set to zero, as there is no subsequent node to interact with:

$$Q_{\text{channel}}[N_{\text{nodes}} - 1] = 0 \tag{3.27}$$

Finally, the total heat transfer $Q_{\text{channel}}^{\text{total}}$ is summed across all nodes to provide an overall assessment of the cooling effectiveness.

2. **Iterative Solver for Temperature, Pressure, and Flow Characteristics:** The outlet temperature and pressure for each node are determined using an iterative solver, which also calculates key flow characteristics such as Reynolds number, friction factor, and pressure drop. This iterative process ensures an accurate representation of the fluid dynamics within the channel:

- The average temperature $T_{\text{avg}}[i]$ and pressure $p_{\text{avg}}[i]$ at each node are calculated as the midpoint between the inlet and outlet guesses:

$$T_{\text{avg}}[i] = \frac{T_{\text{inlet}}[i] + T_{\text{outlet\_guess}}[i]}{2} \tag{3.28}$$

$$p_{\text{avg}}[i] = \frac{p_{\text{inlet}}[i] + p_{\text{outlet\_guess}}[i]}{2} \tag{3.29}$$

These averages are crucial for accurately determining the fluid properties using the CoolProp library, which provides detailed thermophysical data for hydrogen,

including specific heat capacity, viscosity, density, thermal conductivity, and the specific gas constant.

- The Reynolds number $\mathrm{Re}_c[i]$ is calculated to determine the flow regime (laminar, turbulent, or transitional) within the cooling channel. It is computed using:

$$\mathrm{Re}_c[i] = \frac{\dot{m}_{c,\text{per\_channel}} \times D_h[i]}{\mu_c[i] \times A_{\text{node}}[i]} \tag{3.30}$$

where $\dot{m}_{c,\text{per\_channel}}$ is the mass flow rate per channel, $D_h[i]$ is the hydraulic diameter at node i, $\mu_c[i]$ is the dynamic viscosity, and $A_{\text{node}}[i]$ is the cross-sectional area. The Reynolds number helps classify the flow regime, which directly impacts the frictional losses and heat transfer efficiency.

- **Friction Factor Calculation:** The friction factor $\xi(\mathrm{Re}_c[i], \varepsilon_r/D_h)$ is determined using the Churchill correlation, which applies to all flow regimes. The friction factor equation is:

$$\xi(\mathrm{Re}_c[i], \varepsilon_r/D_h) = 8 \left[\left(\frac{8}{\mathrm{Re}_c[i]} \right)^{12} + (K_1 + K_2)^{-3/2} \right]^{1/12} \tag{3.31}$$

with:

$$K_1 = \left[-2.457 \ln \left(\left(\frac{7}{\mathrm{Re}_c[i]} \right)^{0.9} + 0.27 \frac{\varepsilon_r}{D_h[i]} \right) \right]^{16} \tag{3.32}$$

$$K_2 = \left(\frac{37530}{\mathrm{Re}_c[i]} \right)^{16} \tag{3.33}$$

Here, ε_r represents the absolute roughness of the channel's inner walls. This calculation is crucial for evaluating the frictional losses within the channel as the coolant flows through it. The friction factor correlation is sourced from Churchill's work on friction factor equations, which span all fluid flow regimes [25].

- **Pressure Drop Calculation:** The pressure drop $\Delta p[i]$ across each node is calculated using the following formula:

$$\Delta p[i] = \xi[i] \cdot \frac{L_{\text{node}}}{D_h[i]} \cdot \frac{\dot{m}^2_{c,\text{per\_channel}}}{2 \cdot \rho_c[i] \cdot A_{\text{node}}[i]^2} \tag{3.34}$$

where $\xi[i]$ is the friction factor, L_{node} is the length of the node, $\rho_c[i]$ is the coolant density, and $A_{\text{node}}[i]$ is the cross-sectional area. In this model, entrance and exit pressure drops are assumed to be zero, focusing solely on the core frictional losses. The pressure difference due to height variations between entry and exit points is also neglected, as gravitational effects are minimal compared to frictional forces.

- **Outlet Temperature Calculation:** The outlet temperature $T_{\text{outlet\_new}}[i]$ for each

node is iteratively updated based on the heat transfer rate and mass flow rate:

$$T_{\text{outlet\_new}}[i] = \frac{Q_{\text{channel}}[i]}{\dot{m}_{c,\text{per\_channel}} \cdot c_{p_c}[i]} + T_{\text{inlet}}[i] \tag{3.35}$$

where $Q_{\text{channel}}[i]$ is the heat transfer rate, $\dot{m}_{c,\text{per\_channel}}$ is the mass flow rate per channel, and $c_{p_c}[i]$ is the specific heat capacity at node i. This calculation ensures that the temperature increase in the coolant is proportional to the heat absorbed from the combustor.

- The outlet pressure $p_{\text{outlet\_new}}[i]$ is similarly iteratively updated based on the pressure drop:

$$p_{\text{outlet\_new}}[i] = p_{\text{inlet}}[i] - \Delta p[i] \tag{3.36}$$

- The iteration continues until the temperature and pressure differences between successive iterations fall within a predefined tolerance, ensuring that the model has converged to an accurate solution.

3. **Sequential Node Continuity:** For cooling channels with multiple nodes, the outlet temperature $T_{\text{outlet}}[i]$ and pressure $p_{\text{outlet}}[i]$ at each node i serve as the inlet conditions for the subsequent node $i + 1$. This sequential approach maintains continuity in the fluid properties and ensures that the model accurately represents the dynamics within the cooling channels.

The final outlet temperature and pressure for each node are recorded, completing the calculation of the cooling channel's behavior from inlet to outlet. The total heat transfer Q_c^{total} across all nodes is summed to provide an overall assessment of the cooling effectiveness.

This section outlines a comprehensive model for understanding the cooling dynamics within gas turbine engines, focusing on how hydrogen, as a coolant, interacts with the system. The accurate prediction of fluid properties and heat transfer ensures that the cooling system can be optimized for maximum efficiency, supporting the broader operational goals of the gas turbine.

3.2.4 Flowchart

Following the explanation of the computational methodologies for the cold fluid (cooling channels), the flowchart in Figure 3.4 provides a clear visual representation of the steps involved in calculating the cold fluid properties. This diagram shows the iterative process, starting with the initial setup of inlet conditions and geometric parameters, through to the final calculations for pressure drop and heat transfer rate.

The flowchart highlights the key stages in the process, including the iterative solving for outlet conditions and the use of CoolProp to obtain thermodynamic properties such as viscosity, density, and specific heat. It also emphasizes the importance of convergence within a set

tolerance, ensuring accuracy in the predictions of outlet temperature and pressure. This methodology allows for the determination of the cold fluid's contribution to the overall performance of the heat exchanger.

For a more detailed understanding of the code structure and implementation, please refer to the Python code provided in Annex A.2.

3.3 Performance Evaluation

In this section, we delve into the evaluation of the heat exchanger's performance within the gas turbine system. The heat exchanger is a critical component, ensuring efficient thermal management by facilitating the transfer of heat between the hot combustion gases and the coolant, hydrogen. Evaluating its performance involves a thorough assessment of key metrics.

These performance metrics are essential for understanding how effectively the heat exchanger operates under varying conditions. They provide valuable insights into the heat exchanger's capacity to transfer heat, identify potential areas for optimization, and ensure that the system adheres to the required thermal performance standards. The computational models developed in this study are designed to integrate these metrics, offering a comprehensive analysis of the heat exchanger's behavior, while accounting for the complex interactions between fluid properties and thermal gradients present within the system.

3.3.1 Computational Modeling of Heat Exchanger Performance

The efficacy of a heat exchanger is fundamentally gauged by its ability to transfer heat between hot and cold fluids efficiently. Computational modeling serves as a crucial tool in this evaluation, offering detailed insights into the dynamics of heat transfer, fluid flow behavior, and the overall effectiveness of the heat exchanger under various operational scenarios.

To quantify the key performance metrics of the heat exchanger, various computational approaches and models are employed, focusing on the overall heat transfer coefficient (U), the number of transfer units (NTU), and the effectiveness (ε). These methodologies are integrated into the computational framework to evaluate the heat exchanger's thermal performance comprehensively. Such rigorous analysis not only facilitates the optimization of the heat exchanger's design and operation but also ensures that it meets the stringent performance criteria necessary for efficient and reliable operation within the gas turbine system.

3.3.1.1 Calculation of Overall Heat Transfer Coefficient (U)

The overall heat transfer coefficient (U) is a critical parameter that encapsulates the heat exchanger's ability to transfer heat between the hot and cold fluids. This coefficient considers

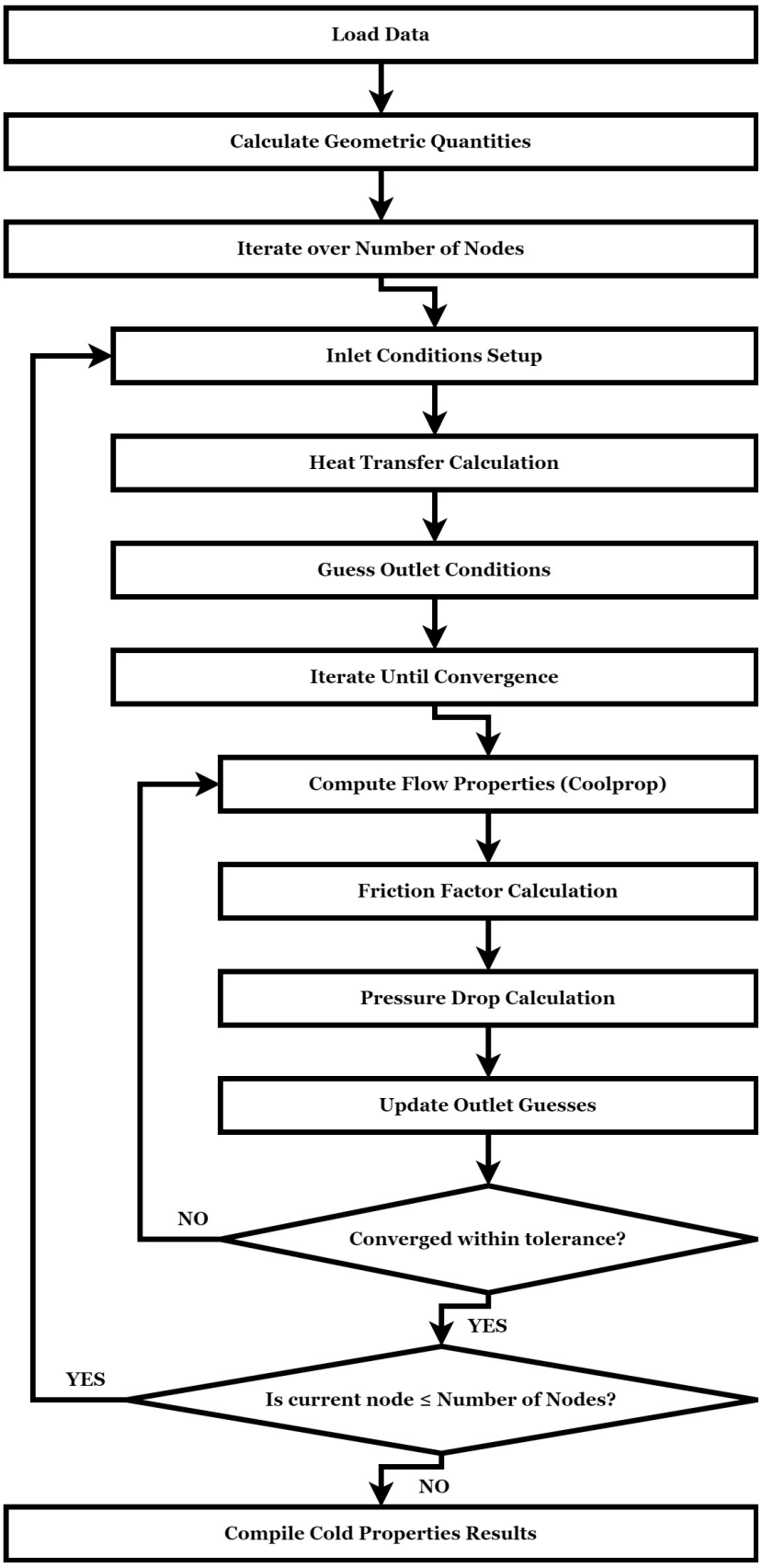

Figure 3.4: Flowchart of Cold Fluid (Cooling Channels) Calculations

the convective heat transfer coefficients on both sides of the heat exchanger and the thermal resistance due to conduction through the exchanger's materials. The approach to calculating U differs depending on whether the system is modeled as a single-node or a multi-node system.

Method 1: Single Node Model

1. **Calculation of Nusselt Number (Nu):**

   - For single-node models, the calculation begins with determining the Nusselt number (Nu), as discussed in (2.2.2.3), is a dimensionless number that describes the ratio of convective to conductive heat transfer across the boundary layer of the fluid. The Dittus-Boelter equation is applied to calculate the Nusselt number for turbulent flow:

   $$Nu_c = 0.023 \cdot Re_c^{0.8} \cdot Pr_c^{0.4} \tag{3.37}$$

   where Re_c is the Reynolds number for the cold fluid, and Pr_c is the Prandtl number.

   - The Dittus-Boelter equation was chosen for its simplicity and widespread application in engineering practices, particularly for turbulent flow in smooth pipes, which is relevant to the operating conditions of this system. This correlation is especially advantageous due to its empirical basis and ease of use, making it highly suitable for initial design calculations. However, it is important to note that this correlation is best suited for flows with moderate temperature gradients and may not accurately capture effects in systems with large temperature differences or non-circular geometries. A detailed comparison of this correlation with other Nusselt number correlations can be found in heat transfer literature, such as in the textbooks by Bergman et al. [26] and by Shah and Sekulic [27].

2. **Calculation of Convective Heat Transfer Coefficients:**

   - With the Nusselt number calculated, the convective heat transfer coefficient for the cold fluid (h_c) is determined using:

   $$h_c = \frac{Nu \cdot k_c}{D_{h,c}} \tag{3.38}$$

   - The convective heat transfer coefficient for the hot fluid (h_h) can be similarly calculated if needed, though, in this model, it is typically provided as part of the input data.

3. **Computation of Overall Heat Transfer Coefficient (U):**

   - The overall heat transfer coefficient U is computed by considering the thermal

resistances in series for the hot and cold fluids:

$$U = \frac{1}{\frac{1}{h_h} + \frac{1}{h_c}} \tag{3.39}$$

This equation is a specific application of the general relationship for the overall heat transfer coefficient, as described by equation (2.18).

- This equation accounts for the thermal resistances due to convection from the hot fluid to the heat exchanger surface, conduction through the exchanger material, and convection from the exchanger surface to the cold fluid, providing a comprehensive measure of the exchanger's thermal performance.

Method 2: Multi-Node Model

1. **Application of Logarithmic Mean Temperature Difference (LMTD):**

   - For multi-node models, where the temperature difference between the hot and cold fluids varies along the length of the exchanger, the Logarithmic Mean Temperature Difference (LMTD) is utilized. The general formula for LMTD, as discussed in (2.2.3.3), is:

$$LMTD = \frac{\Delta T_1 - \Delta T_2}{\ln\left(\frac{\Delta T_1}{\Delta T_2}\right)} \tag{3.40}$$

   where ΔT_1 and ΔT_2 represent the temperature differences at the two ends of the heat exchanger. These temperature differences, ΔT_1 and ΔT_2, vary depending on whether the heat exchanger is configured in parallel flow or counterflow, as outlined in (2.22) and (2.23).

   - This method is chosen over the direct calculation of U as used in the single-node model because it better captures the varying temperature gradients across the length of the heat exchanger, making it more suitable for systems where temperature changes significantly from inlet to outlet, as described in the Literature Review.

2. **Calculation of Overall Heat Transfer Coefficient (U):**

   - The overall heat transfer coefficient U in the multi-node model is calculated using the total heat transfer rate Q_{h} from the hot fluid and the heat exchanger's surface area A, considering the LMTD:

$$U = \frac{Q_{\text{h}}}{A \times \text{LMTD}} \tag{3.41}$$

   This equation is derived from (2.24), where the relationship between the heat transfer rate Q, the overall heat transfer coefficient U, the surface area A, and the log mean temperature difference LMTD is established.

- This approach allows for a more accurate calculation of U, particularly in systems with significant temperature variation along the exchanger's length, ensuring that the thermal performance is accurately represented.

3.3.1.2 Calculation of NTU

1. **Calculation of Heat Capacity Rates:**

   - The heat capacity rate for the hot fluid (C_h) and the cold fluid (C_c) are first calculated based on the mass flow rate ($\dot{m}$) and the specific heat capacity (c_p) at constant pressure for each fluid as shown in (2.19). These are given by:

$$C_h = \dot{m}_h \cdot c_{p,h} \tag{3.42}$$

$$C_c = \dot{m}_c \cdot c_{p,c} \tag{3.43}$$

   - The minimum and maximum heat capacity rates are determined as:

$$C_{\text{min}} = \min(C_h, C_c) \tag{3.44}$$

$$C_{\text{max}} = \max(C_h, C_c) \tag{3.45}$$

     These values are essential for calculating NTU and further evaluating the heat exchanger's effectiveness.

2. **Calculation of NTU:**

   - The NTU is then calculated using the overall heat transfer coefficient (U), the total surface area of the combustion chamber (A), and the minimum heat capacity rate (C_{min}) as defined in (2.25):

$$NTU = \frac{U \cdot A}{C_{\text{min}}} \tag{3.46}$$

   - This formula indicates that NTU is directly proportional to the heat transfer capability of the exchanger (represented by $U \cdot A$) and inversely proportional to the smallest heat capacity rate of the fluids.
   - The NTU value obtained provides a measure of the potential heat transfer in the exchanger relative to the thermal capacity of the fluid with the smallest heat capacity rate.

By calculating the NTU, the performance of the heat exchanger can be effectively evaluated, providing insights into how efficiently the system can transfer heat between the hot and cold

fluids under the given operating conditions. This metric is a fundamental component in the analysis and optimization of heat exchanger design and operation.

3.3.1.3 Effectiveness Calculation

The effectiveness (ε) of the heat exchanger is a crucial metric that quantifies the ratio of the actual heat transfer to the maximum possible heat transfer within the system. In the context of this work, the effectiveness is computed based on the Number of Transfer Units (NTU) method, which is well-established in heat exchanger theory. The relationship between effectiveness and NTU varies depending on the flow configuration, specifically whether the heat exchanger operates in a counterflow or parallel flow mode.

The empirical equations used in this work for calculating effectiveness (ε) are derived from the fundamental principles of heat exchanger theory and are detailed in the literature. These equations, known as the ε-NTU relations, provide a direct way to determine the effectiveness based on the calculated NTU and the capacity rate ratio (C_r), as shown in (2.20). As mentioned in the literature review (Chapter (2)), these relations are pivotal for understanding the performance of various types of heat exchangers, including those used in high-temperature environments like gas turbines.

For a counterflow heat exchanger, the effectiveness is calculated using the following relation:

$$\varepsilon = \begin{cases} \frac{1-\exp(-\text{NTU}\cdot(1-C_r))}{1-C_r\cdot\exp(-\text{NTU}\cdot(1-C_r))} & \text{if } C_r < 1 \\ \frac{\text{NTU}}{1+\text{NTU}} & \text{if } C_r = 1 \end{cases} \tag{3.47}$$

For a parallel flow heat exchanger, the effectiveness is given by:

$$\varepsilon = \frac{1-\exp(-\text{NTU}\cdot(1+C_r))}{1+C_r} \tag{3.48}$$

These ε-NTU relations are crucial in the design and analysis of heat exchangers as they provide a straightforward method to predict the thermal performance without requiring detailed knowledge of the temperature distribution within the heat exchanger. The derivation and thorough discussion of these relations are provided in the reference text by Saari [28], which is also mentioned in the literature review.

In this section provides a comprehensive evaluation of the heat exchanger's performance within the gas turbine system, emphasizing the critical metrics of overall heat transfer coefficient (U), number of transfer units (NTU), and effectiveness (ε). Through a detailed computational approach, we examined how these metrics influence the efficiency of heat transfer between the hot combustion gases and the hydrogen coolant. The computational models implemented effectively capture the complex thermal interactions within the system, offering

insights into the factors that drive performance under various operating conditions. By integrating these performance metrics, we can ensure that the heat exchanger meets the desired thermal management objectives, supporting the overall efficiency and reliability of the gas turbine system.

3.3.2 Flowchart

In Figure 3.5, the computational process for evaluating the heat exchanger's performance is visually represented. This flowchart provides an overview of the steps involved in calculating key performance metrics, including the overall heat transfer coefficient (U), the Number of Transfer Units (NTU), and the effectiveness (ε).

The process begins by determining whether the number of nodes used in the hot and cold fluid calculations exceeds one, which dictates the approach taken for calculating the heat transfer coefficient. Depending on the result, either the Log Mean Temperature Difference (LMTD) method or Nusselt-Prandtl-based calculations are used to compute the overall heat transfer coefficient. This value is subsequently used to calculate the NTU and effectiveness of the heat exchanger, two key metrics that indicate how efficiently the heat exchanger operates.

The final step involves compiling all calculated performance results, providing a comprehensive overview of the heat exchanger's behavior under the simulated conditions. For further details on the code and methodology, please refer to Annex A.2, where the complete Python code is provided.

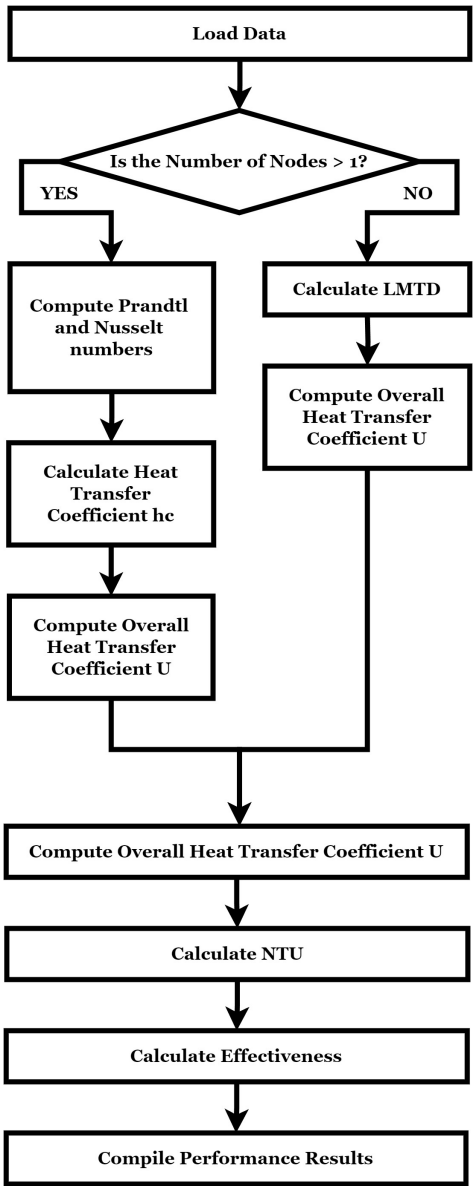

Figure 3.5: Flowchart of Performance Evaluation Calculations

Chapter 4

Results

4.1 Model Validation

The objective of this section is to validate the computational model developed for heat exchanger analysis in gas turbines by comparing its predictions with computational data from the work of V. Fernández-Villacé and G. Paniagua [29]. Their study employs a detailed numerical model to evaluate the performance of an air turbo-rocket expander engine, particularly its heat exchanger (regenerator), across a range of Mach numbers from 1.5 to 4.5. This provides a valuable computational dataset for validating key performance metrics such as heat transfer rates and pressure drops under varying conditions.

The work of V. Fernández-Villacé and G. Paniagua relies on a multi-dimensional computational model that evaluates the behavior of different engine components, including the combustor and cooling system. Their results serve as a comprehensive basis for comparison with the single-node mode in this thesis, ensuring that the simplified model can be validated under different operating conditions.

This thesis focuses on the single-node mode validation, which simplifies the heat exchanger system into a single control volume, averaging spatial variations in temperature and flow. While multi-nodal methods could offer a more detailed spatial resolution, capturing effects such as thermal gradients and localized flow behavior, they are excluded from this validation. The decision to focus on the single-node mode was driven by the thesis' scope, prioritizing an assessment of system-level performance before moving on to more complex simulations.

This validation aims to confirm that the single-node model accurately predicts key metrics such as heat transfer and pressure drop under varying Mach conditions. Additionally, the model's predictions for heat exchanger effectiveness and NTU will be compared to reference values from *Fundamentals of Heat Exchanger Design* by Shah and Sekulić [27], which offers typical benchmarks for heat exchanger performance in industrial gas turbine applications.

4.1.1 Input Data for the Computational Model

The validation process was conducted based on the assumptions and computational data from V. Fernández-Villacé and G. Paniagua's work on an air turbo-rocket expander engine. The input data for the model were chosen to match the computational conditions as closely as possible, ensuring consistency between the simulations and the literature. The specific input files used for the model, containing data for the different Mach numbers, are provided

in the annexes (see Annex A.1).

4.1.1.1 Combustor

- The assumptions made by V. Fernández-Villacé and G. Paniagua for the combustor are completely compatible with those made for the combustion chamber in our model, as shown in Section 3.1.1. Both works assume ideal gas behavior for the hot gases, as well as chemically frozen flow after combustion. These assumptions ensure that the gas composition remains constant and uniform throughout the entire combustor.
- The combustor input parameters, such as mass flow rate, stagnation temperature, and pressure, were adjusted according to the aircraft Mach numbers (ranging from 1.5 to 4.5). Only a single value for the overall combustor stagnation temperature was provided, corresponding to the uniform temperature across the combustor. This restriction necessitated the use of a single-node method, as a multi-node approach would require more detailed temperature profiles.
- All the information is taken directly from Table 5 in the work of V. Fernández-Villacé and G. Paniagua, with the exception of:
  - **Combustor mass flow calculation:** The combustor mass flow rate was not directly available. It was calculated by first determining the air mass flow from the overall air mass flow of the Low Speed Intake, minus the percentage of air bled from the system, and then dividing by the 6 air turbo-rocket engines. This air mass flow was then summed with the hydrogen mass flow, which was calculated separately as described in Table 4.2. This total combustor mass flow reflects the combined contribution of both air and hydrogen flowing through the combustor for each engine.
  - **Throat length calculation:** The throat length was derived by correlating the given combustor length with data extracted from Fig 6.a of the work by V. Fernández-Villacé and G. Paniagua.
  - **Combustor sectional area:** This was taken directly from Table 1 of V. Fernández-Villacé and G. Paniagua's work, which details the dimensions of the air turbo-rocket components.

The combustor input data is summarized in the following Table 4.1.

4.1.1.2 Cooling Channels

- The assumptions made by V. Fernández-Villacé and G. Paniagua for the cooling channels are fully compatible with those used in our model, as described in Section 3.2.1 of the present work. Both models assume real gas behavior for hydrogen, allowing for more accurate thermophysical property calculations under extreme conditions.

Table 4.1: Combustor Input Data for the Computational Model Across Different Mach Numbers

Mach Number	Combustor Mass Flow Rate (kg/s)	Combustor Stagnation Temperature (K)	Combustor Stagnation Pressure (Pa)	Combustion Chamber Dimensions			
				Combustor Sectional Area (m^2)	Combustor Length (m)	Combustor Throat Sectional Area (m^2)	Combustor Throat Length (m)
1.5	228.8	2290	112000	3.183	10.8	2.895	1.2
2	220.8	2310	109000			2.895	
3	202.9	2480	137000			2.167	
4	177.1	2110	329000			0.667	
4.5	152.5	2270	429000			0.458	

- Since all the tank conditions (temperature, pressure, and pump pressure ratio) are known from V. Fernández-Villacé's work [30], it was possible to apply the method described in **Tank Conditions** (3.2.3.1) for calculating the inlet conditions of the cooling channels. This ensures an accurate determination of the hydrogen coolant's inlet pressure, temperature, and mass flow rate.
- All the information is taken directly from Table 5 in the work of V. Fernández-Villacé and G. Paniagua, except for:
  - **Hydrogen mass flow calculation:** The hydrogen mass flow rate was not directly available and was instead calculated as the overall hydrogen mass flow rate minus the percentage of that flow used by the ramjet engine. The remaining hydrogen flow was then divided by the 6 air turbo-rocket engines.
  - **Number of channels and dimensions:** The number of cooling channels and their dimensions (inlet width, inlet height, outlet height) were taken directly from Table 4 of V. Fernández-Villacé and G. Paniagua's work. These dimensions remained consistent with their design for the cooling system, which also utilized variable channel heights.

Table 4.2 shows the cooling channel input data.

Table 4.2: Cooling Channels Input Data for the Computational Model Across Different Mach Numbers

Mach Number	Cooling Channel Mass Flow Rate (kg/s)	Hydrogen Initial Temperature (K)	Hydrogen Initial Pressure (Pa)	Pump Pressure Ratio	Cooling Channel Dimensions					
					Number of Channels	Inlet Width (m)	Inlet Height (m)	Outlet Width (m)	Outlet Height (m)	Inner Walls Rugosity (m)
1.5	6.93	20	300000	16	94	0.066	0.003	0.066	0.005	5e-5
2	6.70			12						
3	6.14			7						
4	2.60			5						
4.5	2.31			4						

4.1.1.3 Flow Configuration

The flow configuration was set to **parallel flow** to ensure consistency with the work of V. Fernández-Villacé and G. Paniagua. In parallel flow configuration, the hydrogen coolant and the hot gases from the combustor flow in the same direction through the heat exchanger. This

setup was chosen because it mirrors the conditions analyzed in their study, ensuring that the results remain comparable.

4.1.2 Results: Predicted and Reference Data

In this section, the results from the computational model are compared with reference data from V. Fernández-Villacé and G. Paniagua [29] for heat transfer rate and pressure drop. Additionally, the model's predictions for effectiveness and NTU are benchmarked against values from "Fundamentals of Heat Exchanger Design" by Shah and Sekulić [27]. These comparisons aim to validate the model's accuracy across a range of Mach numbers and heat exchanger performance metrics.

Another important result comparison is the outlet temperature of the cooling channels. However, since this data is not directly available in the work of V. Fernández-Villacé and G. Paniagua—where only the temperature after the combustor heat exchanger and nozzle heat exchanger is reported—the model's predictions for outlet temperature will only be compared to pressure drop or outlet pressure and overall heat transfer. These comparisons provide a comprehensive assessment of the model's accuracy in predicting the heat exchanger's behavior under different operating conditions.

The detailed results files, which contain all the calculated parameters for the combustor and cooling channels (e.g., heat transfer rate, fluid properties, and flow conditions), are included in the annexes. These files present the results for five different conditions (aircraft Mach 1.5, 2, 3, 4, and 4.5) and can be found in Annex A.3.

4.1.2.1 Heat Transfer Rate

The heat transfer rate is a fundamental parameter in evaluating the performance of the heat exchanger, representing the amount of thermal energy transferred from the hot gases in the combustor to the coolant in the cooling channels. This comparison assesses how well the computational model predicts heat transfer across different Mach numbers, using reference data from V. Fernández-Villacé and G. Paniagua [29].

To obtain the heat transfer rate for a single air turbo-rocket engine, the overall heat transfer rate for the entire system was first calculated. Then, only the heat transfer occurring within the air turbo-rocket combustion chambers was considered. The final value for a single engine was obtained by dividing this heat transfer by 6, as the system consists of six air turbo-rocket engines.

Table 4.3 presents the model's predicted heat transfer rates alongside the reference values for each Mach number. The percentage error is included to quantify the deviations between the two sets of data, providing a clear metric for evaluating the accuracy of the model under varying operational conditions.

Table 4.3: Comparison of Heat Transfer Rates Between the Model Prediction and V. Fernández-Villacé and G. Paniagua's Data

Mach Number	Heat Transfer [MW]		Percentage Error [%]
	Predicted Values	Literature Values	
1.5	41.0	43.4	5.53
2	40.0	43.1	7.19
3	5.40	42.8	87.4
4	0.0803	23.2	99.7
4.5	0.0263	22.7	99.9

4.1.2.2 Pressure Drop

Pressure drop across the cooling channels is another key performance metric for evaluating the effectiveness of the heat exchanger. It reflects the resistance to flow experienced by the coolant as it passes through the cooling channels, which directly affects the overall efficiency of the cooling system.

The outlet pressure of the cooling channels is not explicitly provided in the reference data from V. Fernández-Villacé and G. Paniagua [29]. Instead, the inlet pressure is known, and the percentage of pressure drop through the heat exchanger located in the combustion chamber of the air turbo-rocket is provided. This percentage was used to calculate the outlet pressure, allowing for a direct comparison between the predicted and reference pressure drop values.

Table 4.4 compares the pressure drop values predicted by the computational model with the reference values from V. Fernández-Villacé and G. Paniagua. The percentage error for each Mach number is also provided to quantify the deviation between the model and the literature data.

Table 4.4: Comparison of Pressure Drop Between the Model Prediction and V. Fernández-Villacé and G. Paniagua's Data

Mach Number	Input Pressure [Pa]		Outlet Pressure [Pa]		Pressure Drop		
	Predicted Values	Literature Values	Predicted Values	Literature Values	Predicted Values [Pa]	Literature Values [Pa]	Error [%]
1.5	4.8e6	4.7e6	4.399e6	4.4e6	0.401e6	0.3e6	11.4
2	3.6e6	3.7e6	3.084e6	3.3e6	0.516e6	0.4e6	29.0
3	2.1e6	2.2e6	1.971e6	1.6e6	0.129e6	0.6e6	78.5
4	1.5e6	1.5e6	1.496e6	1.3e6	0.004e6	0.2e6	98.0
4.5	1.2e6	1.1e6	1.197e6	0.88e6	0.003e6	0.22e6	98.6

4.1.2.3 Effectiveness and NTU

The effectiveness (ε) and number of transfer units (NTU) are important performance metrics for heat exchangers, indicating how well the system transfers heat relative to its theoretical maximum. The values predicted by the model are compared with the approximate benchmarks provided by Shah and Sekulić in "Fundamentals of Heat Exchanger Design" [27]. These benchmarks suggest that regenerators in industrial gas turbines typically exhibit

NTU values around 10, with corresponding **effectiveness values close to 90%**.

Table 4.5 presents the model-predicted effectiveness and NTU values for various Mach numbers. These values are then compared qualitatively with the reference ranges from Shah and Sekulić, which provide a general framework for expected NTU and effectiveness in regenerators.

Table 4.5: Effectiveness (ε) and NTU Predicted by the Model

Mach Number	Effectiveness (ε)	NTU
1.5	0.812	2.77
2	0.813	2.80
3	0.562	0.925
4	0.411	0.540
4.5	0.343	0.426

While the comparison focuses on the alignment of the predicted values with the approximate ranges given by Shah and Sekulić, the effectiveness and NTU values predicted by the model vary across the Mach number range, providing insights into the performance of the heat exchanger.

4.1.3 Discussion of Results

The results from the computational model highlight a clear distinction in performance between lower and higher aircraft Mach numbers. At aircraft Mach 1.5 and 2, the model demonstrates reasonable accuracy, providing satisfactory predictions for heat transfer rates, pressure drops, NTU, and effectiveness. However, as the aircraft Mach number increases to 3, 4, and 4.5, the model's accuracy diminishes significantly. The most critical issue is the substantial underestimation of the heat transfer rate, which in turn affects the accuracy of other performance metrics such as pressure drop, NTU, and effectiveness. This discrepancy suggests that the methods and assumptions employed by the model, particularly in handling higher aircraft Mach numbers, are insufficient to capture the complex physical phenomena occurring in those regimes.

One of the key contributors to the model's underestimation of the heat transfer rate is the treatment of throat area and geometry, which directly affects local gas velocity and heat transfer rates. The throat is a critical region where flow typically reaches a Mach number of 1 (choked flow), and any changes in its geometry directly affect the overall gas velocity and heat transfer rates. However, in the single-node model, the detailed behavior inside the combustor and throat, including localized velocity variations and boundary layer effects, cannot be explicitly captured. Although the model provides an overall Mach number for the combustor, it cannot account for the rapid acceleration, viscous effects, and boundary layer interactions that occur in regions like the throat.

As the aircraft transitions to higher aircraft Mach numbers (such as from Mach 2 to 3 and beyond), the throat sectional area decreases significantly. While the model does not directly

simulate the detailed flow behavior in these regions, we infer that the reduction in throat area leads to an increase in local gas velocity, which likely reduces boundary layer thickness and decreases the efficiency of heat transfer. The Bartz formula 3.12, used to estimate the convective heat transfer coefficient in high-speed flows, is highly sensitive to geometric changes. Bartz (1965) [24] notes that rapid changes in geometry, especially in accelerating flows, can lead to inaccuracies in the predicted heat transfer rates. Because the single-node method does not evaluate variations in velocity and boundary layer development directly, the model relies on the empirical Bartz correlation, which may not fully capture the complex flow phenomena at the throat, including turbulent boundary layers and rapid acceleration. This limitation likely contributes to the underestimation of the heat transfer rate.

These challenges persist and worsen at even higher aircraft Mach numbers, such as Mach 4 and 4.5, where the heat transfer coefficient continues to drop sharply. At these extreme conditions, we infer that the flow accelerates rapidly through the throat, further reducing boundary layer thickness and exacerbating the limitations of the Bartz formula. The model, constrained by the single-node approach and the use of empirical correlations, is not equipped to handle the dramatic changes in geometry and local flow properties at these high Mach numbers, leading to significantly lower predicted heat transfer rates.

Additionally, the single-node model's assumption of steady-state, quasi-one-dimensional (quasi-1D) flow, while simplifying the treatment of flow through the combustor and throat, is insufficient for high aircraft Mach number conditions. As the aircraft Mach number increases, the model becomes less capable of accurately predicting the flow properties, particularly the velocity inside the combustor. The simplifications inherent in this approach fail to capture localized phenomena, and as a result, the combustor Mach number tends to be inaccurately predicted across different aircraft Mach numbers, compounding the inaccuracies in heat transfer predictions.

Moreover, the inviscid flow assumption, which neglects viscosity and boundary layer thickening, becomes a significant limitation at higher aircraft Mach numbers. Viscous effects, such as drag and dissipation, become more pronounced in regions like the throat, even though the combustor flow remains subsonic. The model's inability to capture these effects results in an underestimation of the heat transfer rate and other flow properties, particularly at aircraft Mach 3 and above.

The model's predictions for effectiveness and NTU also reflect these limitations. The NTU values, which are expected to be around 10 for regenerators in gas turbine applications, are significantly lower in the model predictions, particularly for aircraft Mach numbers 1.5 and 2, where NTU values of approximately 2.77 and 2.80 were observed, respectively. Similarly, the effectiveness values predicted by the model—around 81% for aircraft Mach 1.5 and 2—fall short of the expected values, which ideally should approach 90%. These discrepancies can be attributed to the averaging inherent in the single-node configuration. While the heat transfer rate itself is accurately predicted, the model cannot account for spatial variations in temperature and flow properties across the heat exchanger, which are critical for accurately determining NTU and effectiveness. The oversimplification of the temperature profile leads

to underestimation in these metrics, despite the correct heat transfer rate, which further highlights the limitations of the single-node model.

Based on the ideal gas assumption, the relationship between stagnation and static temperature also becomes increasingly unreliable at higher aircraft Mach numbers. At Mach 3 and beyond, real gas effects, such as hydrogen dissociation and changes in specific heat capacity, begin to dominate, further distorting the predicted combustor Mach number and heat transfer rate. The model assumes constant thermodynamic properties, such as specific heat and the gas constant, for ideal gases at moderate aircraft Mach numbers but breaks down under higher conditions where real gas behavior is significant.

Finally, the simplified treatment of mass flow rate and velocity further limits the model's accuracy at higher aircraft Mach numbers. The model assumes that mass flow is conserved and calculates velocity based on the Mach number and static temperature, but as the flow heats up and accelerates through the combustor and throat, these simplified gas dynamic relations fail to account for variations in gas composition and state. This introduces further errors in the predicted velocity and Mach number inside the combustor, which, when combined with the limitations of the single-node method and ideal gas assumptions, leads to inaccurate predictions of heat transfer rate and flow behavior at aircraft Mach 3 and above.

In summary, while the computational model performs adequately at lower aircraft Mach numbers, its inability to accurately predict heat transfer rates at higher aircraft Mach numbers exposes the limitations of the underlying assumptions, particularly in dealing with complex flow phenomena and geometric variations in the combustor and throat. The model's use of empirical correlations, such as the Bartz formula, and its simplified treatment of flow properties and gas dynamics fail to account for the significant changes in behavior at higher aircraft Mach numbers. Addressing these limitations will be crucial for improving the accuracy of future simulations, particularly for high-speed flow conditions.

4.2 Parametric Studies

The parametric studies presented in this section aim to evaluate the sensitivity of the heat exchanger's performance to various key design and operating parameters, specifically within the framework of the single-node method. As with the validation process, the parametric studies are limited to the single-node configuration, providing an overall system perspective rather than capturing detailed spatial variations. Despite this limitation, these studies offer valuable insights into how changes in factors such as stagnation temperature, mass flow rate, throat area, and cooling channel geometry affect critical performance metrics, including heat transfer rate, convective heat transfer coefficient, and pressure drop.

It is important to note that the current version of the code is not fully optimized for parametric studies. The code does not support automated interval-based analysis, requiring each parameter variation to be conducted manually, one by one. This limitation adds complexity and time to the parametric studies but still allows for a systematic evaluation of key factors

influencing the system's performance.

The selection of parameters for these studies is based on their relevance to the overall thermal and fluid dynamic behavior of the system. The performance of the heat exchanger is susceptible to both the thermodynamic properties of the working fluids and the geometric configuration of the flow paths. Therefore, a systematic evaluation of these parameters is crucial for understanding the limitations of the current model and identifying potential improvements for future designs.

By varying these parameters, the following subsections explore the individual and combined effects on the heat exchanger's performance, providing key insights that can be applied to optimize the system under different operating conditions.

4.2.1 Parametric Study 1: Influence of Combustor Stagnation Temperature and Mass Flow Rate on Heat Transfer Performance

The first parametric study was designed to explore the relationship between the heat transfer rate and two critical parameters: combustor stagnation temperature and combustor mass flow rate. These parameters were chosen because they directly affect the convective heat transfer rate, making them essential factors in determining the overall thermal exchange in the system. Their influence is particularly important for the design and optimization of high-performance engines, where efficient heat management is vital for performance and safety. The rest of the initial parameters were kept the same as in the validation study for aircraft Mach 1.5, ensuring consistency with the baseline case.

The stagnation temperature, representing the total temperature of the gas entering the combustor, varied between 1800 K and 3000 K. This range covers typical operational conditions of high-speed propulsion systems, such as air turbo-rocket engines, where gas temperatures often reach these high values. Stagnation temperature directly influences the thermal energy available in the flow, and thus, the potential heat transfer rate. As the stagnation temperature increases, the difference between the gas and wall temperatures rises, leading to an increase in the heat transfer rate.

Simultaneously, the combustor mass flow rate was varied between 100 kg/s and 300 kg/s. This range reflects typical operating conditions in similar propulsion systems, where changes in combustor mass flow have a substantial effect on both heat transfer rate and overall system performance. Higher combustor mass flow rates increase the capacity of the system to transport thermal energy, enhancing the heat transfer rate, while also impacting other factors such as pressure drop.

These two parameters were studied together as they jointly determine the convective heat transfer rate, described by the fundamental equation used in the model (see Equation 3.13).

Analyzing these parameters in tandem provides a comprehensive understanding of how combustor mass flow rate and stagnation temperature interact to drive the overall heat transfer

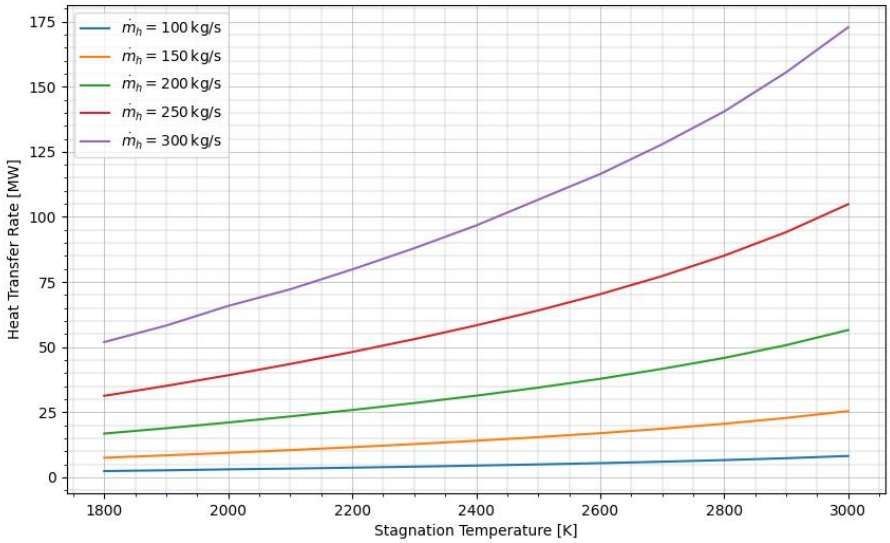

Figure 4.1: Heat Transfer Rate vs. Stagnation Temperature for Different Mass Flow Rates

performance.

The results of this study, presented in Figure 4.1, show that the heat transfer rate increases significantly with both higher stagnation temperatures and combustor mass flow rates. Larger stagnation temperatures provide more thermal energy to the flow, while higher mass flow rates allow for more effective heat transfer to the cooling channels.

As depicted in the figure, increasing the stagnation temperature from 1800 K to 3000 K leads to a sharp rise in heat transfer rates. This effect is further amplified with higher mass flow rates, where the heat transfer rate reaches up to 175 MW at 300 kg/s and 3000 K. At the lower end, with a mass flow rate of 100 kg/s, the heat transfer rate reaches about 25 MW at the same temperature.

This study underscores the sensitivity of the combustor's heat transfer rate to variations in both combustor stagnation temperature and mass flow rate. It suggests that optimizing these parameters is critical for improving thermal efficiency in the system, particularly in scenarios involving high temperatures and large mass flows where significant improvements in heat transfer performance can be achieved.

4.2.2 Parametric Study 2: Influence of Throat Area and Stagnation Temperature on Convective Heat Transfer Coefficient and Heat Transfer Rate

The second parametric study evaluated how variations in the combustor throat section area and stagnation temperature influence two critical performance parameters: the convective heat transfer coefficient and the overall heat transfer rate. These parameters were chosen due to their significant impact on the heat exchanger's performance, particularly in high-speed

propulsion systems where efficient heat management is essential for system optimization and safety. The rest of the initial parameters were kept the same as in the validation study for aircraft Mach 1.5, ensuring consistency with the baseline case.

The throat area of the combustor is a critical geometric feature that directly affects the gas velocity and, consequently, the heat transfer performance of the system. As discussed in the validation section (4.1.3), the model's underestimation of the heat transfer rate at higher aircraft Mach numbers was partially attributed to the limitations in capturing the flow behavior within the throat area. In particular, the single-node method does not resolve the local variations in velocity and boundary layer development that occur in regions like the throat. These effects become increasingly important as the aircraft Mach number rises, leading to a significant reduction in the predicted heat transfer rate.

The convective heat transfer coefficient is directly related to how efficiently heat is transferred from the hot gas inside the combustor to the cooling channels. This coefficient depends on both the gas flow properties and the surface area available for heat exchange. To further investigate this, the parametric study varied the combustor throat area between 1.5 m^2 and 2.895 m^2, allowing us to explore how changes in this critical geometric feature affect the convective heat transfer coefficient and heat transfer rate. The stagnation temperature was varied between 1800 K and 3000 K to represent the typical operating conditions of high-speed propulsion systems. Stagnation temperature directly influences the thermal energy available for heat exchange, while the throat area governs the flow characteristics and local velocities through the combustor.

These two parameters were studied together because they both strongly influence the convective heat transfer process. The convective heat transfer coefficient (h_h) and the heat transfer rate (Q) are connected through the fundamental equation for heat transfer (see Equation 3.13). Higher stagnation temperatures provide more thermal energy for heat exchange, while larger throat areas allow for higher gas velocities, enhancing the convective heat transfer coefficient.

The results of this parametric study are presented in Figure 4.2, with the left plot showing the heat transfer rate and the right plot depicting the convective heat transfer coefficient as a function of throat area and stagnation temperature.

As shown in the left plot, the heat transfer rate increases significantly with both higher stagnation temperatures and larger throat areas. For stagnation temperatures of 3000 K, the heat transfer rate reaches values exceeding 80 MW at a throat area of 2.895 m^2. This trend is consistent with the hypothesis discussed in the validation section, where the underestimation of heat transfer rates at higher Mach numbers was linked to the inability of the single-node method to capture the geometric and flow variations in the throat region. The increasing throat area allows for a higher local velocity, which enhances the heat exchange between the gas and the cooling channels.

On the right plot, the convective heat transfer coefficient also rises with increasing throat area and stagnation temperature. The higher the throat area, the greater the local velocity,

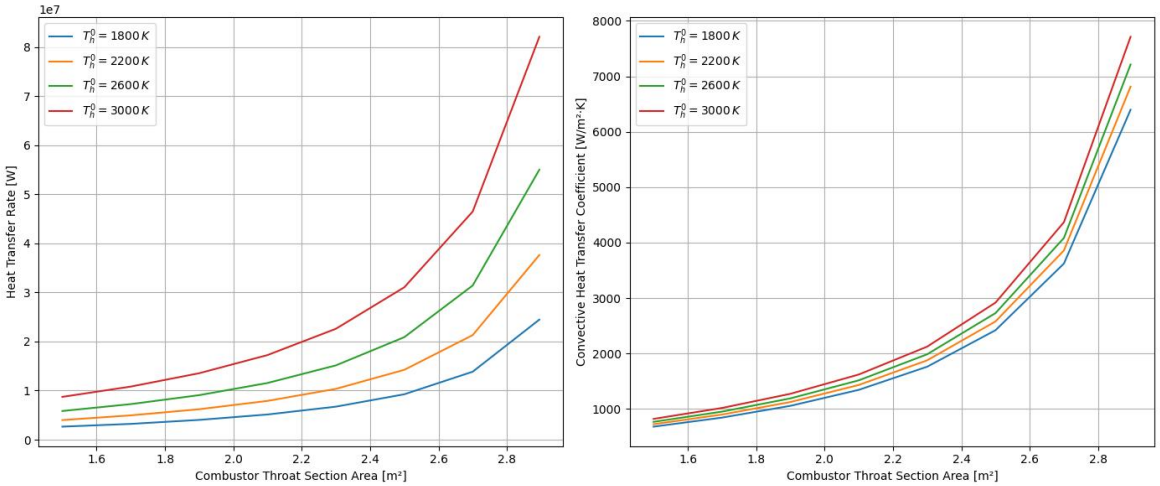

Figure 4.2: Heat Transfer Rate (left) and Convective Heat Transfer Coefficient (right) vs. Throat Area for Different Stagnation Temperatures (T_h^0).

resulting in a more efficient convective heat transfer process. At a stagnation temperature of 3000 K and a throat area of 2.895 m², the convective heat transfer coefficient approaches 7700 W/m²·K.

This study reinforces the earlier observations from the validation section (4.1.3), highlighting the sensitivity of both the convective heat transfer coefficient and the heat transfer rate to variations in the combustor throat area and stagnation temperature. These findings further emphasize the limitations of the single-node model, which does not fully capture the localized flow behavior in the throat region. The results suggest that optimizing the throat area is crucial for enhancing the heat transfer performance of the combustor, particularly at high stagnation temperatures.

In summary, this parametric study demonstrates that the throat area and stagnation temperature strongly influence both the heat transfer rate and the convective heat transfer coefficient. This insight highlights the importance of considering these parameters in the design of high-performance heat exchangers for propulsion systems, where maximizing heat transfer is essential for overall efficiency.

4.2.3 Parametric Study 3: Influence of Hydrogen Mass Flow and Pump Pressure Ratio on Pressure Drop

The third parametric study was conducted to explore the relationship between the hydrogen mass flow rate and the pump pressure ratio, and how these parameters impact the pressure drop across the cooling channels. These parameters are critical in determining the cooling system's performance, as they directly influence the fluid dynamics within the system.

The hydrogen mass flow rate varied between 2 kg/s and 8 kg/s, covering a range of typical operating conditions for high-performance cooling systems. Increasing the mass flow rate leads to higher fluid velocity, which in turn increases the frictional forces and pressure drop.

The pump pressure ratio, which controls the pressure difference driving the coolant through the channels, was varied between 7 and 19. The rest of the initial parameters were kept the same as in the validation study for aircraft Mach 1.5, ensuring consistency with the baseline case.

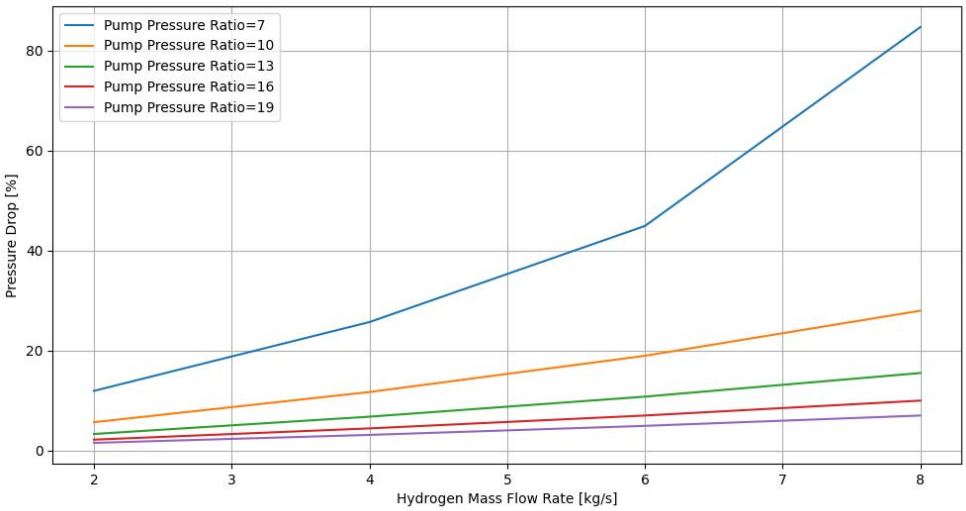

Figure 4.3: Pressure Drop along the Cooling Channels vs Hydrogen Mass Flow for Different Pump Pressure Ratios

These two parameters were studied together to better understand their combined effect on the cooling system's pressure drop. As the hydrogen mass flow rate increases, the fluid experiences higher resistance within the cooling channels, leading to increased pressure losses. Simultaneously, varying the pump pressure ratio directly influences the system's ability to drive the coolant through the channels, affecting the overall pressure drop.

The results of this study, presented in Figure 4.3, show a clear relationship: increasing the hydrogen mass flow rate leads to a significant rise in pressure drop, particularly at lower pump pressure ratios. For a pump pressure ratio of 7, the pressure drop exceeds 80% at the highest mass flow rate of 8 kg/s, indicating that systems with lower pump pressure ratios may struggle to maintain efficient cooling at high flow rates.

At higher pump pressure ratios, such as 16 and 19, the pressure drop remains relatively moderate even as the mass flow rate increases. This result highlights the importance of selecting appropriate pressure ratios to manage flow resistance effectively. As discussed in Parametric Study 4, this trade-off between pressure drop and cooling performance becomes particularly relevant when considering geometric changes in cooling channels.

In conclusion, this parametric study emphasizes the need to balance the hydrogen mass flow rate with the appropriate pump pressure ratio to optimize cooling performance while minimizing pressure drop. Systems operating with higher pump pressure ratios can better handle high-mass-flow conditions, reducing the overall pressure losses and ensuring efficient cooling channel operation.

4.2.4 Parametric Study 4: Influence of Cooling Channel Configuration and Hydrogen Mass Flow on Pressure Drop

The fourth parametric study explores the relationship between the pressure drop along the cooling channels and two important factors: hydrogen mass flow and cooling channel configuration. These parameters are critical because they directly influence the cooling system's performance in propulsion systems, particularly in the context of high-speed engines where hydrogen is commonly used as a coolant. Efficient cooling is essential for maintaining structural integrity and ensuring the thermal efficiency of the system.

In this study, the hydrogen mass flow was varied between 2 kg/s and 10 kg/s, covering a range typical for similar propulsion systems. The mass flow rate affects both the cooling capacity and the pressure drop along the channels. Higher mass flow rates lead to increased fluid friction and resistance, which results in greater pressure losses.

Simultaneously, three different cooling channel configurations were analyzed:

- Configuration 1: Cooling Channel Width = 0.07755 m, Number of Channels = 80
- Configuration 2: Cooling Channel Width = 0.06204 m, Number of Channels = 100
- Configuration 3: Cooling Channel Width = 0.0517 m, Number of Channels = 120

The choice of these configurations was made to maintain a constant total surface area of the cooling channels, achieved by varying both the width and the number of channels. This design ensures that any changes in pressure drop are attributed to the geometric effects of channel size and flow distribution, rather than changes in surface area. The width and number of channels were selected such that their product—the total surface area—remained the same across all configurations. This allows us to isolate the impact of channel geometry on the pressure drop while keeping the heat transfer surface area constant. The rest of the initial parameters were kept the same as in the validation study for aircraft Mach 1.5, ensuring consistency with the baseline case.

The results of this study, presented in Figure 4.4, demonstrate a clear trend: as the hydrogen mass flow increases, the pressure drop rises across all configurations. The narrower cooling channels, coupled with a greater number of channels, lead to slightly higher pressure drops, especially at higher mass flow rates. This is primarily due to increased friction and reduced cross-sectional area, which increases flow resistance. At a hydrogen mass flow rate of 10 kg/s, the pressure drop reaches approximately 14 for the narrowest channels (0.0517 m, 120 channels).

This study underscores the sensitivity of the pressure drop to both hydrogen mass flow and cooling channel configuration. As expected, increasing the mass flow rate results in a significant rise in pressure drop, which is more pronounced in narrower channels.

In Parametric Study 3 (4.2.3), we observed that the pressure drop increases as the pump pressure ratio decreases, with hydrogen mass flow playing a key role in driving these changes.

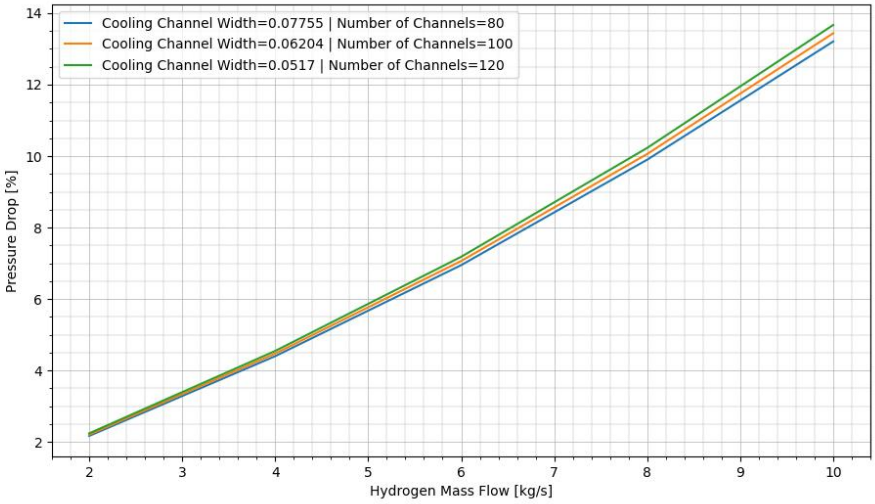

Figure 4.4: Pressure Drop along the Cooling Channels vs Hydrogen Mass Flow for Different Channel Configurations

Here, we extend that analysis by focusing on the geometric configurations of the cooling channels, revealing that the narrower channel configurations exacerbate pressure losses. The trade-off between optimizing cooling system design for heat transfer efficiency and minimizing pressure losses is even more pronounced when both geometric and mass flow effects are considered.

While narrower channels may improve convective heat transfer by increasing surface area, they also lead to higher pressure drops, which may necessitate more powerful pumps or compressors to maintain flow rates. Managing this trade-off is crucial in practical applications to ensure efficient cooling without excessive demands on the system.

Additionally, selecting the appropriate mass flow rate is vital. As mass flow increases, the pressure drop becomes more significant, particularly in more restrictive configurations. For instance, at 10 kg/s, the pressure drop for Configuration 3 is near 14 percent, which could be excessive for certain applications. Therefore, designers must carefully consider both cooling channel geometry and operational mass flow rates to keep pressure losses within acceptable limits while ensuring efficient thermal management.

This parametric study highlights the importance of channel geometry and mass flow rates in the design of efficient cooling systems. While narrower channels can increase the convective heat transfer rate by providing more surface area for heat exchange, they also result in higher pressure losses. Therefore, it is crucial to find a balance between achieving efficient heat transfer and minimizing pressure drop, particularly in high-mass-flow scenarios. When combined with the findings from Parametric Study 3, it is evident that both pump pressure ratio and channel configuration play vital roles in managing pressure losses within the system.

4.2.5 Parametric Study 5: Influence of Combustor Stagnation Temperature and Flow Configuration on Effectiveness

The fifth parametric study aimed to evaluate the effectiveness of the cooling system as a function of combustor stagnation temperature for two distinct flow configurations: parallel flow and counter flow. The primary objective was to analyze how different flow configurations impact the heat exchanger's ability to transfer heat under varying thermal conditions. Effectiveness, as a measure of heat exchanger performance, indicates how well the system approaches the theoretical maximum heat transfer, making this study particularly relevant for assessing overall thermal efficiency.

In this study, the stagnation temperature was varied between 1800 K and 3000 K, which reflects the operational range typically observed in high-speed propulsion systems. These high stagnation temperatures play a critical role in determining the heat transfer potential, as they represent the total thermal energy available in the flow. The flow configuration, whether parallel or counterflow, affects how the hot gas interacts with the cooling channels, ultimately influencing the effectiveness of the system. The rest of the initial parameters in this study were kept the same as in the validation study for aircraft Mach 1.5, ensuring consistency with prior analyses.

The results of this parametric study are presented in Figure 4.5, which shows the effectiveness as a function of stagnation temperature for both parallel and counterflow configurations.

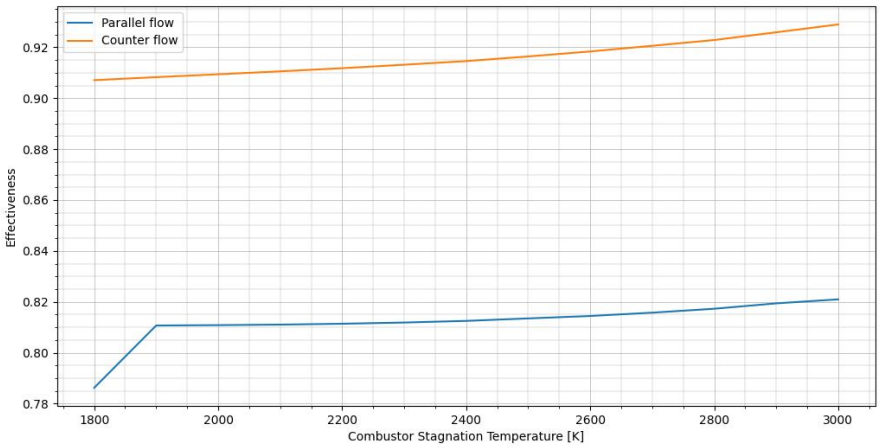

Figure 4.5: Effectiveness vs Stagnation Temperature for Parallel and Counter Flow Configurations

From the figure, it is evident that counterflow consistently outperforms parallel flow in terms of effectiveness across the entire range of stagnation temperatures. For instance, at a stagnation temperature of 3000 K, the effectiveness of the counter flow configuration reaches approximately 0.929, while the parallel flow configuration exhibits an effectiveness of about 0.821. This substantial difference is attributed to the advantages of counterflow configurations, which maintain a higher temperature gradient between the cooling fluid and the hot gas over a larger portion of the heat exchanger, leading to more efficient heat transfer.

The explanation for this divergence stems from the empirical correlations used to estimate the effectiveness, as discussed in the methodology (3.3.1.3). These correlations account for the interaction of flow configurations, gas properties, and temperature profiles. In parallel flow configurations, the temperature difference between the gas and coolant decreases more rapidly along the length of the heat exchanger, which limits the overall heat transfer efficiency. On the other hand, in counterflow systems, the higher average temperature difference between the fluids across the heat exchanger's length leads to a higher overall effectiveness.

The parallel flow configuration shows relatively stable but lower effectiveness values, ranging from approximately 0.786 at 1800 K to 0.821 at 3000 K. The increase in effectiveness with higher stagnation temperatures is modest in the parallel configuration, highlighting its limitations in achieving high heat transfer performance compared to counter flow.

On the other hand, the counter flow configuration shows higher effectiveness values, beginning at approximately 0.907 at 1800 K and rising steadily to 0.929 at 3000 K. This upward trend reflects the superior thermal performance of counter flow systems, which consistently maintain a higher temperature difference between the working fluids, thus improving overall heat transfer efficiency.

This study highlights the significant influence of flow configuration on the effectiveness of the cooling system. While both configurations benefit from increasing stagnation temperatures, counterflow is more effective in utilizing the thermal energy available, leading to higher heat transfer efficiency. The results suggest that for high-temperature propulsion systems, counterflow configurations should be prioritized to optimize thermal performance and ensure efficient cooling.

In conclusion, this study demonstrates the substantial benefits of counter-flow configurations in terms of effectiveness, particularly at higher stagnation temperatures. As system designers aim to optimize thermal management in propulsion systems, the choice of flow configuration will be a key factor in achieving maximum heat transfer performance.

Chapter 5

Conclusion

5.1 Summary

This thesis presented a comprehensive computational evaluation of heat exchangers in hydrogen-fueled gas turbines, focusing on key performance metrics such as heat transfer rates, pressure drop, NTU, and effectiveness across a range of aircraft Mach numbers. The primary objective was to assess the performance of a simplified computational tool employing a single-node method, aimed at providing preliminary design insights for hydrogen-fueled propulsion systems incorporating heat exchangers.

The validation of the computational model demonstrated that the tool can predict heat transfer rates with reasonable accuracy at lower aircraft Mach numbers (Mach 1.5 and 2), where the flow behavior and thermal exchange within the combustor and cooling channels remain more stable and well-aligned with the model's assumptions. However, at higher aircraft Mach numbers (Mach 3, 4, and 4.5), the model's performance diminishes significantly, with a pronounced underestimation of the heat transfer rate. This decline in accuracy is largely attributed to the inherent limitations of the single-node method, which oversimplifies the flow and temperature gradients within the combustor and cooling channels. Moreover, the empirical correlations used for heat transfer predictions, particularly the Bartz formula, become less accurate as the throat area decreases, leading to complex phenomena such as boundary layer thinning and rapid flow acceleration that are not fully captured.

Despite these limitations, the results highlight the model's utility as a quick, computationally inexpensive tool for evaluating heat exchanger performance in the early design stages. The heat transfer predictions at aircraft Mach 1.5 and 2 align well with reference data, validating the model's suitability for preliminary analyses. The single-node approach enabled the identification of critical factors affecting heat transfer efficiency in hydrogen-fueled propulsion systems and offered insights into areas where design improvements could be made, such as optimizing throat geometry and accounting for boundary layer effects.

In addition to the validation studies, this work incorporated several parametric studies to further explore the sensitivity of key parameters, such as combustor stagnation temperature, mass flow rate, throat area, cooling channel configuration, and pump pressure ratio, on the performance of the heat exchanger. These parametric studies provided deeper insights into the relationship between these parameters and the heat transfer rate, convective heat transfer coefficient, and pressure drop. The results from these studies underscored the importance of selecting appropriate design configurations and operational parameters to op-

timize the thermal management of hydrogen-fueled propulsion systems.

The model's predictions for pressure drop, NTU, and effectiveness further reflect the challenges of accurately capturing the complex physical phenomena within the combustor and cooling channels. While the pressure drop predictions generally followed expected trends, the NTU and effectiveness values were lower than anticipated, even at aircraft Mach 1.5 and 2. These discrepancies are linked to the simplification of flow properties and the uniform treatment of temperature distribution, which limit the model's ability to represent the detailed thermal behavior of the system accurately. The results underscore the importance of refining the thermal and fluid dynamic modeling approaches to better capture these intricate flow characteristics, especially at higher speeds.

The insights gained from this work contribute to the broader understanding of thermal management in hydrogen-fueled gas turbines and provide a strong foundation for future research aimed at enhancing the model's accuracy. The multi-node method, although outlined but not validated in this study, offers a promising path forward. By incorporating localized flow and temperature variations, the multi-node approach has the potential to significantly improve the model's predictive capabilities in high-speed flow conditions, addressing the limitations observed in this study and yielding more precise results for future propulsion system applications.

5.2 Future Work

While this thesis has focused on validating the single-node method for predicting the performance of hydrogen-fueled propulsion systems with heat exchangers, the model also incorporates a multi-node approach that has yet to be validated. Future work should prioritize the validation of this multi-node method, as it offers the potential to provide more accurate and detailed predictions by capturing spatial variations in temperature, pressure, and velocity within the combustor and cooling channels. This would enable a better understanding of localized flow phenomena, such as boundary layer development and temperature gradients, which are particularly important at higher aircraft Mach numbers and in more complex flow conditions.

The multi-node approach could greatly enhance the model's accuracy, particularly for the prediction of heat transfer rates, pressure drops, NTU, and effectiveness in regions like the throat, where rapid acceleration and geometric changes play a crucial role. Validation of this approach could be performed using experimental data or high-fidelity computational methods such as computational fluid dynamics (CFD).

In addition to validating the multi-node method, future work should involve conducting parametric studies specifically tailored to the multi-node configuration. These studies could explore the effects of combustor and cooling channel geometries, flow configurations, and operating conditions on system performance. This would provide deeper insights into the spatial variations in temperature and flow properties that the single-node method cannot

capture, thereby optimizing the heat exchanger design for hydrogen-fueled propulsion systems. By systematically varying these parameters, the multi-node method could reveal new design considerations that are critical for improving heat transfer efficiency, reducing pressure losses, and enhancing overall system performance.

Another important direction for future work is the incorporation of wall interaction effects and heat transfer resistance into the model. The current approach neglects the thermal resistance at the interface between the gas and cooling channel walls, which can significantly influence the heat transfer process. Adding this feature would allow for more accurate predictions of the overall heat transfer rates and could help refine the design of the cooling channels by accounting for the material properties and wall thicknesses that influence thermal resistance.

Refining the empirical correlations used for heat transfer predictions, such as the Bartz formula, is also a critical area for future improvement. These correlations, while useful for preliminary evaluations, may not fully capture the complexities of high-speed, compressible flows, especially in regions like the throat where the flow undergoes rapid changes. More advanced models that account for real gas effects and detailed flow behavior, particularly at elevated temperatures, should be explored. For hydrogen, real gas effects such as dissociation and variable specific heat capacities become significant and should be incorporated in future iterations of the model to increase its accuracy.

Moreover, integrating the multi-node model with advanced thermodynamic libraries or CFD techniques would enable a more comprehensive evaluation of the propulsion system under a wider range of conditions. This would allow the model to be applied to a broader range of Mach numbers and geometries, making it a versatile tool for designing efficient and high-performance hydrogen-fueled propulsion systems with heat exchangers.

Lastly, experimental validation remains a crucial aspect of future work. While this thesis has compared the model with computational data, real-world experiments are necessary to evaluate its accuracy comprehensively. Experimental validation would also help identify any discrepancies between the model's predictions and actual system behavior, providing feedback for further model refinements.

Through the validation of the multi-node approach, the inclusion of parametric studies, the addition of wall interaction effects, and experimental validation, the model can be developed into a robust computational tool for the optimization of hydrogen-fueled propulsion systems with heat exchangers.

Bibliography

[1] A. Ghazvini and V. Narayanan, "Improving combustion efficiency," *International Journal of Hydrogen Energy*, vol. 36, no. 7, pp. 4276–4284, 2011. 9

[2] C. F. McDonald, "Heat exchangers and thermal efficiency," *Journal of Engineering for Gas Turbines and Power*, vol. 111, no. 3, pp. 449–456, 1989. 9

[3] H. Zhao, Y. Chen, and T. Smith, "Mitigating pulsating combustion with heat exchangers," *Combustion Science and Technology*, vol. 191, no. 2, pp. 220–234, 2019. 9

[4] S. Moskowitz and G. Richards, "Controlling temperature gradients to extend turbine component life," *Journal of Engineering for Gas Turbines and Power*, vol. 105, no. 2, pp. 456–462, 1983. 9

[5] D. Smyth, "Advantages of ceramic heat exchangers," *Ceramic Engineering and Science Proceedings*, vol. 18, no. 2, pp. 219–226, 1997. 9

[6] A. Ganji and R. F. Mulligan, "Heat recirculation and emission reduction," *Journal of Heat Transfer*, vol. 98, no. 4, pp. 654–659, 1976. 9

[7] Y. Cao and M. Xu, "Recuperative heat exchangers in micro-gas turbines," *Applied Thermal Engineering*, vol. 27, no. 8, pp. 1365–1371, 2007. 9

[8] K. Marksberry and J. Lindahl, "Efficient use of fuel and heat energy," *Energy*, vol. 5, no. 8, pp. 775–782, 1980. 9

[9] J. Dixon, J. Verdicchio, D. Benito, A. Karl, and K. Tham, "Recent developments in gas turbine component temperature prediction methods, using computational fluid dynamics and optimization tools, in conjunction with more conventional finite element analysis techniques," *Proceedings of the Institution of Mechanical Engineers, Part A: Journal of Power and Energy*, vol. 218, pp. 241–255, 2004. 26, 30

[10] Y. Hassan, "High-fidelity experimental measurements for modeling and simulation of nuclear engineering applications," *Nuclear Engineering and Design*, vol. 354, p. 110181, 2019. 30

[11] C. Salpingidou, D. Misirlis, Z. Vlahostergios, M. Flourous, S. Donnerhack, and K. Yakinthos, "Numerical modeling of heat exchangers in gas turbines using cfd computations and thermodynamic cycle analysis tools," *Chemical Engineering Transactions*, vol. 52, pp. 517–522, 2016. 30

[12] L. Mangani, D. R. Launchbury, E. Casartelli, and G. Romanelli, "Development of high order les solver for heat transfer applications based on the open source openfoam framework," in *Proceedings of ASME Turbo Expo 2015: Turbine Technical Conference and Exposition*. American Society of Mechanical Engineers, 2015, pp. GT2015–43 279. 30

[13] O. Högblom and R. Andersson, "Multiphysics cfd simulation for design and analysis of thermoelectric power generation," *Energies*, vol. 13, no. 17, p. 4344, 2020. 30

[14] A. Amerini, S. Paccati, and A. Andreini, "Computational optimization of a loosely-coupled strategy for scale-resolving cht cfd simulation of gas turbine combustors," *Energies*, 2023. 30

[15] S. Kubakh and V. Tsapar, "Simulation of a shell-tube heat exchanger in the oil and gas industry," *Proceedings of the NTUU "Igor Sikorsky KPI". Series: Chemical engineering, ecology and resource saving*, 2023. 30

[16] B. Sundén, "Computational fluid dynamics in research and design of heat exchangers," *Heat Transfer Engineering*, vol. 28, no. 10, pp. 898–910, 2007. 31

[17] K. Menzies, "Large eddy simulation applications in gas turbines," *Philosophical Transactions of the Royal Society A: Mathematical, Physical and Engineering Sciences*, vol. 367, pp. 2827–2838, 2009. 31

[18] L. Gicquel, G. Staffelbach, and T. Poinsot, "Large eddy simulations of gaseous flames in gas turbine combustion chambers," *Progress in Energy and Combustion Science*, vol. 38, pp. 782–817, 2012. 31

[19] S. Jauré, F. Duchaine, G. Staffelbach, and L. Gicquel, "Massively parallel conjugate heat transfer methods relying on large eddy simulation applied to an aeronautical combustor," *Computational Science & Discovery*, vol. 6, p. 015008, 2013. 31

[20] S. Camporeale, B. Fortunato, and A. Dumas, "Dynamic modelling of recuperative gas turbines," *Proceedings of the Institution of Mechanical Engineers, Part A: Journal of Power and Energy*, vol. 214, pp. 213–225, 2000. 31

[21] A. Vollant, G. Balarac, and C. Corre, "Subgrid-scale scalar flux modelling based on optimal estimation theory and machine-learning procedures," *Journal of Turbulence*, vol. 18, no. 9, pp. 854–878, 2017. 31

[22] M. Carnevale, F. Montomoli, A. D'Ammaro, and S. Salvadori, "Uncertainty quantification: A stochastic method for heat transfer prediction using les," *Journal of Turbomachinery-transactions of The Asme*, vol. 135, p. 051021, 2012. 31

[23] N. Tanatsugu, M. Oguma, T. Mizutani, and T. Yano, "Thermal design of a hydrogen heater for an air turboramjet engine," *Experimental Thermal and Fluid Science*, vol. 10, no. 3, pp. 248–257, 1995. 45

[24] D. R. Bartz, "Turbulent boundary-layer heat transfer from rapidly accelerating flow of rocket combustion gases and of heated air," *Advances in Heat Transfer*, vol. 2, pp. 1–108, 1965. 45, 73

[25] S. W. Churchill, "Friction factor equation spans all fluid-flow regimes," *Chemical Engineering*, vol. 84, pp. 91–92, 1977. 56

[26] T. L. Bergman, A. S. Lavine, F. P. Incropera, and D. P. DeWitt, *Fundamentals of Heat and Mass Transfer*, 7th ed. Hoboken, NJ: John Wiley & Sons, 2011. 60

[27] R. K. Shah and D. P. Sekulić, *Fundamentals of Heat Exchanger Design*. Hoboken, New Jersey: John Wiley & Sons, Inc., 2003. 60, 67, 70, 71

[28] K. Saari, *Heat Exchanger Dimensioning*. Lappeenranta University of Technology, 2020. 63

[29] V. Fernández-Villacé and G. Paniagua, "Installed performance evaluation of an airturbo-rocket expander engine," *Journal of Propulsion and Power*, vol. 21, no. 4, pp. 768–776, 2005. 67, 70, 71

[30] I. Rodríguez-Miranda, V. Fernández-Villacé, and G. Paniagua, "Modeling, analysis, and optimization of the air-turborocket expander engine," *Journal of Propulsion and Power*, vol. 29, no. 5, pp. 1011–1022, 2013, presented at the 18th AIAA/3AF International Space Planes and Hypersonic Systems and Technologies Conference, Tours, France, September 24–28, 2012. [Online]. Available: https://arc.aiaa.org/doi/abs/10.2514/1.B34781 69

Appendix A

Code Files

A.1 Input Files

A.1.1 Aircraft Mach 1.5

```
{
  "combustor": {
    "mass_flow_rate_kg_s": 228.8,
    "stagnation_temperature_K": [2290],
    "stagnation_pressure_Pa": 112000,
    "combustor_dimensions": {
      "length_m": 10.8,
      "sectional_area_m2": 3.183,
      "throat_sectional_area_m2": 2.895,
      "throat_length_m": 1.2
    }
  },
  "cooling_channels": {
    "mass_flow_rate_kg_s": 6.93,
    "hydrogen_initial_conditions": {
      "tank_or_inlet": "tank",
      "temperature_K": 20,
      "pressure_Pa": 300000,
      "pump_pressure_ratio_for_tank_conditions": 16
    },
    "channel_dimensions": {
      "number_of_channels": 94,
      "width_inlet_m": 0.066,
      "width_outlet_m": 0.066,
      "height_inlet_m": 0.003,
      "height_outlet_m": 0.005,
      "inner_walls_rugosity_m": 5e-5
    }
  },
  "parallelflow_or_counterflow": "parallelflow"
}
```

A.1.2 Aircraft Mach 2

```
{
    "combustor": {
      "mass_flow_rate_kg_s": 220.8,
      "stagnation_temperature_K": [2310],
      "stagnation_pressure_Pa": 109000,
      "combustor_dimensions": {
        "length_m": 10.8,
        "sectional_area_m2": 3.183,
        "throat_sectional_area_m2": 2.895,
        "throat_length_m": 1.2
      }
    },
    "cooling_channels": {
      "mass_flow_rate_kg_s": 6.70,
      "hydrogen_initial_conditions": {
        "tank_or_inlet": "tank",
        "temperature_K": 20,
        "pressure_Pa": 300000,
        "pump_pressure_ratio_for_tank_conditions": 12
      },
      "channel_dimensions": {
        "number_of_channels": 94,
        "width_inlet_m": 0.066,
        "width_outlet_m": 0.066,
        "height_inlet_m": 0.003,
        "height_outlet_m": 0.005,
        "inner_walls_rugosity_m": 50e-6
      }
    },
    "parallelflow_or_counterflow": "parallelflow"
  }
```

A.1.3 Aircraft Mach 3

```
{
    "combustor": {
      "mass_flow_rate_kg_s": 202.9,
      "stagnation_temperature_K": [2480],
      "stagnation_pressure_Pa": 137000,
      "combustor_dimensions": {
```

```
        "length_m": 10.8,
        "sectional_area_m2": 3.183,
        "throat_sectional_area_m2": 2.167,
        "throat_length_m": 1.2
      }
    },
    "cooling_channels": {
      "mass_flow_rate_kg_s": 6.14,
      "hydrogen_initial_conditions": {
        "tank_or_inlet": "tank",
        "temperature_K": 20,
        "pressure_Pa": 300000,
        "pump_pressure_ratio_for_tank_conditions": 7
      },
      "channel_dimensions": {
        "number_of_channels": 94,
        "width_inlet_m": 0.066,
        "width_outlet_m": 0.066,
        "height_inlet_m": 0.003,
        "height_outlet_m": 0.005,
        "inner_walls_rugosity_m": 50e-6
      }
    },
    "parallelflow_or_counterflow": "parallelflow"
  }
```

A.1.4 Aircraft Mach 4

```
{
    "combustor": {
      "mass_flow_rate_kg_s": 177.1,
      "stagnation_temperature_K": [2110],
      "stagnation_pressure_Pa": 329000,
      "combustor_dimensions": {
        "length_m": 10.8,
        "sectional_area_m2": 3.183,
        "throat_sectional_area_m2": 0.667,
        "throat_length_m": 1.2
      }
    },
    "cooling_channels": {
      "mass_flow_rate_kg_s": 2.60,
```

```
      "hydrogen_initial_conditions": {
        "tank_or_inlet": "tank",
        "temperature_K": 20,
        "pressure_Pa": 300000,
        "pump_pressure_ratio_for_tank_conditions": 5
      },
      "channel_dimensions": {
        "number_of_channels": 94,
        "width_inlet_m": 0.066,
        "width_outlet_m": 0.066,
        "height_inlet_m": 0.003,
        "height_outlet_m": 0.005,
        "inner_walls_rugosity_m": 50e-6

      }
    },
    "parallelflow_or_counterflow": "parallelflow"
  }
```

A.1.5 Aircraft Mach 4.5

```
{
    "combustor": {
      "mass_flow_rate_kg_s": 152.5,
      "stagnation_temperature_K": [2270],
      "stagnation_pressure_Pa": 429000,
      "combustor_dimensions": {
        "length_m": 10.8,
        "sectional_area_m2": 3.183,
        "throat_sectional_area_m2": 0.458,
        "throat_length_m": 1.2
      }
    },
    "cooling_channels": {
      "mass_flow_rate_kg_s": 2.31,
      "hydrogen_initial_conditions": {
        "tank_or_inlet": "tank",
        "temperature_K": 20,
        "pressure_Pa": 300000,
        "pump_pressure_ratio_for_tank_conditions": 4
      },
      "channel_dimensions": {
```

```
        "number_of_channels": 94,
        "width_inlet_m": 0.066,
        "width_outlet_m": 0.066,
        "height_inlet_m": 0.003,
        "height_outlet_m": 0.005,
        "inner_walls_rugosity_m": 50e-6
      }
    },
    "parallelflow_or_counterflow": "parallelflow"
  }
```

A.2 Pyhton Code

```
import cantera as ct
import numpy as np
import json
from scipy.optimize import fsolve
from utils.cantera_utils import canterah
from utils.coolprop_utils import coolprop
from utils.data_utils import read_input_data

def validate_input(data, key, expected_type=None, min_value=None,
    max_value=None, list_type=None):
    if key not in data:
        raise KeyError(f"Missing key: '{key}' in input data.")

    value = data[key]

    if expected_type and not isinstance(value, expected_type):
        raise TypeError(f"Invalid type for key '{key}'. Expected {
            expected_type}, got {type(value)}.")

    if isinstance(value, (int, float)) and min_value is not None and
        value < min_value:
        raise ValueError(f"Value for '{key}' should be >= {min_value},
            got {value}.")

    if isinstance(value, (int, float)) and max_value is not None and
        value > max_value:
        raise ValueError(f"Value for '{key}' should be <= {max_value},
            got {value}.")

    if list_type and isinstance(value, list):
        if not all(isinstance(item, list_type) for item in value):
```

```
            raise ValueError(f"All elements of the list for '{key}' should be of type {list_type}.")
        if min_value is not None and any(item < min_value for item in value):
            raise ValueError(f"All elements of the list for '{key}' should be >= {min_value}.")
        if max_value is not None and any(item > max_value for item in value):
            raise ValueError(f"All elements of the list for '{key}' should be <= {max_value}.")
    return value

class HeatExchanger:
    def __init__(self, config_path):
        self.config = read_input_data(config_path)
        self.max_iterations = 100
        self.tolerance = 1e-6

    def run(self):
        hot_properties = self.calculate_hot_properties()
        cold_properties = self.calculate_cold_properties(
            hot_properties['Q_h'],
            hot_properties['N_nodes'],
            hot_properties['combustor_length']
        )
        performance_results = self.calculate_performance(hot_properties, cold_properties)
        results = self.compile_results(hot_properties, cold_properties, performance_results)
        with open('results_Ma_1_5.json', 'w') as file:
            json.dump(results, file, indent=4)
        print(f"Results saved to results_Ma_1_5.json")

    def calculate_hot_properties(self):

        data = self.config

        m_dot_h = validate_input(data['combustor'], 'mass_flow_rate_kg_s', expected_type=(int, float), min_value=0)
        p_h_stag = validate_input(data['combustor'], 'stagnation_pressure_Pa', expected_type=(int, float), min_value=0)
        T_h_stag = validate_input(data['combustor'], 'stagnation_temperature_K', expected_type=list, list_type=(int, float), min_value=0)
        if isinstance(T_h_stag, list):
            N_nodes = len(T_h_stag)

```

```
        combustor_dimensions = validate_input(data['combustor'], '
            combustor_dimensions', expected_type=dict)
        combustor_length = validate_input(combustor_dimensions, 'length_m
            ', expected_type=(int, float), min_value=0)
        combustor_length_per_node = combustor_length / N_nodes
        combustor_sectional_area = validate_input(combustor_dimensions, '
            sectional_area_m2', expected_type=(int, float), min_value=0)
        combustor_diameter = 2 * np.sqrt(combustor_sectional_area / np.pi
            )
        combustor_surface_area = combustor_length * combustor_diameter *
            np.pi
        combustor_surface_area_per_node = combustor_surface_area /
            N_nodes

        throat_sectional_area = validate_input(combustor_dimensions, '
            throat_sectional_area_m2', expected_type=(int, float),
            min_value=0)
        throat_diameter = 2 * np.sqrt(throat_sectional_area / np.pi)
        throat_length = validate_input(combustor_dimensions, '
            throat_length_m', expected_type=(int, float), min_value=0)

        T_h_static = np.zeros(N_nodes)
        p_h_static = np.zeros(N_nodes)
        mu_h_stag = np.zeros(N_nodes)
        k_h_stag = np.zeros(N_nodes)
        cp_h_stag = np.zeros(N_nodes)
        rho_h_stag = np.zeros(N_nodes)
        gamma_h_stag = np.zeros(N_nodes)
        R_h_stag = np.zeros(N_nodes)
        cp_h = np.zeros(N_nodes)
        gamma_h = np.zeros(N_nodes)
        mu_h = np.zeros(N_nodes)
        k_h = np.zeros(N_nodes)
        rho_h = np.zeros(N_nodes)
        R_h = np.zeros(N_nodes)
        Ma_h = np.zeros(N_nodes)
        Pr_h = np.zeros(N_nodes)
        Re_h = np.zeros(N_nodes)
        T_hw_adiabatic = np.zeros(N_nodes)
        h_h = np.zeros(N_nodes)
        Q_h = np.zeros(N_nodes)

        for i in range(N_nodes):
            initial_guess = [T_h_stag[i] / 1.5, 0.5]
            solver_options = {'xtol': 1e-12, 'maxfev': 10000}
            tolerance = 1e-6
            max_iterations = 100
            for iteration in range(max_iterations):
```

```
                props = canterah(T_h_stag[i], p_h_stag)
                gamma_h_stag[i] = props["Gamma"]
                mu_h_stag[i] = props["Viscosity"]
                k_h_stag[i] = props["Thermal_Conductivity"]
                cp_h_stag[i] = props["Specific_Heat_Capacity"]
                rho_h_stag[i] = props["Density"]
                R_h_stag[i] = props["R"]

                def equations(vars):
                    T_h_static, Ma_h = vars
                    eq1 = T_h_static - T_h_stag[i] / (1 + (gamma_h_stag[i
                        ] - 1) / 2 * Ma_h**2)
                    eq2 = Ma_h - m_dot_h / (rho_h_stag[i] *
                        combustor_sectional_area * np.sqrt(gamma_h_stag[i]
                         * R_h_stag[i] * T_h_static))
                    return [eq1, eq2]

                solution = fsolve(equations, initial_guess, xtol=
                    solver_options['xtol'], maxfev=solver_options['maxfev'
                    ])
                T_h_static[i], Ma_h[i] = solution
                if np.abs(T_h_static[i] - initial_guess[0]) < tolerance
                    and np.abs(Ma_h[i] - initial_guess[1]) < tolerance:
                    break
                initial_guess = [T_h_static[i], Ma_h[i]]

                p_h_static[i] = p_h_stag / ((T_h_stag[i]/T_h_static[i])
                    **(gamma_h_stag[i]/(gamma_h_stag[i] - 1)))

        if N_nodes == 1:
            Pr_h[0] = cp_h_stag[0] * mu_h_stag[0] / k_h_stag[0]
            Re_h[0] = m_dot_h * combustor_diameter / mu_h_stag[0] /
                combustor_sectional_area
            T_hw_adiabatic[0] = T_h_static[0] * (1 + 0.5 * Pr_h[0]**(1/3)
                 * (gamma_h_stag[0] - 1) * Ma_h[0]**2)

            props_h = canterah((T_hw_adiabatic[0] + T_h_static[0]) / 2,
                p_h_static[0])
            mu_h[0] = props_h["Viscosity"]
            k_h[0] = props_h["Thermal_Conductivity"]
            cp_h[0] = props_h["Specific_Heat_Capacity"]
            cp_h[0] = props_h["Specific_Heat_Capacity"]
            rho_h[0] = props_h["Density"]
            R_h[0] = props_h["R"]
            gamma_h[0] = props_h["Gamma"]

            h_h[0] = 0.026 * mu_h[0]**0.2 * (k_h[0]/mu_h[0])**0.6 * cp_h
                [0] ** 0.4 * m_dot_h**0.8 / combustor_sectional_area**0.9
```

```
                * (0.25 * np.pi * throat_diameter / ((combustor_diameter -
                 throat_diameter) / throat_length))
138             Q_h[0] = h_h[0] * (T_hw_adiabatic[0] - T_h_static[0]) *
                    combustor_surface_area
139
140         else:
141             for i in range(N_nodes - 1):
142                 props_h = canterah((T_h_static[i] + T_h_static[i+1]) / 2,
                        p_h_static[i])
143                 gamma_h[i] = props_h["Gamma"]
144                 mu_h[i] = props_h["Viscosity"]
145                 k_h[i] = props_h["Thermal_Conductivity"]
146                 cp_h[i] = props_h["Specific_Heat_Capacity"]
147                 rho_h[i] = props_h["Density"]
148                 R_h[i] = props_h["R"]
149                 Q_h[i] = m_dot_h * cp_h[i] * (T_h_stag[i] - T_h_stag[i
                        +1])
150                 Q_h[N_nodes-1] = 0
151
152         Q_h_total = sum(Q_h)
153
154         return {
155             "T_h_static": T_h_static,
156             "p_h_static": p_h_static,
157             "mu_h_stag": mu_h_stag,
158             "k_h_stag": k_h_stag,
159             "cp_h_stag": cp_h_stag,
160             "rho_h_stag": rho_h_stag,
161             "gamma_h_stag": gamma_h_stag,
162             "R_h_stag": R_h_stag,
163             "cp_h": cp_h,
164             "gamma_h": gamma_h,
165             "mu_h": mu_h,
166             "k_h": k_h,
167             "rho_h": rho_h,
168             "R_h": R_h,
169             "Ma_h": Ma_h,
170             "Pr_h": Pr_h,
171             "Re_h": Re_h,
172             "T_hw_adiabatic": T_hw_adiabatic,
173             "h_h": h_h,
174             "Q_h": Q_h,
175             "Q_h_total": Q_h_total,
176             "N_nodes": N_nodes,
177             "combustor_length": combustor_length,
178             "combustor_surface_area": combustor_surface_area,
179             "combustor_surface_area_per_node":
                    combustor_surface_area_per_node
```

```
        }

    def calculate_cold_properties(self, Q_h, N_nodes, combustor_length):
        data = self.config

        m_dot_c = validate_input(data['cooling_channels'], '
            mass_flow_rate_kg_s', expected_type=(int, float), min_value=0)
        channel_dimensions = validate_input(data['cooling_channels'], '
            channel_dimensions', expected_type=dict)
        number_of_channels = validate_input(channel_dimensions, '
            number_of_channels', expected_type=int, min_value=1)
        m_dot_c_per_channel = m_dot_c / number_of_channels

        width_inlet = validate_input(channel_dimensions, 'width_inlet_m',
             expected_type=(int, float), min_value=0)
        width_outlet = validate_input(channel_dimensions, 'width_outlet_m
            ', expected_type=(int, float), min_value=0)
        height_inlet = validate_input(channel_dimensions, 'height_inlet_m
            ', expected_type=(int, float), min_value=0)
        height_outlet = validate_input(channel_dimensions, '
            height_outlet_m', expected_type=(int, float), min_value=0)

        if 'hydrogen_initial_conditions' not in data['cooling_channels']:
            raise KeyError("Missing␣'hydrogen_initial_conditions'␣in␣
                cooling_channels␣section.")

        initial_conditions = data['cooling_channels']['
            hydrogen_initial_conditions']
        tank_or_inlet = validate_input(initial_conditions, 'tank_or_inlet
            ', expected_type=str)

        flow_type = validate_input(data, 'parallelflow_or_counterflow',
            expected_type=str)

        node_channel_width = np.zeros(N_nodes)
        node_channel_height = np.zeros(N_nodes)
        D_h = np.zeros(N_nodes)
        node_sectional_area = np.zeros(N_nodes)
        node_surface_area = np.zeros(N_nodes)
        Q_c = np.zeros(N_nodes)
        T_inlet = np.zeros(N_nodes)
        p_inlet = np.zeros(N_nodes)
        T_outlet_guess = np.zeros(N_nodes)
        p_outlet_guess = np.zeros(N_nodes)
        T_avg = np.zeros(N_nodes)
        p_avg = np.zeros(N_nodes)
        cp_c = np.zeros(N_nodes)
        mu_c = np.zeros(N_nodes)
```

```
        rho_c = np.zeros(N_nodes)
        gamma_c = np.zeros(N_nodes)
        k_c = np.zeros(N_nodes)
        R_c = np.zeros(N_nodes)
        Re_c = np.zeros(N_nodes)
        K_1 = np.zeros(N_nodes)
        K_2 = np.zeros(N_nodes)
        friction_factor = np.zeros(N_nodes)
        delta_p = np.zeros(N_nodes)
        T_outlet_new = np.zeros(N_nodes)
        p_outlet_new = np.zeros(N_nodes)
        T_outlet = np.zeros(N_nodes)
        p_outlet = np.zeros(N_nodes)

        for j in range(N_nodes):
            if N_nodes == 1:
                node_channel_width[j] = (width_inlet + width_outlet) / 2
                node_channel_height[j] = (height_inlet + height_outlet) /
                    2
                D_h[j] = 2 * node_channel_width[j] * node_channel_height[
                    j] / (node_channel_width[j] + node_channel_height[j])
            else:
                node_channel_width[j] = width_inlet + j * (width_outlet -
                    width_inlet) / (N_nodes-1)
                node_channel_height[j] = height_inlet + j * (
                    height_outlet - height_inlet) / (N_nodes - 1)
                D_h[j] = 2 * node_channel_width[j] * node_channel_height[
                    j] / (node_channel_width[j] + node_channel_height[j])

            node_sectional_area[j] = node_channel_width[j] *
                node_channel_height[j]
            node_surface_area[j] = node_channel_width[j] *
                combustor_length / N_nodes
            surface_area_channel = (width_inlet + width_outlet) / 2 *
                combustor_length
            total_surface_area = surface_area_channel *
                number_of_channels

            if j == 0:
                if tank_or_inlet == 'tank':
                    T_tank = validate_input(initial_conditions, '
                        temperature_K', expected_type=(int, float),
                        min_value=0)
                    p_tank = validate_input(initial_conditions, '
                        pressure_Pa', expected_type=(int, float),
                        min_value=0)
                    pump_pressure_ratio = validate_input(
                        initial_conditions, '
```

```
                    pump_pressure_ratio_for_tank_conditions',
                    expected_type=(int, float), min_value=0)

                gas = ct.Solution('liquidvapor.yaml', 'hydrogen')
                gas.TP = T_tank, p_tank
                s = gas.entropy_mass

                def find_T_inlet(T_inlet_guess):
                    gas.TP = float(T_inlet_guess[0]), p_inlet[0]
                    return gas.entropy_mass - s

                T_inlet_guess = np.array([20.0])
                p_inlet[0] = p_tank * pump_pressure_ratio
                T_inlet[0] = fsolve(find_T_inlet, T_inlet_guess)[0]

            elif tank_or_inlet == 'inlet':
                T_inlet[0] = validate_input(initial_conditions, '
                    temperature_K', expected_type=(int, float),
                    min_value=0)
                p_inlet[0] = validate_input(initial_conditions, '
                    pressure_Pa', expected_type=(int, float),
                    min_value=0)

        else:
            T_inlet[j] = T_outlet[j-1]
            p_inlet[j] = p_outlet[j-1]


        if flow_type == 'parallelflow':
            Q_c[j] = Q_h[j] / number_of_channels
        elif flow_type == 'counterflow':
            if N_nodes > 1:
                if j < (N_nodes - 1):
                    Q_c[j] = Q_h[N_nodes - 2 - j] /
                        number_of_channels
                else:
                    Q_c[j] = 0
            else:
                Q_c[j] = Q_h[j] / number_of_channels

        Q_c_total = sum(Q_c)

        T_outlet_guess[j] = T_inlet[j] + 20
        p_outlet_guess[j] = p_inlet[j] * 0.5

        for iteration in range(self.max_iterations):
            T_avg[j] = (T_inlet[j] + T_outlet_guess[j]) / 2
            p_avg[j] = (p_inlet[j] + p_outlet_guess[j]) / 2
```

```
292
293                 if T_avg[j] <= 0 or p_avg[j] <= 0:
294                     raise ValueError(f"Invalid values for T_avg: {T_avg[j
                        ]} or p_avg: {p_avg[j]}. Both must be positive.")
295
296                 props_cool = coolprop(T_avg[j], p_avg[j])
297                 cp_c[j] = props_cool["Specific_Heat_Capacity"]
298                 mu_c[j] = props_cool["Viscosity"]
299                 rho_c[j] = props_cool["Density"]
300                 gamma_c[j] = props_cool["Gamma"]
301                 k_c[j] = props_cool["Thermal_Conductivity"]
302                 R_c[j] = props_cool["R"]
303
304                 Re_c[j] = m_dot_c_per_channel * D_h[j] / mu_c[j] /
                        node_sectional_area[j]
305                 K_1[j] = (-2.457 * np.log((7/Re_c[j])**0.9 + 0.27 * 50e-6
                         / D_h[j]))**16
306                 K_2[j] = (37530/Re_c[j])**16
307                 friction_factor[j] = 8 * ((8/Re_c[j])**12 + (K_1[j] + K_2
                        [j])**(-3/2))**(1/12)
308                 delta_p[j] = friction_factor[j] * combustor_length /
                        N_nodes / D_h[j] * m_dot_c_per_channel**2 / 2 / rho_c[
                        j] / (node_sectional_area[j] ** 2)
309
310                 T_outlet_new[j] = Q_c[j] / (m_dot_c_per_channel * cp_c[j
                        ]) + T_inlet[j]
311                 p_outlet_new[j] = p_inlet[j] - delta_p[j]
312
313                 if abs(T_outlet_new[j] - T_outlet_guess[j]) < self.
                        tolerance and abs(p_outlet_new[j] - p_outlet_guess[j])
                         < self.tolerance:
314                     break
315
316                 T_outlet_guess[j] = T_outlet_new[j]
317                 p_outlet_guess[j] = p_outlet_new[j]
318
319             T_outlet[j] = T_outlet_new[j]
320             p_outlet[j] = p_outlet_new[j]
321
322         return {
323             "T_inlet": T_inlet,
324             "p_inlet": p_inlet,
325             "T_outlet": T_outlet,
326             "p_outlet": p_outlet,
327             "cp_c": cp_c,
328             "mu_c": mu_c,
329             "rho_c": rho_c,
330             "gamma_c": gamma_c,
```

```
            "k_c": k_c,
            "R_c": R_c,
            "Re_c": Re_c,
            "friction_factor": friction_factor,
            "node_channel_width": node_channel_width,
            "node_channel_height": node_channel_height,
            "D_h": D_h,
            "node_sectional_area": node_sectional_area,
            "node_surface_area": node_surface_area,
            "Q_c": Q_c,
            "Q_c_total": Q_c_total
        }

    def calculate_performance(self, hot_properties, cold_properties):
        data = self.config
        m_dot_h = data['combustor']['mass_flow_rate_kg_s']
        m_dot_c = data['cooling_channels']['mass_flow_rate_kg_s']
        T_h_static = hot_properties['T_h_static']
        N_nodes = hot_properties['N_nodes']
        Q_h_total = hot_properties['Q_h_total']
        combustor_surface_area = hot_properties['combustor_surface_area']
        h_h = hot_properties['h_h']
        T_inlet = cold_properties['T_inlet']
        T_outlet = cold_properties['T_outlet']
        Re_c = cold_properties['Re_c']
        k_c = cold_properties['k_c']
        cp_c = cold_properties['cp_c']
        mu_c = cold_properties['mu_c']
        D_h = cold_properties['D_h']

        if N_nodes == 1:
            Pr_c = cp_c[0] * mu_c[0] / k_c[0]
            Nu = 0.023 * Re_c[0] ** 0.8 * Pr_c ** 0.4
            h_c = Nu * k_c[0] / D_h[0]

            U = 1 / (1/h_h[0] + 1/h_c)

        else:
            if data['parallelflow_or_counterflow'] == 'counterflow':
                delta_T1 = T_h_static[0] - T_outlet[-1]
                delta_T2 = T_h_static[-1] - T_inlet[0]
            else:
                delta_T1 = T_h_static[0] - T_inlet[0]
                delta_T2 = T_h_static[-1] - T_outlet[-1]

            if delta_T1 == delta_T2:
                LMTD = delta_T1
            else:
```

```
                LMTD = (delta_T1 - delta_T2) / np.log(delta_T1 / delta_T2
                    )

            U = Q_h_total / (combustor_surface_area * LMTD)

        C_min = min(m_dot_h * min(hot_properties['cp_h']), m_dot_c * min(
            cold_properties['cp_c']))
        C_max = max(m_dot_h * max(hot_properties['cp_h']), m_dot_c * max(
            cold_properties['cp_c']))

        iteration = 0
        epsilon = 0
        NTU = U * combustor_surface_area / C_min
        C_r = C_min / C_max

        if data['parallelflow_or_counterflow'] == 'counterflow':
            if C_r < 1:
                epsilon = (1 - np.exp(-NTU * (1 - C_r))) / (1 - C_r * np.
                    exp(-NTU * (1 - C_r)))
            else:
                epsilon = NTU / (1 + NTU)
        else:
            epsilon = (1 - np.exp(-NTU * (1 + C_r))) / (1 + C_r)

        return {
            # "LMTD": LMTD,
            "C_min": C_min,
            "C_max": C_max,
            "U": U,
            "Effectiveness": epsilon,
            "NTU": NTU
        }

    def compile_results(self, hot_properties, cold_properties,
        performance_results):
        results = {
            "Performance": {
                "Heat Transfer (Q) [W]": hot_properties['Q_h_total'],
                "Heat Transfer per Node (Q) [W]": hot_properties['Q_h'].
                    tolist(),
                "Heat Transfer Per Channel (Q) [W]": cold_properties['
                    Q_c_total'],
                # "Logarithmic Mean Temperature Difference (LMTD)":
                    performance_results['LMTD'],
                "Minimum Heat Capacity Rate (C_min)": performance_results
                    ['C_min'],
                "Maximum Heat Capacity Rate (C_max)": performance_results
                    ['C_max'],
```

```
                "Overall Heat Transfer Coefficient (U)":
                    performance_results['U'],
                "Effectiveness": performance_results['Effectiveness'],
                "Number of Transfer Units (NTU)": performance_results['
                    NTU'],
            },
            "Combustor Flow Properties": {
                "Inlet Temperature [K]": hot_properties['T_h_static'][0],
                "Outlet Temperature [K]": hot_properties['T_h_static'
                    ][-1],
                "Inlet Pressure [Pa]": hot_properties['p_h_static'][0],
                "Outlet Pressure [Pa]": hot_properties['p_h_static'][-1],
                "Convection Heat Transfer Coefficient [(W/m^2.K)]":
                    hot_properties['h_h'].tolist(),
                "Mach Number (Ma)": hot_properties['Ma_h'].tolist(),
                "Reynolds Number (Re)": hot_properties['Re_h'].tolist(),
                "Prandtl Number (Pr)": hot_properties['Pr_h'].tolist(),
                "Ratio of Specific Heats": hot_properties['gamma_h'].
                    tolist(),
                "Viscosity [Pa.s]": hot_properties['mu_h'].tolist(),
                "Thermal Conductivity [W/(m.K)]": hot_properties['k_h'].
                    tolist(),
                "Isobaric Specific Heat Capacity [J/(K.kg)]":
                    hot_properties['cp_h'].tolist(),
                "Density [kg/m^3]": hot_properties['rho_h'].tolist(),
                "Specific gas constant (R) [J/(kg.K)]": hot_properties['
                    R_h'].tolist(),
            },
            "Cooling Channels Flow Properties": {
                "Inlet Temperature [K]": cold_properties['T_inlet'][0],
                "Outlet Temperature [K]": cold_properties['T_outlet'
                    ][-1],
                "Inlet Pressure [Pa]": cold_properties['p_inlet'][0],
                "Outlet Pressure [Pa]": cold_properties['p_outlet'][-1],
                "Reynolds Number (Re)": cold_properties['Re_c'].tolist(),
                "Ratio of Specific Heats": cold_properties['gamma_c'].
                    tolist(),
                "Viscosity [Pa.s]": cold_properties['mu_c'].tolist(),
                "Thermal Conductivity [W/(m.K)]": cold_properties['k_c'].
                    tolist(),
                "Isobaric Specific Heat Capacity [J/(K.kg)]":
                    cold_properties['cp_c'].tolist(),
                "Density [kg/m^3]": cold_properties['rho_c'].tolist(),
                "Specific gas constant (R) [J/(kg.K)]": cold_properties['
                    R_c'].tolist(),
            },
        }
        return results
```

```python

if __name__ == "__main__":
    exchanger = HeatExchanger('config/settings.json')
    exchanger.run()
```

A.3 Result Files

A.3.1 Aircraft Mach 1.5


```
{
    "Performance": {
        "Heat Transfer (Q) [W]": 41084499.75911759,
        "Heat Transfer per Node (Q) [W]": [
            41084499.75911759
        ],
        "Heat Transfer Per Channel (Q) [W]": 437069.1463735914,
        "Minimum Heat Capacity Rate (C_min)": 97790.7781796189,
        "Maximum Heat Capacity Rate (C_max)": 526595.4128343121,
        "Overall Heat Transfer Coefficient (U)": 3966.4326354529553
            ,
        "Effectiveness": 0.811801883371927,
        "Number of Transfer Units (NTU)": 2.770442797328226
    },
    "Combustor Flow Properties": {
        "Inlet Temperature [K]": 2181.5615433609114,
        "Outlet Temperature [K]": 2181.5615433609114,
        "Inlet Pressure [Pa]": 88735.49346083775,
        "Outlet Pressure [Pa]": 88735.49346083775,
        "Convection Heat Transfer Coefficient [(W/m^2.K)]": [
            6901.972445691828
        ],
        "Mach Number (Ma)": [
            0.6146090754608768
        ],
        "Reynolds Number (Re)": [
            2044769.0172889591
        ],
        "Prandtl Number (Pr)": [
            0.5190669088036622
        ],
        "Ratio of Specific Heats": [
```

```
            1.2646285664144277
        ],
        "Viscosity [Pa.s]": [
            6.937806539957478e-05
        ],
        "Thermal Conductivity [W/(m.K)]": [
            0.30748245731840085
        ],
        "Isobaric Specific Heat Capacity [J/(K.kg)]": [
            2301.5533777723426
        ],
        "Density [kg/m^3]": [
            0.08280300595516525
        ],
        "Specific gas constant (R) [J/(kg.K)]": [
            481.6092148013255
        ]
    },
    "Cooling Channels Flow Properties": {
        "Inlet Temperature [K]": 21.885912815886805,
        "Outlet Temperature [K]": 442.0124372582522,
        "Inlet Pressure [Pa]": 4800000.0,
        "Outlet Pressure [Pa]": 4398422.898085685,
        "Reynolds Number (Re)": [
            278909.7724600424
        ],
        "Ratio of Specific Heats": [
            1.4362757872104315
        ],
        "Viscosity [Pa.s]": [
            7.552202133846608e-06
        ],
        "Thermal Conductivity [W/(m.K)]": [
            0.1573180192443501
        ],
        "Isobaric Specific Heat Capacity [J/(K.kg)]": [
            14111.22340254241
        ],
        "Density [kg/m^3]": [
            4.6625162759660075
        ],
        "Specific gas constant (R) [J/(kg.K)]": [
```

```
            4124.487568704487
        ]
    }
}
```


A.3.2 Aircraft Mach 2


```
{
    "Performance": {
        "Heat Transfer (Q) [W]": 40035068.93972615,
        "Heat Transfer per Node (Q) [W]": [
            40035068.93972615
        ],
        "Heat Transfer Per Channel (Q) [W]": 425904.98872049095,
        "Minimum Heat Capacity Rate (C_min)": 94275.54148017314,
        "Maximum Heat Capacity Rate (C_max)": 508983.64036101295,
        "Overall Heat Transfer Coefficient (U)": 3858.5972740281945
        ,
        "Effectiveness": 0.8130188893866711,
        "Number of Transfer Units (NTU)": 2.795615401874379
    },
    "Combustor Flow Properties": {
        "Inlet Temperature [K]": 2201.590470152145,
        "Outlet Temperature [K]": 2201.590470152145,
        "Inlet Pressure [Pa]": 86519.94777719291,
        "Outlet Pressure [Pa]": 86519.94777719291,
        "Convection Heat Transfer Coefficient [(W/m^2.K)]": [
            6728.474600209347
        ],
        "Mach Number (Ma)": [
            0.6121643398344854
        ],
        "Reynolds Number (Re)": [
            1961414.4494689475
        ],
        "Prandtl Number (Pr)": [
            0.5188340698898607
        ],
        "Ratio of Specific Heats": [
            1.2642001830040355
        ],
        "Viscosity [Pa.s]": [
```

```
            6.981031223316646e-05
        ],
        "Thermal Conductivity [W/(m.K)]": [
            0.3099876555517471
        ],
        "Isobaric Specific Heat Capacity [J/(K.kg)]": [
            2305.1795306205295
        ],
        "Density [kg/m^3]": [
            0.07999255522672905
        ],
        "Specific gas constant (R) [J/(kg.K)]": [
            481.7503288125663
        ]
    },
    "Cooling Channels Flow Properties": {
        "Inlet Temperature [K]": 21.419776529398746,
        "Outlet Temperature [K]": 446.0799620998611,
        "Inlet Pressure [Pa]": 3600000.0,
        "Outlet Pressure [Pa]": 3083598.137129771,
        "Reynolds Number (Re)": [
            269115.6028952283
        ],
        "Ratio of Specific Heats": [
            1.4317568495174762
        ],
        "Viscosity [Pa.s]": [
            7.5672838818140756e-06
        ],
        "Thermal Conductivity [W/(m.K)]": [
            0.15693625905613895
        ],
        "Isobaric Specific Heat Capacity [J/(K.kg)]": [
            14070.976340324349
        ],
        "Density [kg/m^3]": [
            3.3904720441593486
        ],
        "Specific gas constant (R) [J/(kg.K)]": [
            4124.487568704487
        ]
    }
```

```
}
```

A.3.3 Aircraft Mach 3


```
{
    "Performance": {
        "Heat Transfer (Q) [W]": 5396553.851767567,
        "Heat Transfer per Node (Q) [W]": [
            5396553.851767567
        ],
        "Heat Transfer Per Channel (Q) [W]": 57410.147359229435,
        "Minimum Heat Capacity Rate (C_min)": 88671.6611578511,
        "Maximum Heat Capacity Rate (C_max)": 474312.1838646167,
        "Overall Heat Transfer Coefficient (U)": 1201.4089738132702
           ,
        "Effectiveness": 0.5616221880760733,
        "Number of Transfer Units (NTU)": 0.9254501578248346
    },
    "Combustor Flow Properties": {
        "Inlet Temperature [K]": 2413.536228341871,
        "Outlet Temperature [K]": 2413.536228341871,
        "Inlet Pressure [Pa]": 120103.78121179315,
        "Outlet Pressure [Pa]": 120103.78121179315,
        "Convection Heat Transfer Coefficient [(W/m^2.K)]": [
            1481.504188621291
        ],
        "Mach Number (Ma)": [
            0.4601976136118965
        ],
        "Reynolds Number (Re)": [
            1716021.5095626255
        ],
        "Prandtl Number (Pr)": [
            0.5165887281402254
        ],
        "Ratio of Specific Heats": [
            1.2606570935985248
        ],
        "Viscosity [Pa.s]": [
            7.39521566749158e-05
        ],
        "Thermal Conductivity [W/(m.K)]": [
```

```
            0.33433666129993905
        ],
        "Isobaric Specific Heat Capacity [J/(K.kg)]": [
            2337.6647800128962
        ],
        "Density [kg/m^3]": [
            0.101830126439787
        ],
        "Specific gas constant (R) [J/(kg.K)]": [
            483.3423065319669
        ]
    },
    "Cooling Channels Flow Properties": {
        "Inlet Temperature [K]": 20.803834146052953,
        "Outlet Temperature [K]": 81.66379528020556,
        "Inlet Pressure [Pa]": 2100000.0,
        "Outlet Pressure [Pa]": 1971222.221950959,
        "Reynolds Number (Re)": [
            662044.1355238423
        ],
        "Ratio of Specific Heats": [
            2.22026042321453
        ],
        "Viscosity [Pa.s]": [
            2.818938040587902e-06
        ],
        "Thermal Conductivity [W/(m.K)]": [
            0.049793913558062494
        ],
        "Isobaric Specific Heat Capacity [J/(K.kg)]": [
            14441.638625057181
        ],
        "Density [kg/m^3]": [
            11.336746141072767
        ],
        "Specific gas constant (R) [J/(kg.K)]": [
            4124.487568704487
        ]
    }
}
```

A.3.4 Aircraft Mach 4


```
{
    "Performance": {
        "Heat Transfer (Q) [W]": 80265.61519533055,
        "Heat Transfer per Node (Q) [W]": [
            80265.61519533055
        ],
        "Heat Transfer Per Channel (Q) [W]": 853.8895233545803,
        "Minimum Heat Capacity Rate (C_min)": 26116.036342146257,
        "Maximum Heat Capacity Rate (C_max)": 403570.064463156,
        "Overall Heat Transfer Coefficient (U)": 206.4835669607565,
        "Effectiveness": 0.41070945308286466,
        "Number of Transfer Units (NTU)": 0.5400391393594532
    },
    "Combustor Flow Properties": {
        "Inlet Temperature [K]": 2103.542851386716,
        "Outlet Temperature [K]": 2103.542851386716,
        "Inlet Pressure [Pa]": 324254.04425201786,
        "Outlet Pressure [Pa]": 324254.04425201786,
        "Convection Heat Transfer Coefficient [(W/m^2.K)]": [
            226.28053338648212
        ],
        "Mach Number (Ma)": [
            0.15154597591307825
        ],
        "Reynolds Number (Re)": [
            1675242.3135926016
        ],
        "Prandtl Number (Pr)": [
            0.5202159557234665
        ],
        "Ratio of Specific Heats": [
            1.2674289351025856
        ],
        "Viscosity [Pa.s]": [
            6.677691621219585e-05
        ],
        "Thermal Conductivity [W/(m.K)]": [
            0.2925190404141158
        ],
        "Isobaric Specific Heat Capacity [J/(K.kg)]": [
            2278.7694210229024
```

```
        ],
        "Density [kg/m^3]": [
            0.3201939470018703
        ],
        "Specific gas constant (R) [J/(kg.K)]": [
            480.82291853244186
        ]
    },
    "Cooling Channels Flow Properties": {
        "Inlet Temperature [K]": 20.544902277302967,
        "Outlet Temperature [K]": 23.618324834377496,
        "Inlet Pressure [Pa]": 1500000.0,
        "Outlet Pressure [Pa]": 1496142.7995688429,
        "Reynolds Number (Re)": [
            60463.55385287846
        ],
        "Ratio of Specific Heats": [
            1.7357532663586743
        ],
        "Viscosity [Pa.s]": [
            1.30702465514005e-05
        ],
        "Thermal Conductivity [W/(m.K)]": [
            0.10643883731935605
        ],
        "Isobaric Specific Heat Capacity [J/(K.kg)]": [
            10044.629362363945
        ],
        "Density [kg/m^3]": [
            70.75761136442102
        ],
        "Specific gas constant (R) [J/(kg.K)]": [
            4124.487568704487
        ]
    }
}
```


A.3.5 Aircraft Mach 4.5


```
{
    "Performance": {
        "Heat Transfer (Q) [W]": 26329.087865688714,
```

```
        "Heat Transfer per Node (Q) [W]": [
            26329.087865688714
        ],
        "Heat Transfer Per Channel (Q) [W]": 280.09667942222035,
        "Minimum Heat Capacity Rate (C_min)": 22220.822064652846,
        "Maximum Heat Capacity Rate (C_max)": 352085.5659366061,
        "Overall Heat Transfer Coefficient (U)": 138.67898647249808
            ,
        "Effectiveness": 0.34276741495102236,
        "Number of Transfer Units (NTU)": 0.42628253921947645
    },
    "Combustor Flow Properties": {
        "Inlet Temperature [K]": 2266.7779981464782,
        "Outlet Temperature [K]": 2266.7779981464782,
        "Inlet Pressure [Pa]": 426085.7233264978,
        "Outlet Pressure [Pa]": 426085.7233264978,
        "Convection Heat Transfer Coefficient [(W/m^2.K)]": [
            148.73945672836925
        ],
        "Mach Number (Ma)": [
            0.10392118257602517
        ],
        "Reynolds Number (Re)": [
            1371447.7329185593
        ],
        "Prandtl Number (Pr)": [
            0.5203678908138358
        ],
        "Ratio of Specific Heats": [
            1.2632770480127493
        ],
        "Viscosity [Pa.s]": [
            7.028670521414081e-05
        ],
        "Thermal Conductivity [W/(m.K)]": [
            0.31184679019137573
        ],
        "Isobaric Specific Heat Capacity [J/(K.kg)]": [
            2308.7578094203677
        ],
        "Density [kg/m^3]": [
            0.39043346297214865
```

```
        ],
        "Specific gas constant (R) [J/(kg.K)]": [
            481.1636066663041
        ]
    },
    "Cooling Channels Flow Properties": {
        "Inlet Temperature [K]": 20.41228651034427,
        "Outlet Temperature [K]": 21.597170120369256,
        "Inlet Pressure [Pa]": 1200000.0,
        "Outlet Pressure [Pa]": 1196966.271720023,
        "Reynolds Number (Re)": [
            50494.31063881276
        ],
        "Ratio of Specific Heats": [
            1.6836623287670542
        ],
        "Viscosity [Pa.s]": [
            1.390508456679025e-05
        ],
        "Thermal Conductivity [W/(m.K)]": [
            0.10572391676962863
        ],
        "Isobaric Specific Heat Capacity [J/(K.kg)]": [
            9619.403491191708
        ],
        "Density [kg/m^3]": [
            71.56956688903286
        ],
        "Specific gas constant (R) [J/(kg.K)]": [
            4124.487568704487
        ]
    }
}
```